Use of Physical Enhancers for Gastrointestinal and Transdermal Drug Delivery

by

Carl M. Schoellhammer
Bachelor of Science in Chemical Engineering
University of California, Berkeley, 2009

Submitted to the Department of Chemical Engineering in partial fulfillment of the requirements for the degree of

Doctor of Philosophy in Chemical Engineering
at the
Massachusetts Institute of Technology
June 2015

Signature of Author: Signature redacted
Department of Chemical Engineering
April 10th, 2015

Certified By: Signature redacted
Daniel Blankschtein
Professor, Thesis Supervisor

Signature redacted
Robert Langer
Institute Professor, Thesis Supervisor

Accepted By: Signature redacted
Richard Braatz
Professor of Chemical Engineering
Chairman, Committee for Graduate Students

Use of Physical Enhancers for Gastrointestinal and Transdermal Drug Delivery

By

Carl M. Schoellhammer

Submitted to the Department of Chemical Engineering on April 10th, 2015 in partial fulfillment of the requirements of the degree of Doctor of Philosophy in Chemical Engineering

Abstract

The research presented in this thesis represents a significant advance in the field of transdermal- and gastrointestinal (GI)-based drug delivery. With regards to the former, previous work has led to a thorough mechanistic understanding of ultrasound (US)-enhanced transdermal drug delivery. Despite these investigations, it was previously not possible to maximize the efficiency of the permeabilization, or to decrease the required treatment time. In this area, this thesis presents work on the use of a new US treatment modality to both maximize the area of skin that is permeabilized while simultaneously minimizing the required treatment time.

This new method involves the simultaneous use of low- (< 100 kHz) and high- (≥ 1 MHz) frequency US. A proof-of-concept of this method is presented in Chapter 2. Specifically, through the use of aluminum foil pitting experiments, the mechanism of enhancement is elucidated, confirming an increase in transient cavitational events. This method is further shown to lead to enhanced delivery of model permeants to porcine skin *in vitro*.

The new method is further explored in Chapter 3. Specifically, a physiologically relevant experimental setup, utilizing the receiver chamber of a Franz diffusion cell is developed. With this setup, fundamental studies are carried out to investigate the enhancement in localized transport region (LTR) formation versus the enhancement in the resulting skin permeability *in vitro*. The most important finding is that the enhancement in permeability is greater than the enhancement in LTR formation, suggesting that dual-frequency US results in more permeable LTRs, in addition to larger LTRs. This phenomenon was not previously realized. Furthermore, the safety of this method is assessed through blinded histological evaluation of skin samples treated both *in vitro* and *in vivo*. This investigation demonstrated that dual-frequency US results in no greater histological disruption of the skin than that observed using 20 kHz US alone.

The power of physical enhancers, such as US, is underscored by their ability to permeabilize a tissue layer, such as the skin, which is designed to serve as a barrier. The use of physical enhancers in a tissue that lacks this barrier, such as the GI tract, presents an intriguing opportunity to maximize drug delivery while minimizing treatment times. In Chapters 4 and 5, the use of microneedles

and US to facilitate GI-based drug delivery are explored. Specifically, in Chapter 4, the implementation of an ingestible device containing microneedles is investigated. Studies in pigs demonstrated that microinjections of a model biologic in the GI tract results in superior kinetics compared to traditional subcutaneous injection. A model device containing radially protruding microneedles was also found to be capable of being excreted naturally without any adverse events.

Chapter 5 explores the use of US to facilitate rapid delivery to all tissue types of the GI tract. US is demonstrated to be safe and well tolerated. Further, it is found to enable the delivery of a broad range of permeants with a wide range of molecular weights. The clinical use of such a technology is examined in a model of inflammatory bowel disease, and the tolerability and efficacy of rectal-based drug delivery is studied in both small and large animal models *in vivo*.

This thesis advances the current understanding of the use of physical enhancers in skin and GI tissue. In the area of transdermal drug delivery, the insights gained here could lead to more clinically viable devices by reducing the required skin treatment time to achieve a certain level of permeabilization. With respect to the GI tract, this thesis advances for the first time the use of physical enhancers, including investigating the mechanism of enhancement and the cellular and histological effects. This should open the door to a previously unexplored line of research. Indeed, this research could lead to improved therapies and expansion of research techniques applied to the GI tract, as well as to new medical devices to enable local rectal delivery and, eventually, oral administration using ingestible devices.

Thesis Supervisor: Daniel Blankschtein
Title: Herman P. Meissner '29 Professor of Chemical Engineering

Thesis Supervisor: Robert Langer
Title: David H. Koch Institute Professor

Acknowledgements

This thesis was enabled in part by the many people who have helped and supported me throughout my degree. First and foremost, I would like to thank my advisors, Professor Daniel Blankschtein and Professor Robert Langer, for their constant support and guidance both personally and professionally. Professor Blankschtein has always offered his support and encouragement. My research and communication have benefited tremendously from the amount of time he has invested both in completing this thesis, as well as in all of my publications. I am extremely grateful for this. I would like to thank Professor Langer for his tireless efforts in supporting me and guiding me as a scientist. He has taught me to consider the big-picture and to tackle problems that could have tremendous positive impact on the well being of society. I believe my thesis demonstrates this translational research focus. I am indebted to my advisors for this.

I would also like to extend my sincerest gratitude to my committee members, Professor Douglas Hart, Professor J. Christopher Love, and Dr. Giovanni Traverso. They have also invested significant time and effort into my growth and development as a scientist and have supported me during my thesis work at MIT. They all brought a special expertise and pointed my attention to important considerations, which have helped me develop my own strategies for tackling clinically applied research problems.

I would also like to thank all of my friends, collaborators, and colleagues for helping me both personally, and professionally. They helped me maintain my perspective and humor on this challenging journey. I would like to thank the members of the Blankschtein Lab with whom I was able to interact with personally and professionally. This includes the members who initially brought me into the lab and familiarized me with research techniques: Baris Polat, Jennifer Seto, and Jonathan Mendenhall. This is in addition to the current lab members: Matthias Oberli, Diviya Sinha, Vishnu Sresht, Ananth Rajan, and Andreas Reichmuth. I am also indebted to many members of the Langer lab, including: Avi Schroeder, Ross Barman, Angela DiCiccio, Stacy Mo, and Young-Ah Lucy Lee. I would also like to thank my dedicated UROPs, Ruby Maa and Sharanya Srinivasan, for their tireless effort and friendship. All of these individuals have helped me tremendously and I am deeply grateful for the positive impact they have had on me.

Finally, I would like to thank my family. You have never tired in your support for me. I would not be where I am today without all of your help. You never doubted me and continually encouraged me to go as far as I could. Hans, Mike, Tom, Mark, and Katharina, I hope I have made you proud.

To my partner Hallie: I cannot put in words my gratitude for all that you did, do, and will do for me. You are a constant source of firm support, guidance, and understanding for me. This thesis would not be possible without you. I dedicate this thesis to you.

Table of Contents

List of Figures

prevent leakage. The receiver chamber is inspected to ensure that there are no air bubbles present in the PBS. Immediately before treatment, the donor chamber is filled with a solution containing the permeant of interest and an ultrasound horn (either 20, 40, or 60 kHz) is submerged in the permeant solution. (b) Comparison of the amount of glucose delivered to various tissues of the GI tract with (20 kHz) and without (Control) ultrasound. The treatment utilized a 20 kHz ultrasound horn calibrated calorimetrically to 7.5 W/cm^2. The duration of treatment was two minutes with the horn set to pulse (50% duty cycle 5 s on, 5 s off, resulting in one minute of ultrasound exposure). Delivery utilizing ultrasound was significantly greater than passive delivery (two-tailed Student's t-test, $P < 0.03$). (c) Survey of glucose delivery to intestine and colon using 20 and 40 kHz ultrasound at the lowest intensity considered for each frequency. A solution of 1 mg/mL glucose was utilized in the donor chamber. Treatment duration was again two minutes at 50% duty cycle, as described above. Treatment using ultrasound resulted in significantly greater delivery in both tissues. (d) The same survey described in (c) was also performed using 5,000 Da inulin at a concentration of 1 mg/mL in the donor cell. Again, delivery was greater when ultrasound was used. (e) The same survey described in (c) and (d) was then carried out using the clinically relevant compounds hydrocortisone and mesalamine. Both molecules were loaded in the

treatment). The control consisted of recirculating water at room temperature two or five minutes. This is compared to the enhancement in delivery using 20 kHz ultrasound set to an intensity of 7.5 W/cm^2 at a duty cycle of 50% for 2 minutes total (control n = 5, ultrasound n = 3). (*) indicates a statistical difference between the treatment and its respective control determined by a two-tailed Student's t-test. (c) Relative enhancement in glucose delivery to small intestine as a result treatment with 1 MHz ultrasound set to 2 W/cm^2 (5.22 W actual) for 3.4 min (n = 3), stirring of the donor chamber (control n = 5, stirring n = 6), and 40 kHz ultrasound set to an intensity of 13.4 W/cm^2 (control n = 5, ultrasound n = 3). (*) indicates a statistical difference between the treatment and its respective control determined by a two-tailed Student's t-test. (d) Number of pits observed in aluminum foil pitting experiments when treated using 20, 40, or 60 kHz ultrasound for 2 seconds at the highest intensity considered for each frequency (n = 5 for each frequency). (e) Representative images of pitted aluminum foil samples treated with either 20, 40, or 60 kHz ultrasound. The scale bar represents 3 mm. (f) Estimation of pore size radius created in small intestine tissue as a result of ultrasound exposure using the Aqueous Porous Pathway Model. (g) Diagram of the hypothesized mechanism of ultrasound-enhanced GI delivery. Ultrasound emission results in the formation of cavitation bubbles in the fluid (i). As

result of placement of an enema containing 100U insulin without (left) or with (middle) simultaneous 20 kHz ultrasound treatment. Each individual curve is a biological repeat. The bar graph (right) represents the average and standard deviation after 40 minutes of monitoring. The *P*-value represents a two-tailed Student's t-test. 199

Figure 5-4: (a) Colitis induction and treatment schedule. (b) The custom-designed ultrasound probe tip with a shaft diameter of 2 mm. The two bumps shown have a diameter of 3 mm and enhance radial ultrasound emission. (c) Total Fecal Score for healthy animals (Control) and animals with DSS-induced colitis: receiving no treatment (Disease), receiving mesalamine enema daily (Drug Enema QD), receiving mesalamine enema with ultrasound treatment daily (US Treatment QD), and receiving mesalamine enema with ultrasound treatment every other day (US Treatment QOD). All groups were comprised of 5 animals. The * indicates a statistical difference between the ultrasound Treatment groups and those groups receiving no treatment or mesalamine enema alone (one-way analysis of variance testing with multiple comparisons, $P < 0.047$). (d) Histology score of tissue sections at Day 14. The median, 25^{th}, and 75^{th} percentiles are shown. The whiskers indicate the most extreme data points. ** Indicates a statistical difference between the ultrasound QD group and all other colitis groups (one-way analysis of variance testing with multiple comparisons, $P < 2.9 \times 10^{-4}$). (e)

75th percentiles are shown. The whiskers indicate the most extreme data points. The Disease group is shown for comparison. Both the Probe Insertion and US groups had statistically better histology scores than any other group that had disease induced (one-way analysis of variance testing with multiple comparisons, $P < 0.015$). (c) Total fecal score for all three groups over the 14-day period was determined to evaluate for the presence of inflammation leading to worsening fecal scores. A paired, two-tailed t-test between the Probe Insertion and ultrasound groups showed no significant difference between their scores on any day. The largest standard deviation observed in the Total Fecal Score for the Control, Probe Insertion, and US groups over the 14-day trial is 0.54, 2.68, and 3.28, respectively. The average standard deviation for each group over the 14-day trial is 0.17, 0.99, and 1.56, respectively. (d) Cytokine levels of TNF-α (i), IFN-γ (ii) IL-6 (iii), and IL-17 (iv). n = 4 biological repeats for all groups. No statistical difference was found between treatment groups for any cytokine (one-way analysis of variance testing with multiple comparisons). All graphs represent averages and standard deviations. Sample sizes indicated are biological replicates. Toxicity as evaluated through the absence of anemia, low fecal score, low histology scores, and normal cytokine levels supports the likely safety of this drug delivery modality in the GI tract. 223

List of Tables

Chapter 1

Introduction and Background

1.1 Introduction and Background

1.1.1 Importance of Transdermal Drug Delivery

The efficient delivery of drugs into, and across, the skin has been a goal of researchers for decades. The skin is an attractive area for delivery due to its prevalence and ease of access. However, because of the barrier posed by the skin, most compounds are administered with a hypodermic needle [1], [2]. While common, injections have two serious disadvantages: i) pain and needle phobia, and ii) transmission of infectious diseases through needle reuse and unintentional injury.

Injections are unpleasant and painful, which increases needle phobia, resulting in decreased compliance. The significance of this is highlighted by a study, which suggested that 30% of adults suffer from needle phobia [3]-[6]. Even more significant is the risk of unintentional needle injuries to both the patient and physician. This results in hundreds of millions of dollars-worth of additional medical treatment, and increases the transmission of infectious diseases [7]-[10]. In 1999, the World Health Organization estimated that 1.3 million deaths were caused by unsafe needle practices [9]-[11]. In developing countries, it was estimated that 50% of the injections are unsafe. In the United States, there are 800,000 reported cases of needle injuries by medical professionals every year [9], [12], [13].

Despite these disadvantages, needles are required to overcome the barrier properties of the skin. The main barrier to therapeutic delivery is the outermost layer of the skin, the *stratum corneum* (SC). As a result, various methods of skin permeabilization have been explored for their ability to enhance the transport of drugs across the SC.

1.1.2 Skin Architecture and Barrier Function

Skin has been widely studied and its structure is well understood. The first layer of the skin is the epidermis and encompasses the SC. In spite of being only 15-20 μm thick, the SC provides the majority of the barrier function of the skin [7], [14], [15]. It is comprised of densely packed, dead corneocytes filled with keratin, surrounded by a lipid matrix (see Figure 1-1) [16], [17]. This lipid matrix is primarily composed of ceramides (50%), cholesterol (25%), and other free fatty acids, and is estimated to be less than 100 nm wide, limiting passive diffusion to small, lipophilic molecules [18]-[20]. Because of the long, flat, tile-like shape of the corneocytes, the SC is often described as having a "brick-and-mortar" structure [15], [21]. This region is indicated in Figure 1-1.

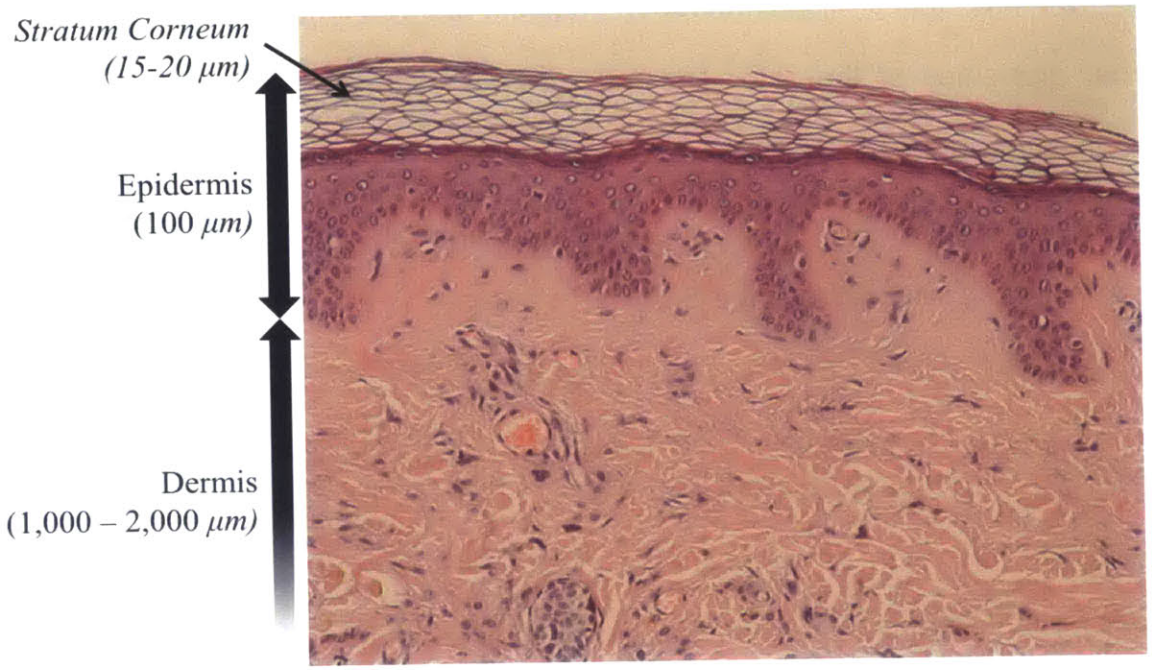

Figure 1-1: Histological cross-section of the skin. The outermost layer of the epidermis, the SC, is composed of dead corneocytes locked in a lipid matrix. Below the SC lies the viable epidermis, comprised of keratinocytes. Below this region is the dermis.

The epidermis itself is approximately 100 μm thick and is composed of keratinocytes below the SC [22]-[24]. These cells continually proliferate, pushing older cells to the surface where they undergo keratinization and programmed cell death, forming the SC [12], [25]. The live keratinocytes directly below the SC also serve a protective function. Upon insult, keratinocytes are able to secrete cytokines and chemokines to stimulate immune function at the site of infection [26]. This signaling can recruit patrolling dendritic cells. Additionally, upon injury, keratinocytes migrate to the site of the wound and form a protective cover over it [1], [6]. The deepest layer of the skin is the dermis, which is between 1,000-2,000 μm in thickness [11], [13]. It is made up of connective tissue, including collagen and elastic fibers, and has macrophages, fibroblasts, and adipocytes throughout [12], [15].

Upon removal of the SC, the epidermis becomes the rate-limiting barrier to transdermal drug delivery (TDD) [3]-[5]. Removal of the viable epidermis and SC resulted in an order-of magnitude increase in delivery over removal of the SC alone [3], [10]. This is an important finding because drugs must reach the capillaries found in the dermis for systemic delivery [8], [10].

1.1.3 New Frontiers: The Gastrointestinal Tract

Just like the skin, the Gastrointestinal (GI) tract could also serve as a unique opportunity for the use of physical enhancers for drug delivery. Oral drug delivery is the preferred route by patients and physicians alike, particularly when compared to parenteral routes [27], [28]. Oral delivery, however, is limited as a

result of poor drug absorption, drug degradation, and first pass metabolism in the liver. This is of particular concern for the biologic class of drugs, which are susceptible to proteases, endonucleases, bacteria, and the extremes in pH encountered in the GI tract [29]. As a result, biologics are not currently orally administrable and require delivery through injection.

As a result, the delivery of macromolecules across the GI tract is one of the most highly investigated areas of research in drug delivery. Approaches being investigated to enable the oral delivery of biologics include chemical modification of the drug, co-administration with enzyme inhibitors, polymeric micro- and nano- carriers, liposome carriers, as well as targeted nanoparticles [30]-[32]. However, these strategies require tedious reformulation of the drug to ensure both compatibility with the specific technique and that the activity of the drug is maintained. Additionally, they lack broad utility, requiring optimization for each drug to be delivered. The use of physical enhancers for oral delivery is an unexplored area rich for academic and clinical investigation. It has the potential to enable oral delivery of substances such as nanoparticles, monoclonal antibodies, or vaccines to modulate mucosal immune responses [33], [34]. Additionally, it has the potential to enable the delivery of new classes of therapeutics such as DNA and RNA-based treatments, the delivery of which requires overcoming several biological barriers [35], [36].

1.1.4 Gastrointestinal Tissue Architecture

The GI tract encompasses the continuous tube from the mouth to the anus. The specific organs that make up the GI tract are the mouth, the pharynx (will not be discussed), the esophagus, the stomach, the small and large intestines, and the colon. The tissue from the esophagus to the anus has four basic layers, and unlike the skin, there is no keratinized cellular layer like the SC. The first, interior-most layer is known as the mucosa, which is a mucous layer composed of: (i) non-keratinized epithelium that comes in direct contact with food in the GI tract, (ii) the lamina propria, which is a layer of connective tissue with a high density of blood vessels, and (iii) the muscularis mucosae, a layer of thin muscle, which in the stomach and the intestine creates folds to enhance surface area for absorption. The second layer is the submucosa, which is made up of collagenous fibers and blood vessels. It also contains lots of nerves to control sensing, movement of the mucosa, and blood flow. The third layer is the muscularis, which is a layer of muscle. From the mouth to the esophagus the muscularis is made of skeletal muscle. Below the esophagus, the muscle is made of smooth muscle cells generally structured in two layers: an inner layer of circular muscle fiber, and an outer layer of longitudinal muscle fiber. The fourth and outer-most layer of the GI tract is the serosa, a layer comprised of connective tissue and epithelium. It acts as the outer-most surrounding of the organs in the peritoneal cavity. Additional details on each tissue type are provided below [37].

1.1.4.1The Mouth

The mouth is formed by the hard and soft palates (top of the mouth), the cheeks, and the tongue. With the exception of the tongue, all these tissues have the same structure as described above, where the mucous membrane is the layer exposed to the mouth cavity. The tongue is composed of skeletal muscle that is then covered by a mucous membrane. The surface of the tongue is covered by papillae, which are elevations of the lamina propria that often contain taste buds.

1.1.4.2The Esophagus

The esophagus is a muscular tube that runs from the back of the mouth down the chest and into the top of the stomach. It is composed of the same three general tissue layers. The outer mucous layer is slightly thicker in the esophagus and the mouth to protect against abrasion. No nutrient absorption takes place in the esophagus, and its general purpose is to transport food into the stomach.

1.1.4.3The Stomach

The stomach is a J-shaped enlargement, which connects the esophagus with the initial part of the small intestine. Although some absorption of nutrients takes place in the stomach, its main function is as a food reservoir, since food absorption and travel through the intestine takes longer than consumption. For a detailed schematic diagram of the various stomach layers, see Figure 1-2.

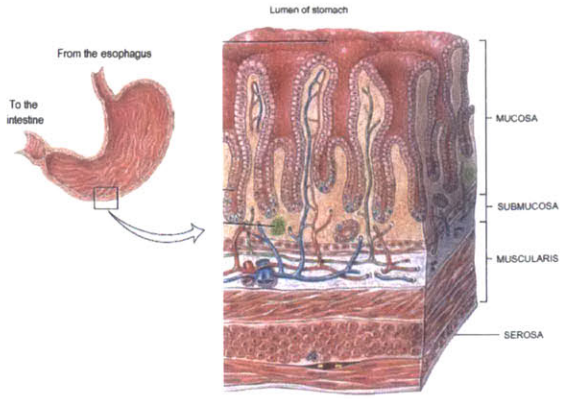

Figure 1-2: Schematic diagram of the stomach wall showing its structure and various layers (adapted from [37]).

The general structure of the stomach is the same as that of the rest of the GI tract. Rather than flat, the top mucous membrane layer is visibly wrinkled, forming deep pits in the surface to maximize surface area. Below the lamina propria, which is covered by the mucous membrane, is the smooth muscle layer. Below that is the submucosa, which is a layer of connective tissue that contains a large density of arteries and blood vessels leading up into the lamina propria. The outer three layers are all smooth muscle that serve to give support to the stomach, as well as to enhance its ability to mix and move the food inside.

1.1.4.4The Intestine

The majority of nutrient absorption takes place in the small intestine. The layers in the intestine are similar to those found in the rest of the GI tract, although the mucous membrane epithelium contains more secretory and absorptive cells, as shown in Figure 1-3.

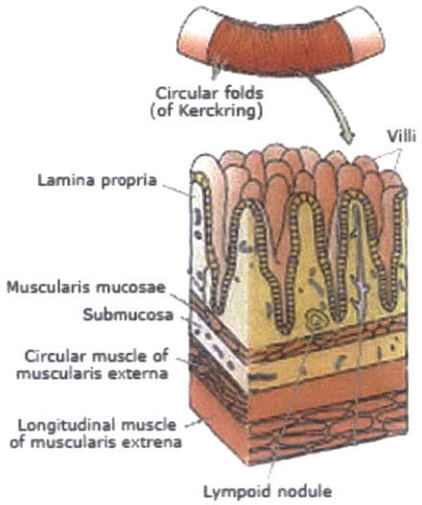

Figure 1-3: Schematic diagram of the intestinal mucosa and submucosa showing the blood flow network and the various types of secretory and absorptive cells lining the epithelium.

The intestine has several unique structural features, which aid in its function of nutrient absorption and digestion. The first feature is the presence of circular folds or rings in the mucosa and submucosa layers around the circumference of the tissue which help increase surface area. The second feature is the villi, which are the finger-like protruding structures in the mucosa shown in Figure 1-3. This again enhances absorptive surface area.

1.1.4.5The Colon

Again, the same general structure of the rest of the GI tract is observed in the colon. The most unique feature of the colon is in the muscularis layer in which the layer of longitudinal muscle fibers are thicker, denser, and localized into three bands which traverse the length of the colon.

1.2 Techniques for Skin Permeabilization

Disruption of the SC allows for a broader class of materials to be delivered into the skin. Additionally, physical insult can activate the immune system at that site, an important feature for vaccination [14], [17]. The methods for skin permeabilization discussed in this review include LFS, MNs, and iontophoresis and electroporation. With the exception of iontophoresis, these methods physically disrupt the SC. While there are several review articles discussing any one particular method, this review aims to discuss those methods regarded as most important, so that comparisons and differences may be highlighted.

1.2.1 Low-Frequency Sonophoresis

LFS employs the use of ultrasound (US) to permeabilize the SC. US is a longitudinal pressure wave with frequencies > 20kHz, the upper limit of hearing [16], [19], [20]. US is typically divided into three frequency ranges: low-frequency (<100kHz), therapeutic (0.7-3MHz), and high-frequency (>3MHz) [21], [23], [24].

The primary mechanism for LFS-enhanced tissue permeability is transient cavitation. When applied to a coupling fluid, LFS nucleates bubbles in solution. The bubbles become unstable as a result of large local pressure gradients, and implode. This results in a jet of liquid that can penetrate the SC [25], [26]. Cavitational effects are inversely correlated with US frequency, making LFS the most efficient for permeabilization [38].

LFS is typically applied to the skin together with a chemical penetration enhancer (CPE), which, together, have been shown to act synergistically [39]. Treatment results in two distinct regions in the skin: localized transport regions (LTRs) and non-localized transport regions (non-LTRs), both with different levels of permeability. LTRs are regions in the skin in which a high degree of fluidization of the SC has taken place due to high concentrations of CPE [40]. The transient cavitation events near the skin surface physically disrupt the skin, while actively pushing CPEs into the skin in those regions. Non-LTRs, while more permeable than native skin, experience fewer cavitation events, and therefore, their CPE content is lower, resulting in lower permeability compared to LTRs [40]-[42].

Current research focuses on two areas: i) enhancing the skin permeability achieved, and ii) miniaturization and optimization of the equipment. With regards to the first, the formation of LTRs is chaotic, and typical treatments only result in 5-10% LTR formation [43], [44]. Therefore, advances in LFS have focused on maximizing LTR formation. One such approach is the simultaneous application of low- and high-frequency US [45]. Introduction of high-frequency US was found to nucleate additional bubbles that collapse under the influence of LFS. This dual-frequency treatment resulted in 40-fold larger LTRs than those achieved with LFS alone (see Figure 1-4). It also resulted in an order-of-magnitude enhancement in the delivery of the permeants that were tested under certain conditions [45]. Achieving greater skin permeability has positive implications on the types and sizes of molecules that can be delivered.

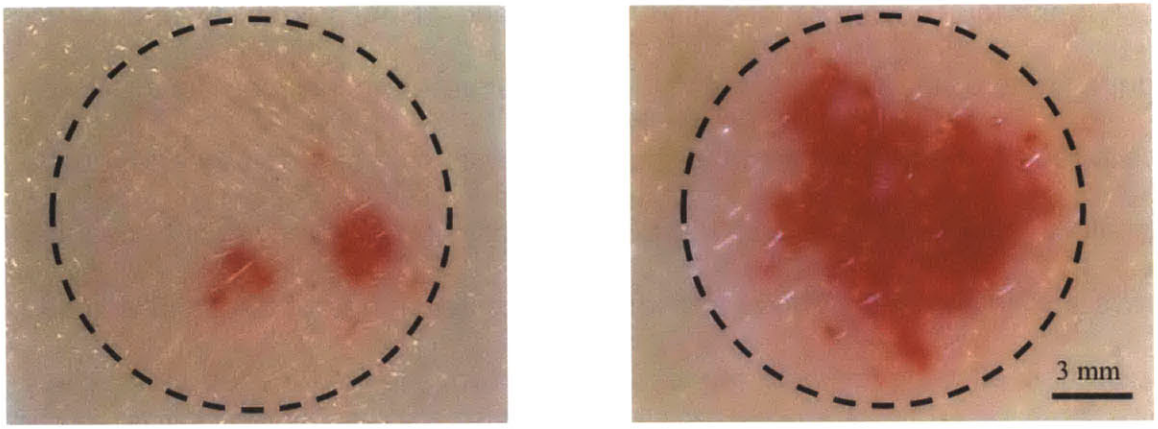

Single Frequency Control

Dual Frequency

Figure 1-4: LTR formation by allura red staining in representative images of skin treated with LFS alone (left) or with dual-frequency US (right). The dotted line indicates the area of the skin exposed to US.

Important advances are also being made in the portability and power requirements of the US equipment. New construction techniques have allowed for the replacement of traditional piezoelectric systems that are bulky and require excitation voltages in excess of 100 V [46]. Today, low-profile cymbal transducer arrays are being used. These transducers take advantage of the flexural mode of vibration, allowing for more modest excitation voltages to be used. In addition to significantly reduced power requirements, these devices have low profiles (< 10 mm), affording greater portability and potential incorporation into wearable patches [46], [47]. Together, enhancements in permeability and further miniaturization of the electrical components could make US a clinically meaningful TDD method.

1.2.2 Microneedles

MNs are thin projectiles with lengths on the order of microns that are used to pierce the SC. Because of their length, the needles do not penetrate deep enough to stimulate nerves, making them painless. There are four types of MNs: i) solid MNs used for pretreatment of the skin followed by the application of a topical cream [48], ii) hollow MNs for infusion of larger quantities of drug into the skin [49], iii) coated MNs where the drug to be delivered is coated onto the surface of solid MNs [50], and iv) dissolving MNs in which the needle itself is a dissolvable material encapsulating the drug [51].

Two main hurdles to clinical adoption of MNs are: i) the ability to scale-up production of these devices, and ii) the range of molecules and the amount that

can be delivered. The latter has received particular attention and strategies to improve delivery depend on the type of MN being investigated. A common factor, however, is the ability to have all MNs penetrate the skin, which maximizes the amount of drug delivered. For dissolving MNs, another important criterion is the dissolution time. Achieving total dissolution of the needles enables less drug to be loaded into the patches and reduces biohazard waste when still intact needles are disposed of. One recent method that address both issues is the manufacturing of biocompatible polymeric MNs on water-soluble, flexible backings [52]. These patches were observed to completely dissolve in 5 minutes in water. In skin, because the backing is water-soluble, there is no need to remove the device, ensuring total dissolution while reducing biohazard waste [52]. Additionally, the flexible backing, shown in Figure 1-5, allows for the patch to contour to the skin, and the localization of insertion forces over fewer MNs compared to rigid backings, thereby increasing the ability of each MN to pierce the SC.

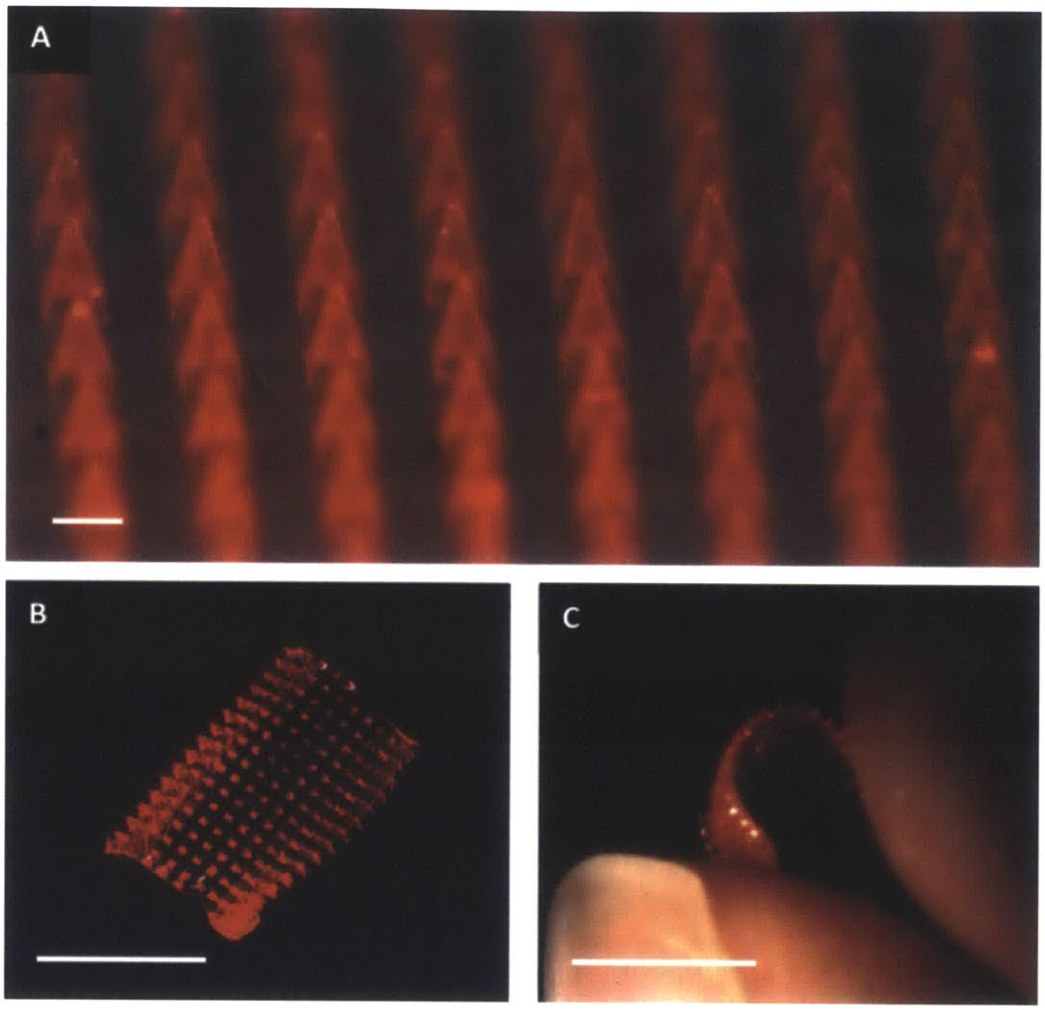

Figure 1-5: Images of a flexible MN patch. (A) The MN morphology is highly reproducible (scale bar: 200 μm). The flexibility of the patch is demonstrated in (B) and (C) (scale bar: 1 cm). Reprinted with permission from [52].

Another recent fabrication method for dissolving needles is the droplet-born air blowing method [53]. Patterned droplets of polymer can be stretched between two plates. Blowing air between the two plates then shapes and cures the MNs. The advantages of this method are the mild temperature and pressure requirements and the short manufacturing time. It was found that MNs fabricated using this method dissolved in 60 minutes *in vitro* [53].

When used as a pretreatment, solid MNs create long-lasting pores in the skin through which macromolecules can diffuse. This method involves application of a MN device to the skin, followed by removal of the device and placement of a medicated cream or patch over the site. The duration over which drug diffuses through the skin, however, depends on the lifetime of the pores. It has recently been shown that pores decrease significantly in size in only 15 minutes [54]. However, simple methods such as occlusion of the treatment site can be used to extend pore life to between 48-72 hours [55]. More advanced methods include the co-delivery of non-specific cyclooxygenase inhibitors. In guinea pigs, this has been shown to increase pore life to 7 days, and has recently been used in humans to deliver naltrexone continuously for 7 days [56], [57]. While promising, the safety of prolonged pore life must be investigated.

Despite these advances, challenges still exist. Dissolving MNs are limited by the practical size of the MN, which controls how much material can be delivered. There are also a limited number of therapeutics that can be coated on the surface of solid MNs [58], [59]. Nevertheless, this TDD method is making an impact in the area of vaccination.

1.2.3 Electrical Techniques

The two primary means of electrically-facilitated TDD are iontophoresis and electroporation. Iontophoresis involves the application of electrical current to drive charged permeants into the skin through electrostatic effects [60], [61]. Typical currents range from 0.1-1.0 mA/cm^2 [60], [62]. While uncharged species can also be delivered through electroosmosis, fluxes observed are low, limiting the utility of this method [61]. Electroporation also uses electricity, albeit to disrupt cellular membranes [63]. Electric pulses of hundreds of volts, lasting for 10 μs-10 ms, are typical and result in the formation of aqueous pores in the lipid bilayers of the SC, as well as in the reversible disruption of cell membranes [64], [65]. While the electric field does provide a driving force, delivery is primarily by passive diffusion through the long-lived pores due to the short duration of the pulses (typically milliseconds) [66]. Iontophoresis, by comparison, has a negligible effect on skin architecture at short treatment times. This is because of the low-voltage nature of the applied electric current. Only at long treatment times do morphological changes start to take place as a result of resistive heating [67]. These two methods are sometimes coupled to achieve greater drug delivery.

Recent studies have demonstrated the utility of these methods for the delivery of a broad range of therapeutics from small molecules, to larger proteins [60], [63], [68]. There has also been work on the miniaturization of the necessary equipment, making it battery-powered and portable [69]. However, there are

several concerns surrounding the clinical applicability or electrical techniques. For example, only charged molecules experience significant enhancement in delivery as a result of this method. With regards to electroporation, its application can rapidly change the electrical resistance of the SC [66]. When this occurs, the pulses are no longer confined to the SC, and may stimulate the lower lying nerves and motor neurons, eliciting pain and muscle contraction. For example, electrophoretic treatments that do not elicit pain can still invoke twitching of the muscles [63]. These concerns have tempered research into the use of electroporation for TDD. Instead, it has found use in other delivery applications. In the field of vaccination, its use in achieving intracellular uptake of DNA-based vaccines by skin resident dendritic cells is an active area of research [64], [70].

1.2.4 Combination Methods

Combinations of skin-permeabilizing methods have also been investigated. Most studies focus on the combination of a skin permeabilizing technology with an active driving force, i.e., MNs and electrical techniques, MNs and US, or US pretreatment followed by iontophoresis. Here, recent developments in the combination of MNs and US with other methods are discussed, followed by an examination of the future prospects of these methods.

1.2.4.1 Microneedles Combined with Electrical Driving Forces

The combination of MNs with either electroporation or iontophoresis is straightforward. The MNs create additional aqueous pores in the skin through which the applied current is conducted. Typically, skin is pretreated with MNs, and then the drug of interest is applied with simultaneous iontophoresis for 4-6 hrs. [71], [72]. Two advantages of this delivery method are the ability to control the flux of drugs through the modulation of the applied current, as well as a reduction in the lag time needed for drugs to penetrate the skin [73]. However, in the case of small molecules, this method only yields additive benefits at best relative to the use of either method alone. This is because little disruption of the SC is necessary to enhance the delivery of small molecules [71]. Finally, the sequential and time-consuming nature of the treatment detracts from its ease-of-use.

Other studies, however, have investigated the simultaneous use of both TDD methods for the delivery of larger molecules. One such study investigated the simultaneous application of MNs and electroporation as a pretreatment before passive delivery of dextran (4.3 kDa) [74]. This study showed a 140-fold enhancement in delivery over control samples, and an almost 7-fold enhancement over electroporation alone, the TDD method that showed the next-best delivery. Additionally, the treatment only utilized 10 pulses over a 10 second period, making treatment rapid [74].

The safety of these TDD methods remains to be investigated. The puncture of the skin with the MNs may allow the current to reach the lower layers

of the skin faster, which could stimulate nerves and motor neurons. However, if proven safe and painless *in vivo*, these combination methods could be useful, particularly those utilizing simultaneous treatments [74], [75].

1.2.4.2Ultrasound Combined with other Transdermal Drug Delivery Methods

Several reports exist on the combined use of MNs and US for drug delivery [76]-[78]. Here, the MNs are used to penetrate the SC and then US is used to further permeate, and actively push drug into the skin [78]. The most interesting is the simultaneous use of both methods. One group constructed a MN device with a 20 kHz piezoelectric crystal such that each MN also was able to conduct US into the skin [78]. The simultaneous treatment and integration into a single device simplifies this method's use. The authors found that simultaneous treatment yielded an enhancement in the delivery of calcein and bovine serum albumin over either method alone [78].

There have also been some studies on the use of US and iontophoresis [79], [80]. Hikima et al. investigated the combined use of 300 kHz US with iontophoresis for molecules with a range of molecular weights (122-1485 Da). Similar to the combined use of MNs and iontophoresis, they found that only larger molecules experienced synergistic enhancement [79]. They did, however, note that US treatment followed by iontophoresis yielded larger fluxes of material than the simultaneous use of both. This is most likely due to permeabilization of the SC by US before the iontophoretic driving force is applied [79]. This

suggests that lower US frequencies, when combined with iontophoresis, may yield greater enhancements.

1.2.4.3Future Prospects of Combination Methods

While the combination methods discussed above show some benefit in delivery over the individual methods, there are challenges associated with their implementation. First, the treatments must be simple to use. This requires that a single device can apply all of the methods used without continual intervention by the patient or physician. Second, safety studies are needed to assess the potential for pain, especially for those methods utilizing electrical modalities. Finally, the specific application should be carefully considered as not every TDD method, or their various combinations, will yield appropriate delivery. Indeed, while each TDD method typically yields an enhancement in delivery relative to passive diffusion for a broad class of drugs, this is not necessarily the case for the enhancement in delivery when using combination methods, relative to each method alone.

1.3 Thesis Objectives

Non-invasive transdermal drug delivery presents an attractive method for drug administration [2], [81]. Recently, there has been renewed research interest in sonophoresis. Two major challenges limiting greater clinical use of sonophoresis are the portability of the equipment required, and the extended treatment times required [43], [82]. Studies addressing the former hurdle have

focused on the use of low-profile cymbal transducer arrays that can be integrated into patches [46], [83]. In addition to portability, these devices minimize the excitation voltages required, thereby reducing power consumption [47].

With regards to the treatment times necessary, a new approach has recently been investigated to increase skin permeabilization efficiency, thereby decreasing the required treatment time [45]. This method takes advantage of dual-frequency US. By simultaneously using both low-frequency (< 60 kHZ) and high-frequency (> 1 MHz) US, I recently showed significant enhancement in the formation of LTRs compared to the use of low-frequency US alone. I also showed that this enhanced LTR formation translated into enhanced delivery of model permeants over a range of molecular weights [45].

In addition to the transdermal route, the delivery of macromolecules across the GI tract is one of the most highly investigated areas of research in drug delivery. Delivery via the GI tract, however, is still limited to small molecules [84]. Even delivery of small molecules can be challenging, with most drugs often requiring specialized formulations to stabilize the active pharmaceutical ingredient and provide optimal absorption in the GI tract. Therefore, a platform that could allow for the delivery of a broad range of therapeutics without the need for time-consuming and costly reformulation could present a paradigm shift in delivery science and have wide clinical impact. Physical methods of drug delivery, such as US, may be capable of delivering macromolecules while circumventing the need for extensive formulation development. Despite being

investigated for other uses, to the best of my knowledge, ultrasound has never been studied for drug delivery in the GI tract.

With the above in mind, my thesis research objectives include:

1. Increasing skin permeability through the development of new strategies to induce greater transient cavitation.
2. Investigating the use of active delivery technologies in the GI tract:
    a. Investigating oral delivery facilitated by the microneedle pill.
    b. Investigating colonic delivery facilitated by ultrasound.

1.4 Thesis Overview

The remainder of this thesis is devoted to investigating the use of novel strategies to facilitate transdermal drug delivery using US, as well as investigating the use of physical enhancers for drug delivery in the GI tract for the first time.

Chapter 2 investigates the simultaneous application of two distinct US frequencies, in the range of 20 kHz to 3 MHz to enhance the efficacy of US exposure. Aluminum foil pitting experiments are utilized to study the effect of two frequencies on cavitational activity. Additionally, *in vitro* tests with porcine skin indicated that the permeability and resulting formation of LTRs are greatly enhanced when two US frequencies (low and high) are used simultaneously. These results were corroborated with glucose (180 Da) and inulin (5000 Da)

transdermal flux experiments, which showed greater permeant delivery both into and through the dual-frequency US pre-treated skin.

Chapter 3 takes the investigation of the use of dual-frequency US further. Building on the studies presented in Chapter 2, the simultaneous use of low- and high-frequency ultrasound is explored in a physiologically relevant experimental setup to enable the translation of this treatment to testing *in vivo*.

This thesis then begins exploring the use of physical enhancers for drug delivery in the GI tract in Chapter 4. Both patients and physicians prefer the oral route of drug delivery. The GI tract, however, limits the bioavailability of certain therapeutics because of its protease and bacteria-rich environment as well as general pH variability from pH 1-7. These extreme environments make oral delivery particularly challenging for the biologic class of therapeutics. In this chapter, proof-of-concept experiments in swine are presented on the use of microneedle-based delivery. Moreover, it is demonstrated that microneedle-containing devices can be passed and excreted from the GI tract safely. These findings strongly support the success of implementation of microneedle technology for use in the GI tract.

In addition to microneedles, the use of ultrasound in the GI tract is explored in Chapter 5. This study represents the first report of US as a modality for enhanced drug delivery via the entire GI tract, with an emphasis on rectal delivery. US increases absorption of model therapeutics in tissue 2-10 fold *ex vivo* depending on location. Furthermore, in small and large animal models *in vivo*, ultrasound leads to an order-of-magnitude enhancement in GI mucosal drug

delivery with minimal histological disruption, including for a biologically active macromolecule (insulin). Finally, in a rodent model of acute colitis, the addition of ultrasound to standard of care treatment was found to result in superior clinical and histological scores of disease activity. The novel use of ultrasound to enhance GI drug delivery could augment the efficacy of GI therapies and broaden the scope of agents delivered locally and systemically through the GI tract.

Finally, this thesis concludes in Chapter 6 with a summary of the findings presented in Chapters 2-5, and proposed potential future directions of research.

1.5 References

[1] M. N. M. Walter, K. T. Wright, H. R. Fuller, S. MacNeil, and W. E. B. Johnson, "Mesenchymal stem cell-conditioned medium accelerates skin wound healing: An in vitro study of fibroblast and keratinocyte scratch assays," *Experimental Cell Research*, vol. 316, no. 7, pp. 1271–1281, Apr. 2010.

[2] M. R. Prausnitz and R. Langer, "Transdermal drug delivery," *Nat Biotechnol*, vol. 26, no. 11, pp. 1261–1268, Nov. 2008.

[3] S. N. Andrews, E. Jeong, and M. R. Prausnitz, "Transdermal Delivery of Molecules is Limited by Full Epidermis, Not Just Stratum Corneum," *Pharm Res*, vol. 30, no. 4, pp. 1099–1109, Nov. 2012.

[4] E. L. Giudice and J. D. Campbell, "Needle-free vaccine delivery," *Advanced drug delivery reviews*, 2006.

[5] C. J. Sokolowski, J. A. Giovannitti Jr., and S. G. Boynes, "Needle Phobia: Etiology, Adverse Consequences, and Patient Management," *Dental Clinics of North America*, vol. 54, no. 4, pp. 731–744, Oct. 2010.

[6] Y. Nir, A. Paz, E. Sabo, and I. Potasman, "Fear of injections in young adults: prevalence and associations," *American Journal of Tropical Medicine and Hygiene*, 2003.

[7] A. Dahlan, H. O. Alpar, P. Stickings, D. Sesardic, and S. Murdan, "Transcutaneous immunisation assisted by low-frequency ultrasound," *International Journal of Pharmaceutics*, vol. 368, no. 1, pp. 123–128, Feb. 2009.

[8] K. Kretsos and G. B. Kasting, "A geometrical model of dermal capillary clearance," *Mathematical biosciences*, 2007.

[9] A. Tezel, S. Paliwal, Z. Shen, and S. Mitragotri, "Low-frequency ultrasound as a transcutaneous immunization adjuvant," *Vaccine*, vol. 23, no. 29, pp. 3800–3807, May 2005.

[10] M. A. Miller and E. Pisani, "The cost of unsafe injections," *Bulletin from the World Health Organization*, 1999.

[11] T. L. Moore, "Seventeen-point dermal ultrasound scoring system--a reliable measure of skin thickness in patients with systemic sclerosis," *Rheumatology*, vol. 42, no. 12, pp. 1559–1563, Jun. 2003.

[12] J. A. McGrath, R. A. J. Eady, and F. M. Pope, "Anatomy and Organization of Human Skin," in *Rook's Textbook of Dermatology*, Blackwell Publishing, Inc., 2008, pp. 45–128.

[13] B. L. Kirkpatrick, V. E. Ricketts, D. S. Reeves, and A. P. MacGowan, "Needlestick injuries among medical students," *Journal of Hospital Infection*, vol. 23, no. 4, pp. 315–317, Apr. 1993.

[14] Z. Ding, E. van Riet, W. Jiskoot, and J. A. Bouwstra, "Advances in transcutaneous vaccine delivery: do all ways lead to Rome?," *Journal of Controlled Release*, vol. 148, no. 3, pp. 266–282, 2010.

[15] J. E. Rim, P. M. Pinsky, and W. W. van Osdol, "Using the method of homogenization to calculate the effective diffusivity of the stratum corneum with permeable corneocytes," *Journal of Biomechanics*, vol. 41, no. 4, pp. 788–796, Jan. 2008.

[16] B. E. Polat, D. Hart, R. Langer, and D. Blankschtein, "Ultrasound-mediated transdermal drug delivery: Mechanisms, scope, and emerging trends," *Journal of Controlled Release*, vol. 152, no. 3, pp. 330–348, Jun. 2011.

[17] M. A. Deli, "Potential use of tight junction modulators to reversibly open membranous barriers and improve drug delivery," *BBA - Biomembranes*, vol. 1788, no. 4, pp. 892–910, Apr. 2009.

[18] A. Brotchie, F. Grieser, and M. Ashokkumar, "Characterization of Acoustic Cavitation Bubbles in Different Sound Fields," *J. Phys. Chem. B*, vol. 114, no. 34, pp. 11010–11016, Sep. 2010.

[19] G. Cevc, "Lipid vesicles and other colloids as drug carriers on the skin," *Advanced drug delivery reviews*, 2004.

[20] K. C. Madison, "Barrier Function of the Skin: 'La Raison d'Être' of the

Epidermis," *J Investig Dermatol*, vol. 121, no. 2, pp. 231–241, Jul. 2003.

[21] B. E. Polat, D. Blankschtein, and R. Langer, "Low-frequency sonophoresis: application to the transdermal delivery of macromolecules and hydrophilic drugs," *Expert Opin. Drug Deliv.*, vol. 7, no. 12, pp. 1415–1432, Dec. 2010.

[22] H.-L. Liu and C.-M. Hsieh, "Single-transducer dual-frequency ultrasound generation to enhance acoustic cavitation," *Ultrasonics - Sonochemistry*, vol. 16, no. 3, pp. 431–438, Mar. 2009.

[23] T. Gambichler, S. Boms, M. Stucker, A. Kreuter, G. Moussa, M. Sand, P. Altmeyer, and K. Hoffmann, "Epidermal thickness assessed by optical coherence tomography and routine histology: preliminary results of method comparison.," *J Eur Acad Dermatol Venerol*, vol. 20, no. 7, pp. 791–795, Jun. 2006.

[24] K. W. Ng, M. Pearton, S. Coulman, A. Anstey, C. Gateley, A. Morrissey, C. Allender, and J. Birchall, "Development of an ex vivo human skin model for intradermal vaccination: Tissue viability and Langerhans cell behaviour," *Vaccine*, vol. 27, no. 43, pp. 5948–5955, Oct. 2009.

[25] M. Ashokkumar, J. Lee, Y. Iida, K. Yasui, T. Kozuka, T. Tuziuti, and A. Towata, "Spatial Distribution of Acoustic Cavitation Bubbles at Different Ultrasound Frequencies," *ChemPhysChem*, vol. 11, no. 8, pp. 1680–1684, Mar. 2010.

[26] C. Scarponi, F. Nasorri, F. Pavani, S. Madonna, R. Sestito, M. Simonacci, O. De Pità, A. Cavani, and C. Albanesi, "Low-Frequency Low-Intensity

Ultrasounds Do Not Influence the Survival and Immune Functions of Cultured Keratinocytes and Dendritic Cells," *Journal of Biomedicine and Biotechnology*, vol. 2009, no. 1, pp. 1–13, 2009.

[27] S. Mignani, S. El Kazzouli, M. Bousmina, and J.-P. Majoral, "Expand classical drug administration ways by emerging routes using dendrimer drug delivery systems: A concise overview," *Advanced drug delivery reviews*, vol. 65, no. 10, pp. 1316–1330, Oct. 2013.

[28] M. M. Borner, P. Schoffski, R. de Wit, F. Caponigro, G. Comella, A. Sulkes, G. Greim, G. J. Peters, K. van der Born, J. Wanders, R. F. de Boer, C. Martin, and P. Fumoleau, "Patient preference and pharmacokinetics of oral modulated UFT versus intravenous fluorouracil and leucovorin: a randomised crossover trial in advanced colorectal cancer.," *Eur J Cancer*, vol. 38, no. 3, pp. 349–358, Feb. 2002.

[29] Y. Aoki, M. Morishita, K. Asai, B. Akikusa, S. Hosoda, and K. Takayama, "Region-Dependent Role of the Mucous/Glycocalyx Layers in Insulin Permeation Across Rat Small Intestinal Membrane," *Pharm Res*, vol. 22, no. 11, pp. 1854–1862, Jul. 2005.

[30] K. Chaturvedi, K. Ganguly, M. N. Nadagouda, and T. M. Aminabhavi, "Polymeric hydrogels for oral insulin delivery.," *Journal of controlled release : official journal of the Controlled Release Society*, vol. 165, no. 2, pp. 129–138, Jan. 2013.

[31] M. A. Radwant and H. Y. Aboul-Enein, "The effect of oral absorption enhancers on the in vivo performance of insulin-loaded

poly(ethylcyanoacrylate) nanospheres in diabetic rats.," *Journal of Microencapsulation*, vol. 19, no. 2, pp. 225–235, Mar. 2002.

[32] "Folate-decorated PLGA nanoparticles as a rationally designed vehicle for the oral delivery of insulin," Sep. 2012.

[33] A. Cerutti, "Location, location, location: B-cell differentiation in the gut lamina propria," *Mucosal Immunol*, vol. 1, no. 1, pp. 8–10, Jan. 2008.

[34] Q. Zhu, J. Talton, G. Zhang, T. Cunningham, Z. Wang, R. C. Waters, J. Kirk, B. A. R. Eppler, D. M. Klinman, Y. Sui, S. Gagnon, I. M. Belyakov, R. J. Mumper, and J. A. Berzofsky, "Large intestine-targeted, nanoparticle-releasing oral vaccine to control genitorectal viral infection," *Nature Publishing Group*, pp. 1–7, Jul. 2012.

[35] C. V. Pecot, G. A. Calin, R. L. Coleman, G. Lopez-Berestein, and A. K. Sood, "RNA interference in the clinic: challenges and future directions," *Nat Rev Cancer*, vol. 11, no. 1, pp. 59–67, Jan. 2011.

[36] M. P. Morrow and D. B. Weiner, "DNA Drugs Come of Age," *Scientific American*, vol. 303, no. 1, pp. 48–53, Jul. 2010.

[37] G. J. Tortora, N. P. Anagnostakos, 1924, *Principles of anatomy and physiology*. Burgess Publishing Co., 1976.

[38] B. E. Polat, D. Blankschtein, and R. Langer, "Low-frequency sonophoresis: application to the transdermal delivery of macromolecules and hydrophilic drugs," *Expert Opin. Drug Deliv.*, vol. 7, no. 12, pp. 1415–1432, Dec. 2010.

[39] A. Tezel, A. Sens, J. Tuchscherer, and S. Mitragotri, "Synergistic effect of

low-frequency ultrasound and surfactants on skin permeability," *Journal of Pharmaceutical Sciences*, vol. 91, no. 1, pp. 91–100, Jan. 2002.

[40] J. Kushner, D. Kim, P. T. C. So, D. Blankschtein, and R. S. Langer, "Dual-Channel Two-Photon Microscopy Study of Transdermal Transport in Skin Treated with Low-Frequency Ultrasound and a Chemical Enhancer," *J Investig Dermatol*, vol. 127, pp. 2832–2846, Jun. 2007.

[41] J. Kushner, D. Blankschtein, and R. Langer, "Evaluation of hydrophilic permeant transport parameters in the localized and non-localized transport regions of skin treated simultaneously with low-frequency ultrasound and sodium lauryl sulfate," *Journal of Pharmaceutical Sciences*, vol. 97, no. 2, pp. 906–918, 2007.

[42] B. E. Polat, P. L. Figueroa, D. Blankschtein, and R. Langer, "Transport pathways and enhancement mechanisms within localized and non-localized transport regions in skin treated with low-frequency sonophoresis and sodium lauryl sulfate," *Journal of Pharmaceutical Sciences*, vol. 100, no. 2, pp. 512–529, Aug. 2010.

[43] M. Ogura, S. Paliwal, and S. Mitragotri, "Low-frequency sonophoresis: Current status and future prospects," *Advanced drug delivery reviews*, vol. 60, no. 10, pp. 1218–1223, Jun. 2008.

[44] R. F. V. Lopez, J. E. Seto, D. Blankschtein, and R. Langer, "Enhancing the transdermal delivery of rigid nanoparticles using the simultaneous application of ultrasound and sodium lauryl sulfate," *Biomaterials*, vol. 32, no. 3, pp. 933–941, Jan. 2011.

[45] C. M. Schoellhammer, B. E. Polat, J. Mendenhall, R. Maa, B. Jones, D. P. Hart, R. Langer, and D. Blankschtein, "Rapid skin permeabilization by the simultaneous application of dual-frequency, high-intensity ultrasound," *Journal of Controlled Release*, vol. 163, no. 2, pp. 154–160, 2012.

[46] Y. Sunny, C. R. Bawiec, A. T. Nguyen, and J. A. Samuels, "Optimization of un-tethered, low voltage, 20-100 kHz flexural transducers for biomedical ultrasonics applications," *Ultrasonics*, 2012.

[47] C. R. Bawiec, Y. Sunny, A. T. Nguyen, and J. A. Samuels, "Finite element static displacement optimization of 20–100kHz flexural transducers for fully portable ultrasound applicator," *Ultrasonics*, 2012.

[48] J.-H. Park, S.-O. Choi, S. Seo, Y. B. Choy, and M. R. Prausnitz, "A microneedle roller for transdermal drug delivery," *European journal of pharmaceutics and biopharmaceutics*, vol. 76, no. 2, pp. 282–289, Oct. 2010.

[49] J. Gupta, E. I. Felner, and M. R. Prausnitz, "Minimally Invasive Insulin Delivery in Subjects with Type 1 Diabetes Using Hollow Microneedles," *Diabetes Technology & Therapeutics*, vol. 11, no. 6, pp. 329–337, Jun. 2009.

[50] Q. Zhu, V. G. Zarnitsyn, L. Ye, Z. Wen, Y. Gao, L. Pan, I. Skountzou, H. S. Gill, M. R. Prausnitz, C. Yang, and R. W. Compans, "Immunization by vaccine-coated microneedle arrays protects against lethal influenza virus challenge," *Proceedings of the National Academy of Sciences*, vol. 106, no. 19, pp. 7968–7973, May 2009.

[51] K. Lee, C. Y. Lee, and H. Jung, "Dissolving microneedles for transdermal drug administration prepared by stepwise controlled drawing of maltose," *Biomaterials*, vol. 32, no. 11, pp. 3134–3140, Apr. 2011.

[52] K. A. Moga, L. R. Bickford, R. D. Geil, S. S. Dunn, A. A. Pandya, Y. Wang, J. H. Fain, C. F. Archuleta, A. T. O'Neill, and J. M. DeSimone, "Rapidly–Dissolvable Microneedle Patches Via a Highly Scalable and Reproducible Soft Lithography Approach," *Adv. Mater.*, vol. 25, no. 36, pp. 5060–5066, 2013.

[53] J. D. Kim, M. Kim, H. Yang, K. Lee, and H. Jung, "Droplet-born air blowing: Novel dissolving microneedle fabrication," *Journal of Controlled Release*, vol. 170, no. 3, pp. 430–436, Sep. 2013.

[54] S. Bal, A. C. Kruithof, H. Liebl, M. Tomerius, J. Bouwstra, J. Lademann, and M. Meinke, "In vivo visualization of microneedle conduits in human skin using laser scanning microscopy," *Laser Phys. Lett.*, vol. 7, no. 3, pp. 242–246, Mar. 2010.

[55] H. Kalluri and A. K. Banga, "Formation and Closure of Microchannels in Skin Following Microporation," *Pharm Res*, vol. 28, no. 1, pp. 82–94, Mar. 2010.

[56] S. L. Banks, K. S. Paudel, N. K. Brogden, C. D. Loftin, and A. L. Stinchcomb, "Diclofenac Enables Prolonged Delivery of Naltrexone Through Microneedle-Treated Skin," *Pharm Res*, vol. 28, no. 5, pp. 1211–1219, Feb. 2011.

[57] N. K. Brogden, S. L. Banks, L. J. Crofford, and A. L. Stinchcomb,

"Diclofenac Enables Unprecedented Week-Long Microneedle-Enhanced Delivery of a Skin Impermeable Medication in Humans," *Pharm Res*, vol. 30, no. 8, pp. 1947–1955, Jun. 2013.

[58] H. S. Gill and M. R. Prausnitz, "Coating formulations for microneedles," *Pharm Res*, 2007.

[59] G. Cevc and U. Vierl, "Nanotechnology and the transdermal route," *Journal of Controlled Release*, vol. 141, no. 3, pp. 277–299, Feb. 2010.

[60] K. Kigasawa, K. Kajimoto, T. Nakamura, S. Hama, K. Kanamura, H. Harashima, and K. Kogure, "Noninvasive and efficient transdermal delivery of CpG-oligodeoxynucleotide for cancer immunotherapy," *Journal of Controlled Release*, vol. 150, no. 3, pp. 256–265, 2011.

[61] N. R. Herr, B. M. Kile, R. M. Carelli, and R. M. Wightman, "Electroosmotic Flow and Its Contribution to Iontophoretic Delivery," *Anal. Chem.*, vol. 80, no. 22, pp. 8635–8641, Nov. 2008.

[62] S. Dubey and Y. N. Kalia, "Non-invasive iontophoretic delivery of enzymatically active ribonuclease A (13.6kDa) across intact porcine and human skins," *Journal of Controlled Release*, vol. 145, no. 3, pp. 203–209, Aug. 2010.

[63] S. M. Sammeta, S. R. K. Vaka, and S. N. Murthy, "Transcutaneous electroporation mediated delivery of doxepin-HPCD complex: A sustained release approach for treatment of postherpetic neuralgia," *Journal of Controlled Release*, vol. 142, no. 3, pp. 361–367, Mar. 2010.

[64] F. Eriksson, T. Tötterman, A.-K. Maltais, P. Pisa, and J. Yachnin, "DNA

vaccine coding for the rhesus prostate specific antigen delivered by intradermal electroporation in patients with relapsed prostate cancer," *Vaccine*, vol. 31, no. 37, pp. 3843–3848, Aug. 2013.

[65] A.-R. Denet, R. Vanbever, and V. Préat, "Skin electroporation for transdermal and topical delivery," *Advanced drug delivery reviews*, vol. 56, no. 5, pp. 659–674, 2004.

[66] B. Zorec, S. Becker, M. Reberšek, D. Miklavčič, and N. Pavšelj, "Skin electroporation for transdermal drug delivery: The influence of the order of different square wave electric pulses," *International Journal of Pharmaceutics*, Sep. 2013.

[67] U. F. Pliquett, C. A. Gusbeth, and J. C. Weaver, "Non-linearity of molecular transport through human skin due to electric stimulus," *Journal of Controlled Release*, vol. 68, no. 3, pp. 373–386, 2000.

[68] K. Kigasawa, K. Kajimoto, S. Hama, A. Saito, K. Kanamura, and K. Kogure, "Noninvasive delivery of siRNA into the epidermis by iontophoresis using an atopic dermatitis-like model rat," *International Journal of Pharmaceutics*, vol. 383, no. 1, pp. 157–160, Jan. 2010.

[69] C. T.-S. Ching, T.-P. Sun, W.-T. Huang, S.-H. Huang, C.-S. Hsiao, and K.-M. Chang, "A circuit design of a low-cost, portable and programmable electroporation device for biomedical applications," *Sensors & Actuators: B. Chemical*, vol. 166, pp. 292–300, May 2012.

[70] B. D. Livingston, S. F. Little, A. Luxembourg, B. Ellefsen, and D. Hannaman, "Comparative performance of a licensed anthrax vaccine

versus electroporation based delivery of a PA encoding DNA vaccine in rhesus macaques," *Vaccine*, vol. 28, no. 4, pp. 1056–1061, Jan. 2010.

[71] N. D. Singh and A. K. Banga, "Controlled delivery of ropinirole hydrochloride through skin using modulated iontophoresis and microneedles," *Journal of Drug Targeting*, vol. 21, no. 4, pp. 354–366, May 2013.

[72] K. R. Pawar, F. Smith, C. S. Kolli, and R. J. Babu, "Effect of Lipophilicity on Microneedle-Mediated Iontophoretic Transdermal Delivery Across Human Skin In Vitro," *Journal of Pharmaceutical Sciences*, vol. 102, no. 10, pp. 3784–3791, Aug. 2013.

[73] V. Kumar and A. K. Banga, "Modulated iontophoretic delivery of small and large molecules through microchannels," *International Journal of Pharmaceutics*, vol. 434, no. 1, pp. 106–114, Sep. 2012.

[74] K. Yan, H. Todo, and K. Sugibayashi, "Transdermal drug delivery by in-skin electroporation using a microneedle array," *International Journal of Pharmaceutics*, vol. 397, no. 1, pp. 77–83, Sep. 2010.

[75] M. J. Garland, E. C. Salvador, K. Migalska, D. A. Woolfson, and R. F. Donnelly, "Dissolving polymeric microneedle arrays for electrically assisted transdermal drug delivery," *Journal of Controlled Release*, vol. 159, no. 1, pp. 52–59, 2012.

[76] T. Han and D. B. Das, "Permeability Enhancement for Transdermal Delivery of Large Molecule Using Low-Frequency Sonophoresis Combined with Microneedles ," *Journal of Pharmaceutical Sciences*, vol.

102, no. 10, 2013.

[77] J. Yoon, D. Park, T. Son, J. Seo, J. S. Nelson, and B. Jung, "A physical method to enhance transdermal delivery of a tissue optical clearing agent: Combination of microneedling and sonophoresis," *Lasers Surg. Med.*, vol. 42, no. 5, pp. 412–417, Jun. 2010.

[78] B. Chen, J. Wei, and C. Iliescu, "Sonophoretic enhanced microneedles array (SEMA)—Improving the efficiency of transdermal drug delivery," *Sensors & Actuators: B. Chemical*, vol. 145, no. 1, pp. 54–60, Mar. 2010.

[79] T. Hikima, S. Ohsumi, K. Shirouzu, and K. Tojo, "Mechanisms of synergistic skin penetration by sonophoresis and iontophoresis," *Biological and Pharmaceutical Bulletin*, vol. 32, pp. 905–909, 2009.

[80] S. Katikaneni, G. Li, A. Badkar, and A. K. Banga, "Transdermal delivery of a ~13 kDa protein—an in vivocomparison of physical enhancement methods," *Journal of Drug Targeting*, vol. 18, no. 2, pp. 141–147, Feb. 2010.

[81] C. M. Schoellhammer, D. Blankschtein, and R. Langer, "Skin permeabilization for transdermal drug delivery: recent advances and future prospects.," *Expert Opin. Drug Deliv.*, vol. 11, no. 3, pp. 393–407, Jan. 2014.

[82] N. B. Smith, "Perspectives on transdermal ultrasound mediated drug delivery," *International Journal of Nanomedicine*, vol. 2, no. 4, pp. 585–594, Apr. 2009.

[83] E.-J. Park, J. Werner, J. Beebe, S. Chan, and N. B. Smith, "Noninvasive

Ultrasonic Glucose Sensing with Large Pigs (~200 Pounds) Using a Lightweight Cymbal Transducer Array and Biosensors," *Journal of Diabetes Science and Technology*, vol. 3, no. 3, pp. 517–523, Apr. 2009.

[84] L. M. Ensign, R. Cone, and J. Hanes, "Oral drug delivery with polymeric nanoparticles: The gastrointestinal mucus barriers," *Advanced drug delivery reviews*, vol. 64, no. 6, pp. 557–570, 2012.

Chapter 2

Rapid Skin Permeabilization by the Simultaneous Application of Dual-Frequency, High-Intensity Ultrasound

2.1. Introduction

Ultrasound-assisted transdermal drug delivery (TDD) has been studied extensively for decades. Work in this area originally focused mainly on using therapeutic and high-frequency ultrasound (US) (>0.7 MHz) to enhance drug delivery through the skin [1]. It was only in the late-1980s and early 1990s that the use of low-frequency US (<100kHz) began to be more widely investigated for drug-delivery applications [2]. This switch occurred primarily because it was recognized that US-enhanced skin permeability results from transient cavitation near the skin surface, which is inversely correlated with the US frequency [3]. Since these discoveries were made, extensive research has been conducted into the mechanisms and applications of low-frequency sonophoresis (LFS) [3].

In addition to low-frequency US treatment, chemical penetration enhancers (CPEs), most often surfactants, have also been studied extensively for their permeability-enhancing abilities. Interestingly, CPEs have been found to act synergistically with low-frequency US in enhancing skin permeability [4]. Upon the application of US and a CPE, two distinct regions of skin are observed, known as localized transport regions (LTRs) and non-localized transport regions (non-LTRs). LTRs are US and CPE-induced regions in the skin in which a high

degree of perturbation of the stratum corneum (SC) has taken place [5]. As a result, transport through the LTRs is greatly enhanced relative to that through native skin. It has been found that LTRs are up to 80-fold more permeable than non-LTRs and that non-LTRs also exhibit enhanced transport relative to native skin when a CPE is present during LFS treatment [1], [6]. Within the LTRs, the SC no longer presents a significant barrier to permeant transport, as the dermis becomes the primary diffusional barrier [6]. In non-LTRs, however, the SC still possesses considerable barrier function [2], [6]. Enhancement within the non-LTRs has been shown to be due to increased penetration of CPEs via acoustic streaming, resulting in a slight disruption of the SC [3], [7]. In LTRs, however, increased enhancement results from the synergistic effects of the simultaneous application of US and CPEs. By causing transient cavitation events near the skin surface, US is able to physically disrupt the skin. These same cavitation events also actively deliver the CPEs into the skin, leading to higher concentrations of CPEs in the LTRs relative to the non-LTRs, which contributes to causing greater skin permeability [3], [5], [6], [8].

LTR formation as a result of US and CPE treatment is an unpredictable and stochastic process. Additionally, even if treatment times in excess of 10 minutes are utilized, typically only 5-10% of the treated skin surface area may result in LTRs [4], [9]. If a larger portion of the treated skin area could reliably and reproducibly form LTRs, greater amounts of drugs could be delivered to, and through, the skin. Furthermore, this would allow for smaller skin areas to be

treated to achieve the same amount of drug delivery, requiring less US power and potentially shorter treatment times.

Building upon the proven methods of US-mediated skin permeability enhancement, a potential method for increasing LTR formation and decreasing treatment times would involve generating more bubbles in the acoustic field adjacent to the skin. These additional bubbles could be nucleated using a second US horn. Specifically, higher frequencies of US (>0.7 MHz) are capable of nucleating a relatively large number of small cavitation bubbles, relative to low-frequency US. Along these lines, recent reports have shown that by combining US horns operating at frequencies in the range of 20 kHz to 3 MHz, acoustic cavitation activity is enhanced compared to that of single US frequencies operating alone [5], [10], [11]. Here, we hypothesize that the addition of a second, high-frequency, US horn oriented parallel to the surface of the skin will nucleate a greater number of bubbles in the vicinity of the skin (see Figure 2-1a). These additional bubbles can then cavitate and collapse in response to acoustic waves generated from a low-frequency US horn oriented perpendicular to the skin surface (see Figures 2-1b and 2-1c), as is done with typical LFS treatments.

2.2. Experimental Section

2.2.1. Materials

Phosphate buffered saline (PBS) and sodium lauryl sulfate (SLS) were obtained from Sigma-Aldrich Company (St. Louis, MO). Allura red was obtained from TCI America (Portland, OR). All chemicals were used as received. ^{3}H-

labeled glucose (20 Ci/mmol activity) and ^{14}C-labeled 5000 Da molecular weight inulin (2 mCi/g activity) were obtained from American Radiolabeled Chemicals, Inc. (St. Louis, MO). The tissue solubilizer Soluene-350 and scintillation cocktail Hionic-Fluor were obtained from Perkin-Elmer (Waltham, MA).

2.2.2. Aluminum Foil Pitting Experiments

In order to gauge the number and radius of acoustic cavitation microjets generated by the applied single- or dual-frequency US treatments, a series of aluminum foil (Reynolds, Richmond, VA) pitting experiments were carried out following previously published protocols [12]. Experiments were conducted in a custom-fabricated 2.2 L tank (see Figure 2-1). The tank was constructed in order to allow for two frequencies of US to be applied simultaneously to aluminum foil and skin samples. Aluminum foil samples were carefully cut into 25-mm by 25-mm squares to avoid wrinkling, and mounted on the receiver compartment of 12 mL Franz diffusion cells (PermeGear, Hellertown, PA). Vacuum grease (Dow Corning, Midland, MI) was utilized to adhere the aluminum foil samples to the receiver compartment of the diffusion cells. The receiver compartments of the diffusion cells were then filled with 12 mL of PBS and placed in the diffusion cell holder in the tank.

Three low-frequency ultrasounds (20, 40, and 60 kHz), in combination with two high-frequency ultrasounds (1 and 3 MHz), were considered in a pairwise fashion (e.g., 20 kHz + 1 MHz, 20 kHz + 3 MHz, etc.). Low-frequency US was generated utilizing three separate US systems (Sonics and Materials, Inc.,

Newtown, CT), each operating at a different frequency: 20 kHz (VCX 500), 40 kHz (VCX 130), and 60 kHz (custom order). 1 and 3 MHz US was generated utilizing a tunable US probe (Enraf Nonius, Rotterdam, The Netherlands). The low-frequency US horn was positioned perpendicular to the aluminum foil surface, offset by 1 cm, with the high-frequency US probe positioned parallel to the aluminum foil surface, approximately 1 cm from the leading edge of the diffusion cell (see Figure 2-1 for a schematic of the experimental setup). The intensities of the low- and high-frequency ultrasounds utilized were 8.0 W/cm^2 and 1.5 W/cm^2, respectively, and were calibrated by calorimetry. The respective intensities were held constant for all the US horns used, and were chosen for consistency with previously published reports of single-frequency US-enhanced transdermal drug delivery [2], [3]. The coupling solution between the US horns and the aluminum foil sample contained either PBS or 1 wt% SLS in PBS. Single-frequency experiments were conducted with the low-frequency US horn operating at the conditions described above and the high-frequency US set to zero intensity (sham ultrasound). Dual-frequency experiments were conducted by first turning on the high-frequency US horn, and then running the low-frequency US horn for 5 s in continuous or pulsed (1s ON: 1s OFF) mode. For each combination of frequencies (3 low x 2 high), coupling solution formulation (PBS or 1% SLS in PBS), and wave pulsing (continuous or pulsed), five replicates were tested for statistical analysis. All the single-frequency samples were repeated 4-5 times.

2.2.3. Collection and Analysis of Aluminum Foil Samples

Following US treatment, samples were removed from the receiver compartment of the diffusion cell, trimmed to the treated area, mounted on heavy stock paper, and then laminated. Samples were then scanned using a Canon CanoScan 8800F at 1200 dpi in grayscale mode and saved in the BMP file format. The pits in each sample were then manually counted and sized using custom software that was developed in house for this purpose (available at: http://web.mit.edu/dbgroup/current_research.shtml). This software allows the user to specify pit centers and radii (assuming hemispherical pits) through direct interaction with the scanned images using any pointing device (e.g., mouse, stylus), thereby facilitating rapid and accurate quantification of the pit population distribution. Pit radii are stored in units of pixels, and then converted into centimeters based on the scan resolution. Pit count and size data collected using this software was then imported into Microsoft Excel (Redmond, WA) for statistical analysis.

2.2.4. Preparation and Treatment of Skin Samples

This procedure has been approved by the MIT Committee on Animal Care. Tissue was procured by Research 87 (Boylston, MA). Previously published protocols were utilized for the storage and preparation of skin samples [13]. Briefly, skin was harvested from the back and flank of female Yorkshire pigs within one hour of sacrificing the animal. Subcutaneous fat was removed from the dermis with a razor blade, and then sectioned into 25-mm strips prior to

storage at −85°C for up to six months. Skin was thawed for 20 minutes in PBS, prior to use in experiments, and then excess hair was trimmed using surgical scissors. Skin was then dermatomed to 700 μm using an electric reciprocating dermatome (Zimmer Orthopedic Surgical Products, Dover, Ohio), and cut into 25 × 25-mm samples. The skin samples were then mounted in the bath as shown in Figure 2-1.

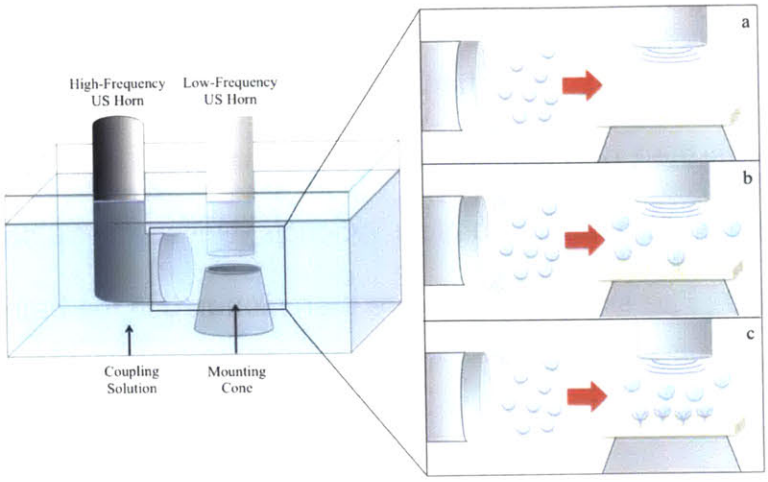

Figure 2-1: Schematic diagram of the setup used showing the coupling solution bath and the mounting cone over which the skin is mounted. For the aluminum foil experiments, the diffusion cell is placed within the rubber cone. It is hypothesized that the high-frequency US horn nucleates small bubbles, which are then pushed below the low-frequency horn by streaming (a). The additional bubbles nucleated by the high-frequency horn grow by rectified diffusion under the influence of the low-frequency horn (b). Once the bubbles reach the threshold size, they collapse against the skin (c).

Skin samples were treated similarly to the procedure described in Section 2.2.2, with the exception that only 20 kHz US was investigated and the low-frequency US horn was positioned 3 mm from the surface of the skin for consistency with prior LFS research [13-15]. The tank was filled with a solution of 1% SLS in PBS until the high-frequency US horn was fully submerged. Skin samples were then suspended over a rubber ring directly below the 20 kHz probe using metal pins. The intensities of the low- and high-frequency US horns were identical to those described in Section 2.2.2. Note that only 1MHz was tested for the high-frequency US because experiments with aluminum foil showed that the resulting pitted area is larger when using 1 MHz than when using 3 MHz (see Section 2.3.2). The 20 kHz probe was set to 50% duty cycle (1s on, 1s off). Treatment time ranged between two and six minutes, which are typical treatment time ranges established from prior LFS research [6], [7], [13].

2.2.5. Quantification of LTR Area in Ultrasound-Treated Skin

Immediately after US treatment, the skin was removed from the tank and washed thoroughly with PBS to remove any residual SLS. The skin samples were then mounted into 15-mm inner-diameter diffusion cells (PermeGear, Hellertown, PA) using the following protocol. High vacuum grease (Dow Corning, Midland, MI) was applied to the inner flange of the donor compartment in order to provide a water-tight seal between the skin and the diffusion cell. The receiver chamber was then filled with PBS and the skin sample was positioned over the receiver chamber with the treated area centered in the diffusion cell. The donor

compartment was then placed on top of the skin and the diffusion cell was clamped tightly. The donor chamber was filled with the dye allura red at a concentration of 0.04 wt% in PBS, and was allowed to sit for 1.5 hours.

After the skin was stained, the allura red solution was removed from the donor compartment, and the skin sample was washed thoroughly with PBS. The skin sample was then gently blotted dry to prepare it for imaging. The skin surface was imaged using a digital camera (Panasonic DMC-ZS7, 12.1 megapixels, shutter speed 1/2000s) positioned approximately 20 cm above the skin. The images were processed using Adobe Photoshop CS5.1 using the following protocol. First, the blue-channel of the image was isolated because this provided the best contrast for measuring the red dyed portion of the skin (see Figure 2-6) [16]. The image was then cropped such that only the portion of skin exposed to allura red was captured (1.5 cm x 1.5 cm). The threshold of the image was then adjusted such that only the dyed portion of the skin was captured (see Figure 2-6c). Once an appropriate threshold level was found, all samples were processed using the same threshold value for consistency. The adjusted image was then opened in ImageJ (National Institutes of Health, Bethesda, MD), and the area was quantified with the "Analyze Particles" option using the default size and circularity options. The reported values were then converted from units of pixels to mm by utilizing standards of known dimensions. All samples below a minimum resolution value of 0.01% LTR area were reported to have an LTR area of 0.

2.2.6. Quantification of Glucose and Inulin Penetration into Treated Skin

After pretreatment of the skin with US, 1 mL of glucose (concentration of 1 mg/mL spiked with 2 μCi/mL tritiated glucose, or $1.8x10^{-3}$ % labeled glucose by mass) was added to the donor compartment of the diffusion cell and allowed to permeate for two hours. At the end of the experiment, the glucose solution was removed, and the donor compartment was washed thoroughly with PBS to remove excess glucose that did not penetrate into the skin. The receiver compartment was collected and the diffusion cell disassembled. The area of the skin exposed to the glucose solution was carefully excised using a razor blade and collected. 10 mL of Soluene 350 was added to each skin sample, and the sample was heated in a water bath between 70-85 ^{o}C to facilitate solubilization of the tissue. Upon solubilization, 5 mL was aliquoted for radiometric analysis. 2 mL aliquots of the receiver solutions from each experiment were also sampled and analyzed. 15 mL of Hionic Fluor Scintillation Cocktail was added to all tissue and receiver solution aliquots and allowed to rest for 40 minutes for the fluorescence signal to equilibrate. The samples were then run on a Tri-Carb Liquid Scintillation Counter (Perkin Elmer) to determine the decompositions per minute (DPM). The resulting DPM values were used to calculate the total mass of glucose delivered to, and through, the skin for each sample using the ratio of labeled to unlabeled glucose and the known activity of the ^{3}H glucose.

Separate skin samples pretreated with US had 1 mL of inulin (concentration of 1 mg/mL spiked with 2 μCi/mL ^{14}C-labeled inulin, or 100 % labeled inulin by mass) added to the donor compartment, and were also allowed

to permeate for two hours. Quantification of inulin delivery followed an identical procedure as that performed for glucose.

2.2.7. Statistical Significance

We have characterized statistical significance using t-tests. F-tests were performed to analyze variances. Statistical significance is defined throughout as $p < 0.05$. All calculations were performed using Microsoft Excel (Redmond, Washington).

2.3. Results and Discussion

2.3.1. Aluminum Foil Pitting

Each aluminum foil pitting experiment was performed in quintuplicate. These experiments aimed to quantify the effect of four different sets of variables on pit size (radius), number of pits, and total pitted area. These variables include: i) the coupling solution composition (with or without SLS), ii) the duty cycle of the low-frequency US horn (100% or 50%), iii) the frequency of the low-frequency US horn (20, 40, or 60kHz), and iv) the use and frequency of the high-frequency US horn (not used, 1, or 3 MHz).

2.3.1.1. Coupling Solution

The effect of SLS in the coupling solution was visible in the number of pits, and therefore, in the total pitted area observed on the aluminum foil. The pit

radius was found to be unaffected by the presence of SLS (the pit radius was only affected by the low-frequency US horn used (Figure 2-2), as expected based on previously published reports on the relationship between cavitation bubble size and US frequency [3]). With regards to the total pitted area, SLS had a greater effect on 40 kHz and 60 kHz compared to 20 kHz, as shown in Figure 2-3. SLS in the coupling solution acted to decrease the number of pits present on the aluminum foil, thereby decreasing the total pitted area when 40 and 60kHz was used.

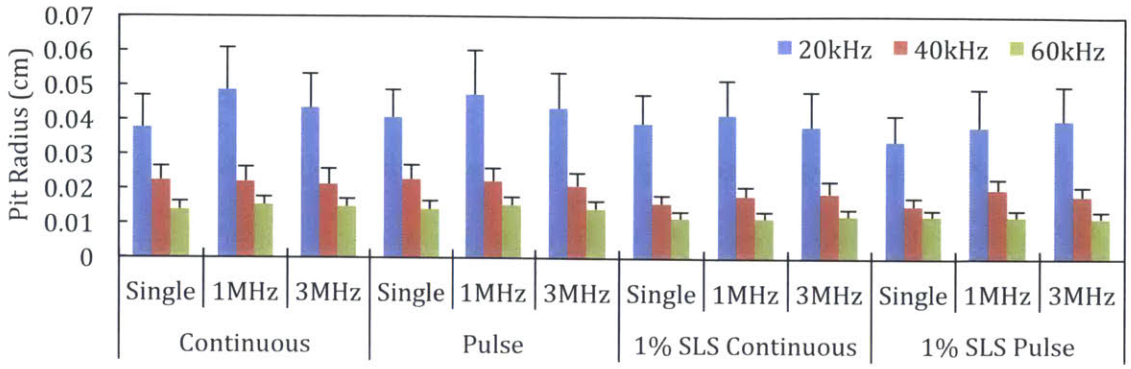

Figure 2-2: Average pit radius due to a variety of treatment conditions. Continuous denotes continuous operation of the low-frequency US horn. Pulse denotes 50% duty cycle of the low-frequency US horn (1s on, 1s off). Error bars represent one standard deviation.

This is consistent with previously published results [4], and can be attributed to the amphiphilic nature of SLS. Briefly, when bubbles are formed, surfactants like SLS preferentially organize at the bubble-liquid interface, thus reducing the bubble surface tension [17]. While this reduction in surface tension does lead to greater bubble growth rates, bubble collapse intensities are decreased [18]. If a charged surfactant like SLS is used, then SLS adsorption onto the bubble-liquid interface also leads to electrostatic repulsions between the charged bubbles, which decreases bubble coalescence. This, in turn, results in fewer bubbles above the threshold size needed to grow via rectified diffusion, when compared to the number of bubbles without SLS. As a result, these smaller bubbles produced at 40-60 kHz simply dissolve back into the solution due to the Laplace Pressure [19]. Also, as the bubble collapse intensities are decreased in the presence of SLS, it is likely that some bubbles do not collapse with sufficient energy to cause observable pitting of the foil and are therefore not accounted for in our analysis. This explains the decreased number of pits observed when SLS is added to the coupling solution.

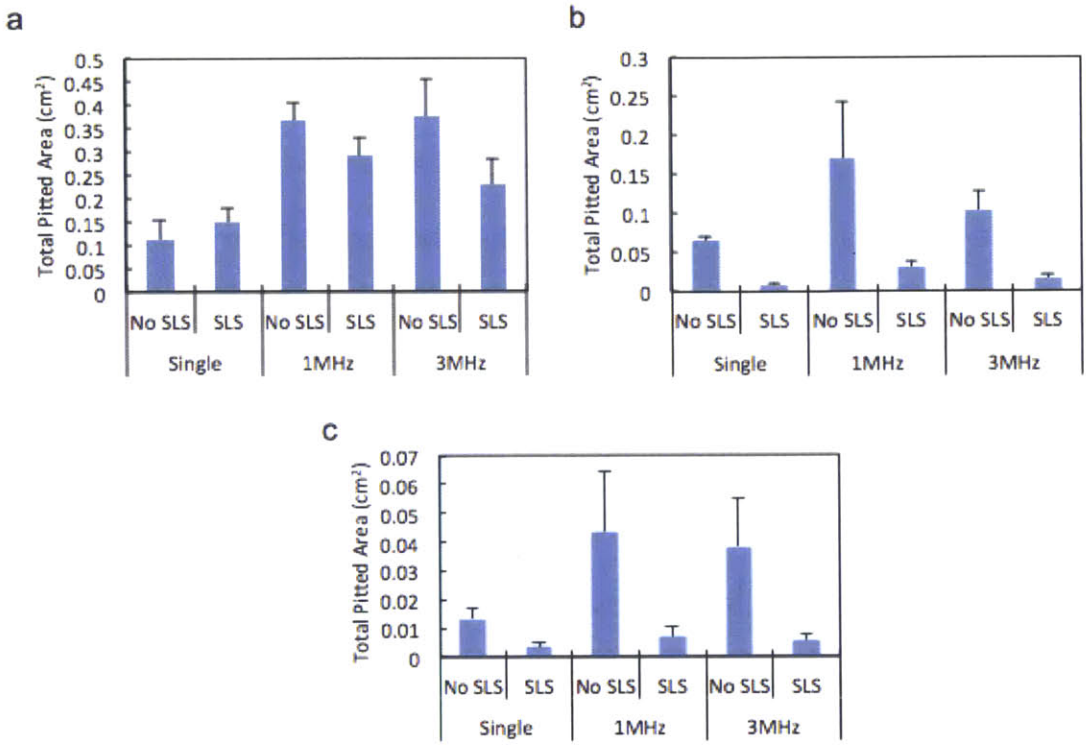

Figure 2-3: The effect of SLS in the coupling solution on the total pitted area for various combinations of low-frequency and high-frequency US: (a) 20 kHz, (b) 40 kHz, and (c) 60 kHz. Error bars represent one standard deviation.

2.3.1.2. Low-Frequency Ultrasound

The low-frequency US used had a consistent effect on pit radius, as shown in Figure 2-2. 20 kHz created the largest pits, followed by 40 kHz, with 60 kHz creating the smallest pits. This trend was independent of the three other variables (SLS, high frequency applied, pulsing). The number of pits observed on the aluminum foil was also found to depend greatly on the low-frequency US used. Without SLS, 40 kHz US consistently produced the largest number of pits (see the blue curve in Figure 2-4). The number of pits generated using 20 and 60 kHz were found to be comparable. Upon addition of SLS, however, the number of pits was found to be inversely correlated with frequency (see the red curve in Figure 2-4), with the number of pits observed using 20 kHz US remaining the same (as discussed in Section 2.3.1.1). The effect of SLS on the number of pits observed is consistent with the discussion presented in Section 2.3.1.1. Specifically, because there is an inverse relationship between cavitation bubble size and applied US frequency, the bubbles generated by 40 and 60 kHz are more susceptible to dissolving back into solution during the OFF pulse phase of the low-frequency horn, thereby resulting in fewer pits at the aluminum foil surface. The duty cycle of the low-frequency US horn was found to have no significant impact on pit radius, number of pits, or total pitted area (data not shown, $p > 0.05$).

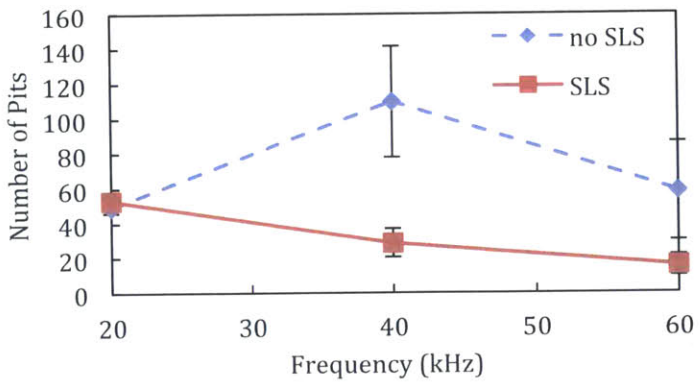

Figure 2-4: Number of pits observed in aluminum foil pitting experiments when treated using 1 MHz US and low-frequency ultrasound (20, 40, and 60 kHz) with and without 1% SLS present in the coupling solution. The red and blue lines are drawn to facilitate observation of trends. Error bars represent one standard deviation.

2.3.1.3. High-Frequency Ultrasound Application

The pit radius was found to be independent of the high-frequency US used (see Figure 2-2). The greatest effect of the high-frequency US used was observed on the number of pits, as expected. Simultaneous use of the high-frequency US horn was found to always produce more pits on the aluminum foil than found in samples treated without using the high-frequency US. While the 1 MHz frequency generally produced more pits than the 3 MHz frequency (and therefore, a larger pitted area), the effect was typically not significant (see the red and green curves in the plot of total pitted area in Figure 2-5). Both 1 MHz and 3 MHz US frequencies produced significantly more pits when compared to using no high-frequency US (except for 60 kHz, $p = 0.11$ and 0.62 for use of 1 and 3 MHz respectively) (data not shown). In the case of 20 and 40 kHz, the high-frequency US horn was observed to nucleate additional bubbles, which could then cavitate and collapse under the influence of the low-frequency US horn. This significant increase in the number of pits leads to a significant increase in the total pitted area, as shown in Figure 2-5. Figure 2-5 reveals that the use of 20 kHz always produces the largest pitted area when compared to using 40 or 60 kHz ($p < 2.2 \times 10^{-5}$ for 20 kHz and 1 MHz compared to 40 or 60 kHz and 1 MHz).

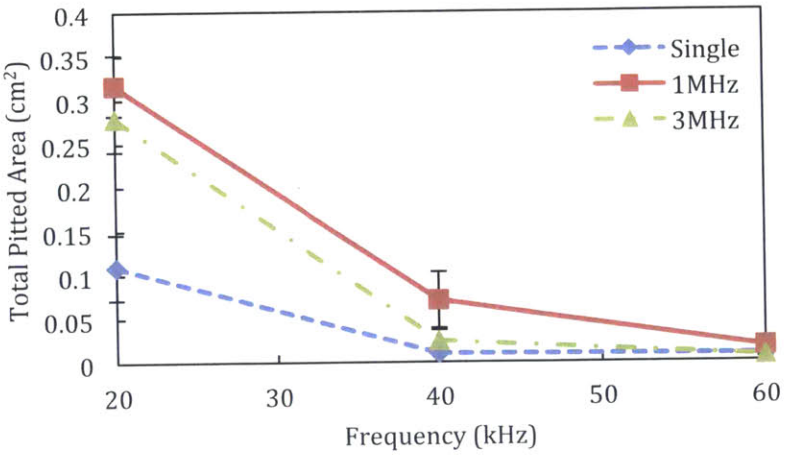

Figure 2-5: Variation of the total pitted area in the aluminum foil pitting experiments as a function of the low- and high-frequency US used. All the experiments were carried out using a coupling solution of 1% SLS, and the low-frequency US was pulsed (1s on, 1s off). The red, green, and blue lines are drawn to facilitate observation of trends. Error bars represent one standard deviation.

The slight decrease in the number of pits observed when using 3 MHz compared to 1 MHz US is thought to be due to the difference in the size of the bubbles nucleated by both frequencies. It is known that the average size of nucleated bubbles is inversely proportional to the applied US frequency [3]. The pits are created by bubbles that collapse under the influence of the low-frequency horn. Not all bubbles, however, can couple to the signal of the low-frequency horn and cavitate. Only bubbles within a specific size range (unique to each US frequency) can couple to the low-frequency US. The 3 MHz horn could be nucleating fewer bubbles with sizes within the range necessary to couple to the low-frequency US horn. In addition, the observed slight decrease in the number of pits could be due to the coupling efficiency of the 3 MHz horn, resulting in a decrease in the number of bubbles that are nucleated. The first explanation suggests that additional US frequencies below 1 MHz may also yield increased pitting. Additionally, there may be an optimal US frequency for use as the high-frequency horn, with respect to the number of pits induced. This interesting possibility may be investigated further using custom-fabricated US horns operating in the range of 100 kHz to 1 MHz.

2.3.2. Skin Permeability

While significant trends were observed in the aluminum foil pitting experiments, it still remained to be seen whether similar trends would be observed when treating skin. Based on the results of the aluminum foil pitting

experiments, it was logical to choose 20 kHz as the low-frequency US for the skin studies, since this frequency consistently yielded samples with the largest total pitted area (see Figure 2-5). Additionally, 1 MHz was chosen as the simultaneous high-frequency US. While the use of 1 MHz US did not produce significantly better results than the use of 3 MHz, the average pitted area using 1MHz was found to be larger than that using 3MHz (see the green and red curves in Figure 2-5). 1% SLS was utilized in the coupling solution because this was shown to have a minimal effect on the pitting results at 20kHz, as discussed in Section 2.3.1.1, and has previously been shown to enhance the efficacy of US pretreatment of the skin [20]. Finally, low-frequency US horn was operated at 50% duty cycle to minimize thermal effects, which is consistent with previously published literature reports [3], [6]. Indeed, even at the longest treatment time of six minutes, the temperature of the water bath was found to increase only by 0.33 ^{o}C. Because work by our group and others has previously shown that a temperature increase of at least 10 ^{o}C is required to increase the skin permeability significantly, it is safe to assume that thermal effects in this case are negligible [2].

Skin was treated using the above conditions for treatment times ranging from two to six minutes. The resulting LTR area vs. treatment time curve is shown in Figure 2-7. Six minute treatments resulted in LTR formation in excess of 27% of the treated skin area in the Dual samples (see Table 2-1). Coverage was less than 5% in the single-frequency samples, in agreement with other published results [9]. For comparison, the Dual samples treated for only four

minutes had comparable LTR coverage to single-frequency samples treated for six minutes. This demonstrates that the use of simultaneous low- and high-frequency US decreases the required treatment time to achieve the same size LTR's.

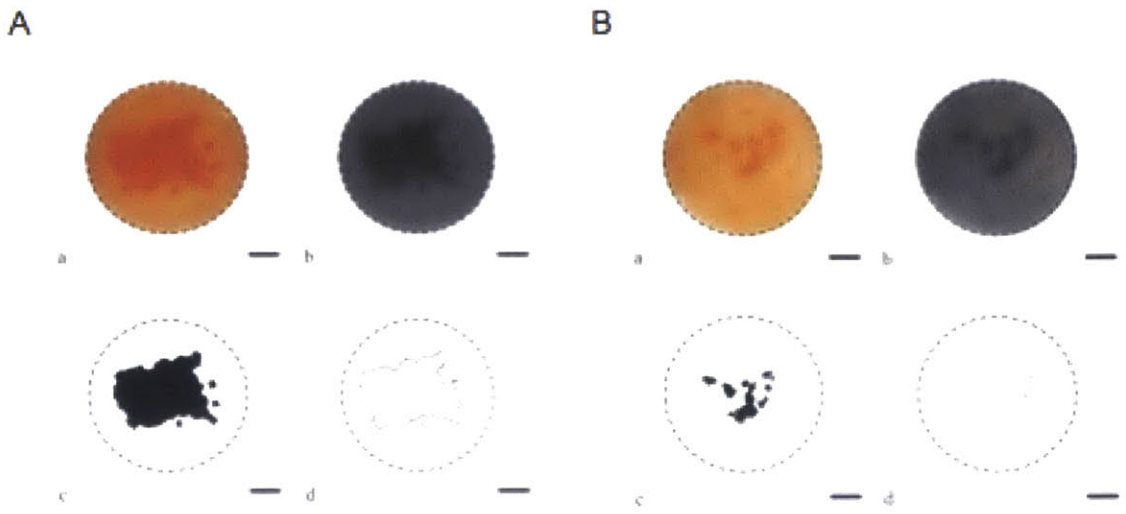

Figure 2-6: Representative images of skin treated with both low- and high-frequency US (A) for six minutes, and of skin treated with only low-frequency US for six minutes (B). Native Image (a). Isolated blue channel (b). Threshold-adjusted image (c). Area measured by ImageJ and outlined (d). The circular dotted line indicates the area of the skin that was treated with US and exposed to the dye allura red. The scale bar in the images represents 3mm.

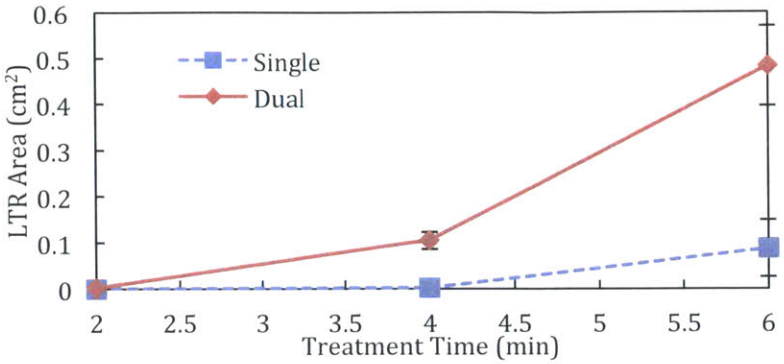

Figure 2-7: Resulting LTR area vs. treatment time for the single- (Single) and dual- frequency (Dual) US treatments. The red and blue lines are drawn to facilitate observation of trends. Error bars represent one standard deviation.

Additionally, when high-frequency US was used, the LTR's formed one contiguous area, contrary to the non-contiguous patterns that typically form using low-frequency US alone. This observation is highlighted in Figure 2-6, which shows skin samples treated with both dual- and single-frequency US for six minutes. The LTR in Figure 2-6A is localized in the center of the skin sample, and is generally contiguous. LTR's exhibiting this type of localization and contiguity are not typically observed in skin samples treated with only low-frequency ultrasound and CPEs (see Figure 2-6B). This phenomenon was observed at all treatment times (no LTR's were observed upon visual inspection in the single-frequency samples treated for two minutes). This suggests that the use of dual-frequency ultrasound also helps to centralize LTR's due to increased cavitational activity focused in the region where the low- and high-frequency ultrasound fields overlap.

Table 2-1: Percent LTR coverage as a result of US pretreatment time for the single-frequency and Dual samples. Enhancement is defined as the Dual value divided by the single-frequency value.

Treatment Time (min)	% LTR Coverage		
	Single	Dual	Enhancement
2	0	0.108	N/A
4	0.143	5.95	41.5
6	4.98	27.4	5.49

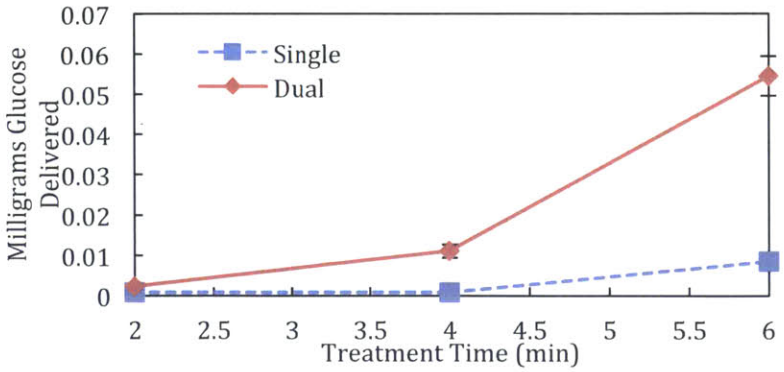

Figure 2-8: Resulting passive glucose delivery to, and through, the skin vs. the US pretreatment time. The red and blue lines are drawn to facilitate observation of trends. Error bars represent one standard deviation.

The enhancement in skin permeability as a result of the application of simultaneous low- and high-frequency US was then quantified by glucose transport. The cumulative mass of glucose delivered passively to, and through, skin pretreated simultaneously with both frequencies was found to be 2.7x, 13.6x, and 6.3x greater than that delivered to the single-frequency samples treated for two, four, and six minutes, respectively (see Figure 2-8 for a plot of glucose delivered vs. treatment time, and Table 2-2 for the actual values). Similar to the resulting LTR sizes, glucose delivery to single-frequency samples pretreated with US for six minutes was comparable to that seen in the Dual samples pretreated for only four minutes. This substantiates the claim that US pretreatment times can be reduced when using dual-frequency ultrasound without any decrease in the amount of compound delivered. Table 2-2 shows that glucose delivery to single-frequency samples treated for four minutes was slightly less than glucose delivery to single-frequency samples treated for two minutes. This was not statistically significant ($p = 0.42$), however, which suggests that there is a minimum treatment time required to achieve increases in delivery when using low-frequency ultrasound alone. The onset of this threshold is reduced with dual-frequency treatment, and less than the treatment time of two minutes. Dual samples treated for four minutes had 4.8x the amount of glucose delivery than Dual samples treated for two minutes (see Glucose Delivery in Table 2-2), which was statistically significant ($p = 0.013$).

Table 2-2: Glucose and inulin delivery as a result of US pretreatment time for the single-frequency and Dual samples. Enhancement is defined as the Dual value divided by the single-frequency value.

Treatment Time (min)	Glucose Delivery			Inulin Delivery		
	Single (mg)	Dual (mg)	Enhancement	Single (mg)	Dual (mg)	Enhancement
2	8.59×10^{-4}	2.32×10^{-3}	2.70	6.34×10^{-4}	1.42×10^{-3}	2.22
4	8.14×10^{-4}	1.11×10^{-2}	13.6	6.06×10^{-4}	2.31×10^{-3}	3.81
6	8.64×10^{-3}	5.46×10^{-2}	6.32	1.82×10^{-3}	3.66×10^{-3}	2.01

Finally, the phenomenon of enhanced delivery using dual-frequency US was quantified using a larger molecule, specifically, inulin (5000 Da). The mass of inulin delivered to, and through, the skin is reported in Table 2-2, and a plot is shown in Figure 2-9. Similar to what was observed with glucose, the four-minute treatment time yielded the greatest enhancement (the enhancements at each time point are reported in Table 2-2). The hypothesis that there is a minimum treatment time required to achieve significant enhancement when using low-frequency US alone is also supported by the inulin results, since there was no significant difference between delivery after two and four minutes of treatment for the single-frequency samples ($p = 0.11$) (see the blue curve in Figure 2-9). This demonstrates the ability of dual-frequency US to enhance delivery of compounds with a wide range of molecular sizes.

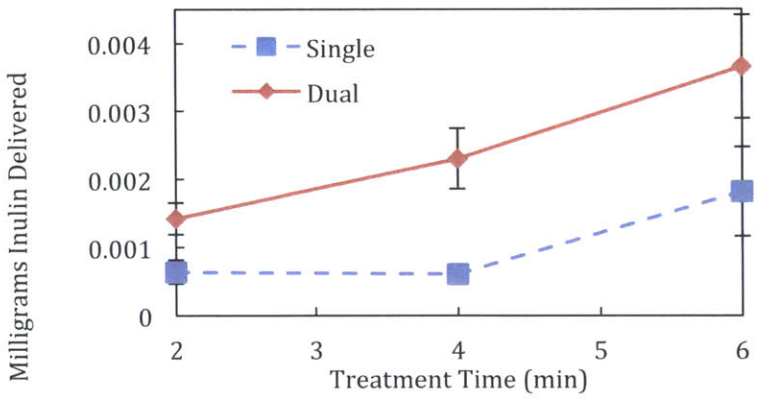

Figure 2-9: Resulting passive inulin delivery to, and through, the skin vs. the US pretreatment time. The red and blue lines are drawn to facilitate observation of trends. Error bars represent one standard deviation.

Interestingly, we found that the enhancement observed in the resulting LTR area was generally greater than the enhancement observed in the case of molecular permeability. In the context of the aqueous-porous pathway model, LTR's have previously been shown to have a greater density of aqueous channels relative to that corresponding to non-LTR's as a result of the ultrasound treatment [6]. This result is consistent with the hypothesis that the dual-frequency ultrasound treatment generates a greater number of bubble collapse events when compared with the single-frequency ultrasound treatment. Nevertheless, in spite of the increased number of channels, larger molecules, such as inulin, may still only "sample" and diffuse through the largest aqueous pores generated. This is why transport of glucose (180 Da) exhibited greater enhancement as a result of the dual-frequency ultrasound treatment than that experienced by inulin (5000 Da). This finding is also consistent with the literature, where it was shown, in the context of the aqueous-porous pathway model, that the estimated pore size generated by the ultrasound treatment depends on the permeant used to probe transport across the skin [6].

2.4. Conclusions

The effect of dual low- and high-frequency US on aluminum foil pitting and skin perturbation was investigated. Aluminum foil pitting experiments were carried out to quantify the number of pits, pit radius, and the total pitted area observed in single- and dual-frequency ultrasound experiments. The number of pits was found to depend strongly on whether high-frequency US was used, with

significantly more pits found using dual-frequency US. This finding was then tested in porcine skin samples in vitro. Skin samples were treated between two and six minutes. The resulting LTR area was found to be significantly greater in samples treated simultaneously with low- and high-frequency US, compared to samples treated with LFS alone, with the maximum LTR coverage exceeding 27% of the treated area. Passive delivery of both glucose (180 Da) and inulin (5000 Da) to, and through, the US-pretreated skin was also found to be significantly enhanced when dual-frequency US was used. Based on our findings, we conclude that dual-frequency US represents a new and viable method for reducing required US treatment times, for decreasing the lag-time associated with transdermal uptake of permeants following US treatment, and for enhancing overall skin permeability.

2.5. References

[1] M. K. Newman, M. Kill, and G. Frampton, "Effects of ultrasound alone and combined with hydrocortisone injections by needle or hypo-spray.," *Am J Phys Med*, vol. 37, no. 4, pp. 206–209, Aug. 1958.

[2] S. Mitragotri, D. A. Edwards, R. Langer, 4, "A mechanistic study of ultrasonically-enhanced transdermal drug delivery.," *J Pharm Sci*, vol. 84, no. 6, pp. 697–706, Jun. 1995.

[3] B. E. Polat, D. Hart, R. Langer, and D. Blankschtein, "Ultrasound-mediated transdermal drug delivery: Mechanisms, scope, and emerging trends," *J Control Release*, vol. 152, no. 3, pp. 330–348, 2011.

[4] A. Tezel, A. Sens, J. Tuchscherer, and S. Mitragotri, "Synergistic effect of low-frequency ultrasound and surfactants on skin permeability," *J Pharm Sci*, vol. 91, no. 1, pp. 91–100, 2002.

[5] J. Kushner, D. Kim, P. T. C. So, D. Blankschtein, and R. S. Langer, "Dual-channel two-photon microscopy study of transdermal transport in skin treated with low-frequency ultrasound and a chemical enhancer," *J Invest Dermatol*, vol. 127, no. 12, pp. 2832–2846, 2007.

[6] J. Kushner, D. Blankschtein, and R. Langer, "Evaluation of hydrophilic permeant transport parameters in the localized and non-localized transport regions of skin treated simultaneously with low-frequency ultrasound and sodium lauryl sulfate," *J Pharm Sci*, vol. 97, no. 2, pp. 906–918, 2008.

[7] B. E. Polat, W. M. Deen, R. Langer, and D. Blankschtein, "A physical mechanism to explain the delivery of chemical penetration enhancers into skin during transdermal sonophoresis - Insight into the observed synergism.," *J Control Release*, Nov. 2011.

[8] B. E. Polat, P. L. Figueroa, D. Blankschtein, and R. Langer, "Transport Pathways and Enhancement Mechanisms Within Localized and Non-Localized Transport Regions in Skin Treated with Low-Frequency Sonophoresis and Sodium Lauryl Sulfate," *J Pharm Sci*, vol. 100, no. 2, pp. 512–529, 2011.

[9] M. Ogura, S. Pahwal, and S. Mitragotri, "Low-frequency sonophoresis: Current status and future prospects," *Adv Drug Deliver Rev*, vol. 60, no.

10, pp. 1218–1223, 2008.

[10] H.-L. Liu and C.-M. Hsieh, "Single-transducer dual-frequency ultrasound generation to enhance acoustic cavitation.," *Ultrason Sonochem*, vol. 16, no. 3, pp. 431–438, Mar. 2009.

[11] H. Hasanzadeh, M. Mokhtari-Dizaji, S. Z. Bathaie, Z. M. Hassan, V. Nilchiani, and H. Goudarzi, "Enhancement and control of acoustic cavitation yield by low-level dual frequency sonication: A subharmonic analysis," *Ultrason Sonochem*, vol. 18, no. 1, pp. 394–400, 2011.

[12] S. Mitragotri, D. Ray, J. Farrell, H. Tang, B. Yu, J. Kost, D. Blankschtein, and R. Langer, "Synergistic effect of low-frequency ultrasound and sodium lauryl sulfate on transdermal transport," *J Pharm Sci*, vol. 89, no. 7, pp. 892–900, 2000.

[13] J. E. Seto, B. E. Polat, R. F. V. Lopez, D. Blankschtein, and R. Langer, "Effects of ultrasound and sodium lauryl sulfate on the transdermal delivery of hydrophilic permeants: Comparative in vitro studies with full-thickness and split-thickness pig and human skin," *J Control Release*, vol. 145, no. 1, pp. 26–32, 2010.

[14] T. Terahara, S. Mitragotri, J. Kost, and R. Langer, "Dependence of low-frequency sonophoresis on ultrasound parameters; distance of the horn and intensity," *International Journal of Pharmaceutics*, vol. 235, pp. 35–42, 2002.

[15] B. E. Polat, J. E. Seto, D. Blankschtein, and R. Langer, "Application of the Aqueous Porous Pathway Model to Quantify the Effect of Sodium Lauryl

Sulfate on Ultrasound-Induced Skin Structural Perturbation," *J Pharm Sci*, vol. 100, no. 4, pp. 1387–1397, 2011.

[16] J. Kushner, D. Blankschtein, and R. Langer, "Experimental demonstration of the existence of highly permeable localize transport regions in low-frequency sonophoresis," *J Pharm Sci*, vol. 93, no. 11, pp. 2733–2745, 2004.

[17] S. Wu, T. Leong, S. Kentish, and M. Ashokkumar, "Frequency Effects during Acoustic Cavitation in Surfactant Solutions," *J Phys Chem B*, vol. 113, no. 52, pp. 16568–16573, 2009.

[18] J. Lee, S. Kentish, and M. Ashokkumar, "Effect of surfactants on the rate of growth of an air bubble by rectified diffusion," *J Phys Chem B*, vol. 109, no. 30, pp. 14595–14598, 2005.

[19] J. Lee, S. Kentish, T. Matula, and M. Ashokkumar, "Effect of surfactants on inertial cavitation activity in a pulsed acoustic field," *J Phys Chem B*, vol. 109, no. 35, pp. 16860–16865, 2005.

[20] I. Lavon, N. Grossman, and J. Kost, "The nature of ultrasound-SLS synergism during enhanced transdermal transport," *J Control Release*, vol. 107, no. 3, pp. 484–494, 2005.

Chapter 3

Applicability and Safety of Dual-Frequency Ultrasonic Treatment for the Transdermal Delivery of Drugs

3.1. Introduction

Non-invasive transdermal drug delivery (TDD) presents an attractive method for drug administration [1], [2]. In addition to the potential benefits of patient compliance associated with painless drug delivery, TDD can reduce first-pass degradation of drugs typically associated with the oral route and enables the delivery of larger molecules limited to subcutaneous injection [1], [2]. Despite countless experimental investigations surrounding this route, its use clinically is largely limited to the delivery of small molecules, such as nicotine and estradiol [3]. This is due in large part to the barrier posed by the outermost layer of the skin, the *stratum corneum* (SC). While there exist several methods to overcome or permeabilize this membrane, each method has associated limitations [4]. Treatment of skin with ultrasound (US) (also known as sonophoresis), for example, has the potential to permeabilize relatively large areas, but typically requires large, bulky equipment and a power source [5]. Recently, there has been renewed research interest in sonophoresis. Two major challenges limiting greater clinical use is the portability of the equipment required and the length of the treatment required [6], [7]. Studies addressing the former hurdle have focused on the use of low-profile cymbal transducer arrays that can be integrated

into patches [8], [9]. In addition to portability, these devices minimize the excitation voltages required, reducing power consumption [10].

With regards to the treatment times necessary, a new approach has recently been investigated to increase permeabilization efficiency, thereby decreasing the required treatment time [11]. This method employs the use of two US frequencies simultaneously. A proof-of-concept study demonstrated that the use of both low- (< 60 kHZ) and high-frequency (> 1 MHz) US together resulted in greater transient cavitation events, as assessed by pitting data, and resulted in larger localized transport regions (LTRs) *in vitro* [11].

While this initial study demonstrated that the simultaneous application of low- and high-frequency US could enhance cavitational activity, the experimental setup required submerging tissue in a tank to allow for both frequencies to be applied simultaneously. This setup could result in artificial enhancement in skin permeability due to the underside of the dermatomed skin layer (epidermis) being exposed to surfactant present in the coupling solution. Additionally, there has never been a mechanistic exploration of the permeability of the resulting LTRs or the safety and tolerability of this new method. Here, we build on this preliminary report of the use of dual-frequency US to first develop an experimental setup which exposes only the top surface of the skin to the coupling solution, while allowing for the simultaneous application of both 20 kHz and 1 MHz US. We then use this setup to explore LTR formation, investigate the mechanistic underpinnings of this modality, and quantify the resulting permeability of treated skin *in vitro* over a range of relevant treatment times. We also examine treated

skin histologically to determine the level of barrier disruption as a result of US treatment. Finally, we utilize this setup to allow for treatment *in vivo* in pigs to examine LTR formation and tolerability.

3.2. Experimental Section

3.2.1. Materials

All chemicals were used as received. Sodium lauryl sulfate (SLS), 4 kDa FITC-labeled dextran, and phosphate buffered saline (PBS) were obtained from Sigma-Aldrich Company (St. Louis, MO). Lysine-fixable 3, 10, and 70 kDa dextrans labeled with Texas Red were purchased from Invitrogen (Carlsbad, CA). Allura red was obtained from TCI America (Portland, OR).

3.2.2. Preparation of Skin Samples and Ultrasonic Treatment

All procedures were approved by the Massachusetts Institute of Technology Committee on Animal Care. Porcine skin was used because of its physiological similarity to human skin [12]. Skin was procured by Research 87 (Boylston, MA). The preparation and storage of skin samples followed previously published protocols [13]. Briefly, back and flank skin was dissected from female Yorkshire pigs within an hour of euthanization. This skin was sectioned into 25-mm wide strips and the subcutaneous fat was removed using a razor blade. The skin was then stored at −85 °C for up to six months. Prior to use in experiments, skin was thawed for 20 minutes in PBS and the hair was trimmed using surgical scissors. The skin was then dermatomed to 700 μm using an electric

reciprocating dermatome (Zimmer Orthopedic Surgical Products, Dover, Ohio), and cut into 25 × 25-mm samples. The skin samples were then mounted in a custom diffusion cell to enable simultaneous sonication of the skin with both 20 kHz and 1 MHz US. Specifically, high vacuum grease (Dow Corning, Midland, MI) was applied to the flange of the custom-built top (FineLine Prototyping, Raleigh, NC) and 15-mm inner-diameter diffusion cell receiver chamber (PermeGear, Hellertown, PA). The skin was applied to the custom-designed top and then sandwiched between the top and receiver chamber. The top and bottom chambers were then clamped together and the receiver chamber was filled with PBS (12 mL) and a small volume of PBS was added to the custom-designed top to keep the skin hydrated until treatment.

Skin samples were treated in a similar fashion to previously reported methods [11], [14], [15]. Specifically, a 20 kHz horn (Sonics and Materials, Inc. Model VCX 500, Newtown, CT) and a 1 MHz horn (Therasound 3 Series, Richmar Corporation, Chattanooga, TN) were employed. The 20 kHz US horn was positioned 3 mm above the skin surface and operated at an intensity of 8 W/cm^2 (by calorimetry) and a 50% duty cycle (1s on, 1s off). The 1 MHz horn was placed on the side of the 20 kHz horn, approximately 5 cm from the leading edge of the skin. The 1 MHz horn was programmed to operate at a power of 2.0 W/cm^2 continuously. The custom diffusion top was filled with 300 mL of a solution of 1 wt% SLS and 0.04 wt% Allura red dye in PBS. The treatment times tested ranged between four and eight minutes, which are within the range of commonly-tested treatment times in the literature [16], [17]. Thermal effects were

determined to be negligible as the temperature increase of the coupling solution was less than 2 °C even at the longest treatment time considered. Prior work has shown that an increase of at least 10 °C is necessary to appreciably permeabilize the skin [18]. Treatments utilizing 20 kHz US alone were used as a control throughout the study. The use of 1 MHz US alone was not tested because it has been established in the literature that high-frequency US (≥ 1 MHz) at typical intensities, such as those used here, do not generate transient cavitation [1]. As a result, there would not be any quantifiable LTR formation and the resulting flux of 4 kDa dextran would not be significantly different than that observed in native skin [18].

3.2.3. Skin Resistivity Measurements

Electrical resistivity has previously been shown to be an accurate measure of skin perturbation [15], [19]. The resistivity across skin samples was determined using a method similar to previously published protocols [17], [20]. Specifically, a 10 Hz sinusoidal wave with root-mean-square voltage of 100 mV was employed (Hewlett Packard Model 33120A, Palo Alto, CA). This signal was then applied across the skin using two Ag/AgCl electrodes (In Vivo Metric, Healdsburg, CA). The resulting current was measured using a multimeter (Fluke, Model 87V, Everett, WA) and the resistance calculated using Ohm's Law. Finally, the resistivity was found by multiplying the resistance by the area of the skin exposed (the diffusion cells have an exposure area of 1.76 cm^2). In all measurements, the background resistance (resistance of PBS in the diffusion cell

without skin) was accounted for by subtracting it from the resistance observed when the skin was mounted in the diffusion cell. All skin samples were ensured to have a starting resistivity of at least 35 $k\Omega.cm^2$, otherwise, the skin sample was considered damaged and discarded [19].

3.2.4. Quantification of LTR Area

Immediately after US treatment, the coupling solution was discarded and the diffusion top and skin were washed thoroughly with PBS to remove any remaining coupling solution. The diffusion cell was then disassembled, the skin removed and placed on a paper towel, and blotted dry to prepare it for imaging. The skin was imaged using a digital camera (Panasonic DMC-ZS7, 12.1 megapixels, shutter speed 1/2000s) positioned approximately 10 cm above the skin. The resulting image was then cropped making sure that only the portion of the skin exposed to US was captured (1.5 cm x 1.5 cm) and processed using ImageJ 1.46r (National Institutes of Health, Bethesda, MD). Specifically, the blue channel of the LTR image was isolated because it has been shown to give the best contrast between LTRs and non-LTRs [21]. The image was then inverted, and the average pixel intensity of non-LTRs was measured. This pixel intensity was subtracted from the entire image to account for variations in lighting at the time of imaging. The image was then re-inverted. The threshold was adjusted using the default value found by ImageJ. Finally, the LTR area was quantified using the "Analyze Particles" function.

3.2.5. Steady-State Dextran Permeability

Once the skin samples were imaged to quantify LTR size, they were remounted in clean diffusion cells using standard glass tops (PermeGear, Hellertown, PA), and filled with PBS. A magnetic stir bar was added to the receiver chamber. The donor chambers were filled with 1.5 mL of 0.1 wt% 4 kDa dextran in PBS. The receiver chambers were magnetically stirred at 500 rpm. To ensure that the lag-phase was overcome, the receiver chambers were sampled between hour 20 and 48. For each sample, a 200 µL aliquot was taken and replaced with an equal volume of fresh PBS. These samples were then placed in 96-well plates and read using a plate reader (Tecan Infinite M200Pro) (excitation: 490 nm, emission: 525 nm). A known standard concentration series was also run to convert the sample emission to concentration. The permeability, P of dextran was then calculated using Eq. 3-1:

$$P = \frac{V_R}{AC_D}\frac{\Delta C_R}{\Delta \mathrm{t}} \tag{3-1}$$

where V_R is the volume of the receiver chamber, A is the area for diffusion, C_D is the concentration of dextran in the donor chamber, and $\Delta C_R/\Delta \mathrm{t}$ is the regression slope of a plot of the receiver chamber concentration with time.

3.2.6. Aqueous Porous Pathway Model

Theoretical pore sizes were estimated using the aqueous porous pathway model [22]. This theory allows for the estimation of theoretical pores in a medium using the permeability of a molecule (calculated from Eq. 3-1) and the electrical

resistivity of the membrane upon the application of a current. Assuming that both the permeant and the ions traverse the same pathway through the skin, a hindrance factor may be calculated for the permeant from known relations [23].

The permeability (*P*) and electrical resistivity (*R*) are related by Eq. 3-2:

$$log(P) = log(C) - log(R) \tag{3-2}$$

where *C* is a constant given by:

$$C = \frac{kT}{2z^2 F c_{ion} e} \frac{D^{\infty}_{permeant} H(\lambda_{permeant})}{D^{\infty}_{ion} H(\lambda_{ion})} \tag{3-3}$$

In Eq. 3-3, *k* is Boltzmann's constant, *T* is the absolute temperature, *z* is the valence of the electrolyte, *F* is Faraday's constant, c_{ion} is the molar concentration of the electrolyte, e is the electronic charge, D^{∞} is the diffusion coefficient of either the permeant or the ion at infinite dilution, λ is the ratio of the radius of either the permeant or the ion to the radius of the aqueous pores in the skin, and $H(\lambda)$ is the hindrance factor for the permeant or the ion [22].

The relation for the hindrance factor is given by [24]:

$$H(\lambda) = 1 + \frac{9}{8}\lambda ln(\lambda) - 1.56034\lambda + 0.528155\lambda^2 + 1.91521\lambda^3 - 2.81903\lambda^4 + 0.270788\lambda^5 + 1.10115\lambda^6 - 0.435933\lambda^7 \tag{3-4}$$

Once *C* is determined from Eq. 3-2, the only unknown quantity present is the skin pore radius in the ratio of the hindrance factors in Eq. 3-3. It is important to note that there is an upper limit on the pore size that can be estimated using Eq. 3-4 based on the permeant selected. The permeant must experience some amount of hindrance as a result of traversing the pores. Because the hindrance factor ranges from 0 to 1 (1 representing no hindrance), an upper limit is set on $H(\lambda)$, above which the pores are considered to be too large to estimate. Here, in this report, the upper limit on the hindrance factor is $H(\lambda) = 0.9$, which has been used previously in the literature [22], [23]. The hydrodynamic radius of 4 kDa dextran is 14 Å. This yields an upper limit on pore size estimates of approximately 870 Å [25]. Finally, the applicability of this theory to pore size estimates in skin has previously been tested by plotting $log(P)$ versus $log(R)$ and requiring that the 95% confidence interval of the regression slope contains the theoretical value of -1 (see Eq. 3-2). Previous work has shown this requirement to hold, and here too, it was ensured that the 95% confidence interval of the regression slope contained the value of -1 [15].

3.2.7. Histology

Individual skin samples were either treated with 20 kHz alone or with 20 kHz + 1 MHz as described in Section 3.2.2. After treatment, these samples were removed from the diffusion cell, washed, and blotted dry. The area exposed to the coupling solution and US was isolated using a scalpel. The treated area was

then sliced into 2 mm-wide sections fixed overnight in 10% formalin. The skin sections were then mounted in paraffin blocks to allow cross sections of the skin to be taken. Two, 8 μm-thick sections separated by a 200 μm step were stained with hematoxylin and eosin and mounted to glass microscope slides for histological examination.

3.2.8. Dextran Diffusion Depth

While US treatment increases the permeability of the skin, there may still exist limitations on the molecular weight of molecules that can diffuse through treated skin. To better understand this size-dependent permeability, dextrans of various sizes labeled with Texas red were allowed to diffuse through treated skin for a set period of time. Specifically, 3, 10, and 70 kDa dextrans labeled with Texas Red were used to image the relative penetration depth of these molecules into the skin. Skin was treated as described in Section 3.2.2 for six or eight minutes. Additionally, untreated skin samples were included as a control. After treatment, the skin samples were mounted in fresh diffusion cells with a magnetic stir bar in the receiver chamber. Only one molecule was allowed to diffuse through any given skin sample. 1-mL of 3, 10, or 70 kDa dextran solution at a concentration of 1 mg/mL in PBS was added to the donor chamber and the receiver chamber was stirred at 500 RPM. The dye was allowed to diffuse for only one hour to ensure that the diffusion front would not reach the receiver chamber. At that point, the dye solution was removed and the skin thoroughly washed with PBS. The skin was then sectioned and fixed overnight in 10%

formalin. Mounting and processing was performed as described in Section 3.2.7 with the exception that the skin was unstained.

The slides were imaged by the microscopy core facility in the Swanson Biotechnology Center (Massachusetts Institute of Technology). Briefly, slides were imaged with an Olympus FV-1000MP multiphoton microscope with a 25x, 1.05 N.A. objective. Samples were excited at 860 nm using a Ti-Sapphire pulsed laser (Spectra-Physics, Santa Clara, CA). Emission for Texas red was collected with a 607/70 nm band-pass filter and collagen was imaged by second harmonic generation at 430 nm. Individual image channels were combined in ImageJ.

3.2.9. *In Vivo* Experiments

All procedures were conducted in accordance with protocols approved by the Massachusetts Institute of Technology Committee on Animal Care. Female Yorkshire pigs approximately 50 kg in size were used for *in vivo* testing. Anesthesia was induced with intramuscular injection of 5 mg/kg Telazol and 2 mg/kg xylazine. A 20 gauge peripheral venous catheter was then placed in a vein in the ear of the animals. Anesthesia was maintained with 1 mg/kg ketamine and 0.3 mg/kg midazolam intravenously. The animals were laid on their side. The hair on the flank of the animal was carefully trimmed away using surgical scissors so as to not damage the skin. The custom-built top was then affixed to the skin using high vacuum grease. Treatment was performed following methods described in Section 3.2.2 with the addition of a plastic spacer connecting the diffusion top to the 20 kHz horn to maintain a distance of 3 mm

from the horn tip to the skin. In this manner, position variability due to breathing of the animal is minimized. Six and eight minute treatments were tested.

Following treatment, the diffusion top was removed and the skin washed with water to remove any excess coupling solution and gently blotted dry. The resulting LTRs were imaged and quantified according to the procedure described in Section 3.2.4. Once the LTRs were imaged, a biopsy was taken for the purpose of histological examination using a punch biopsy with a 3 mm diameter (Miltex, York, PA). The biopsies were fixed in 10% formalin. Histological slides were prepared as described in Section 3.2.7.

3.2.10. Statistical Significance

Statistical significance was defined throughout as $P < 0.05$. *P*-values were determined by one-way analysis-of-variance with multiple comparison testing unless otherwise noted. All calculations were performed in MatLab R2014a (MathWorks, Natick, MA).

3.3. Results and Discussion

3.3.1. *In Vitro* Results

To better understand enhancement in skin permeability as a result of the simultaneous use of 20 kHz + 1 MHz US, a more relevant experimental setup had to be designed to allow for the simultaneous application of both low- and high-frequency US. A custom-built top was designed in AutoCAD 2012 (see Figure 3-1A).

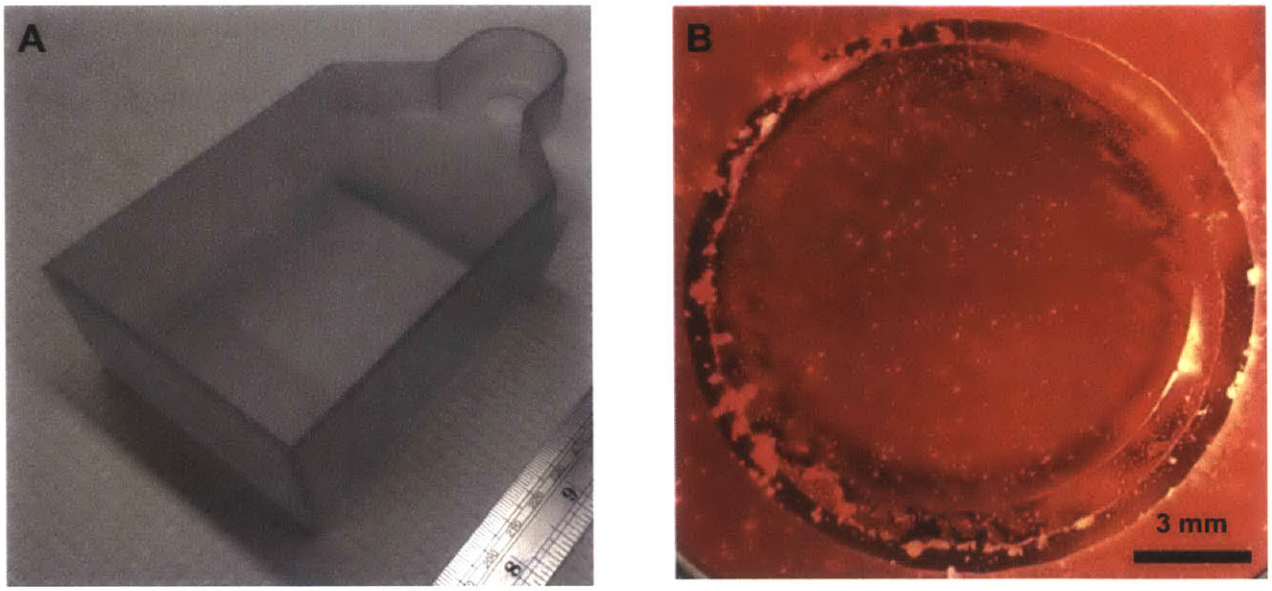

Figure 3-1: A) Custom designed diffusion top used for the study to allow for the simultaneous application of the 20 kHz and 1 MHz US horns. B) View from below the diffusion top looking up through the opening where the skin is normally mounted showing significant bubble formation when the 1 MHz US horn is on. The diffusion top is filled with a coupling solution of 1 wt% SLS and 0.04 wt% Allura red in PBS.

The top was designed so as to allow for unhindered bubble nucleation over the skin by the 1 MHz US horn. It was found that the top allowed for bubbles nucleated by the 1 MHz horn to oscillate over the area of the skin (Figure 3-1B).

Once the top was determined not to hinder bubble formation by the 1 MHz horn, porcine skin samples were treated *in vitro* with the diffusion top and the resulting LTR areas quantified. LTR sizes as a result of either 20 kHz or 20 kHz + 1 MHz US are shown in Figure 3-2A.

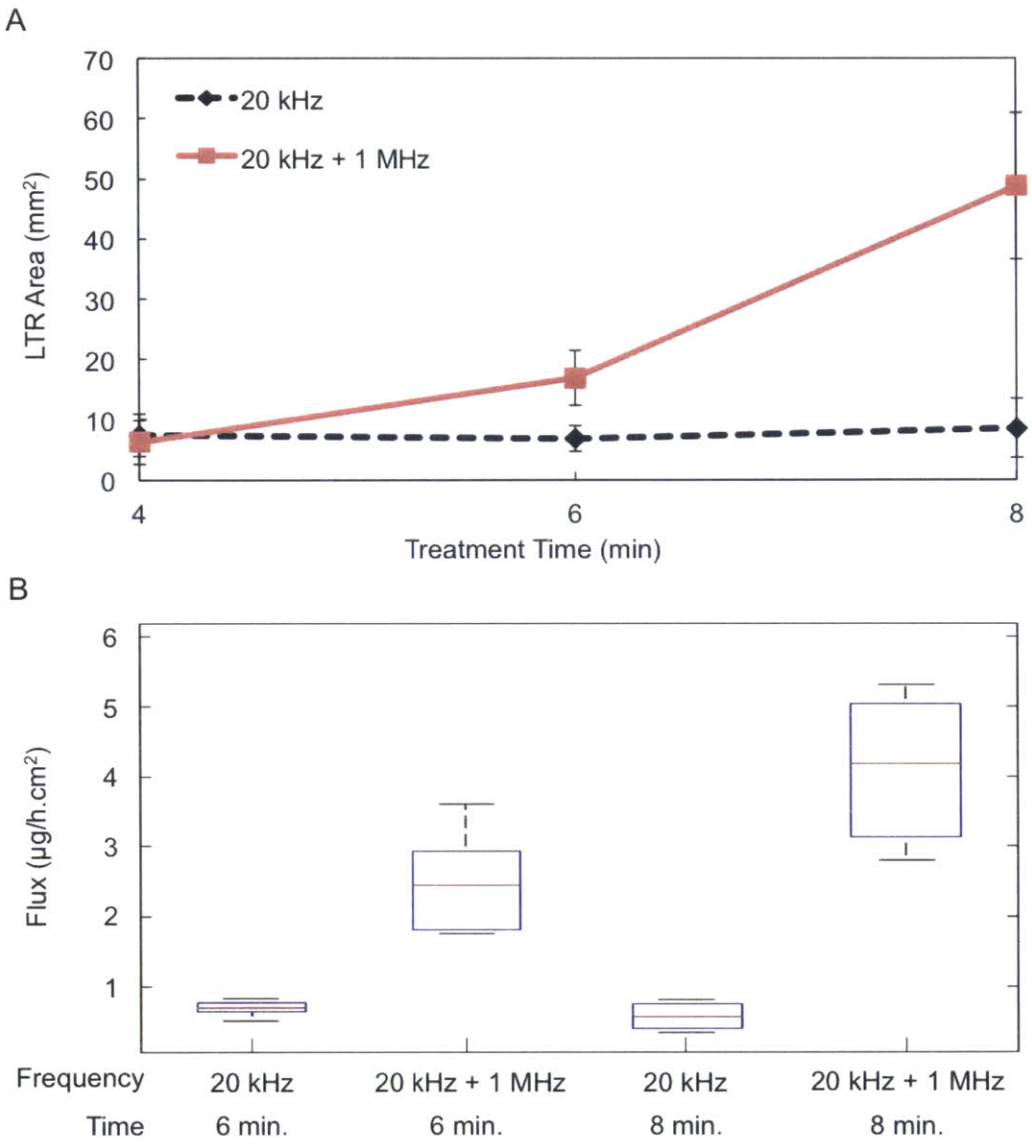

Figure 3-2: A) *In vitro* LTR size vs. treatment time as a result of treatment with either 20 kHz or 20 kHz + 1 MHz US. Each point represents n ≥ 3 biological repeats. Averages and standard deviations are presented. B) Flux of 4 kDa dextran at steady-state as a result of US treatment for either six or eight minutes. The median, 25th, and 75th percentiles are shown. Whiskers indicate the most extreme data points. Each condition represents n ≥ 5 biological repeats.

As shown in Figure 3-2A, a 2.5-fold and nearly 6-fold enhancement in LTR size was observed at treatment times of six and eight minutes, respectively, using both US frequencies simultaneously ($P < 0.0043$). No significant difference in LTR size was observed at the shortest treatment time. Additionally, no significant difference was found between LTR sizes at any treatment time using 20 kHz US alone. This is in clear contrast to what was found using 20 kHz + 1 MHz, in which there is a statistically significant increase in LTR size with increasing treatment time ($P < 0.048$). In this new study, longer treatment times were required compared to the previously published report. This is a result of the experimental setup that was employed in the preliminary report [11]. Specifically, that study employed a tank to allow for skin samples to be exposed to 20 kHz and 1 MHz simultaneously. While treatment utilizing 20 kHz alone was included as a control in that study to validate the phenomenon of enhanced cavitational activity using dual-frequency US, submersion of skin samples in the tank exposed the underlying epidermis to the coupling fluid containing SLS [11]. This results in additional permeabilization of the skin. Therefore, in this present study, the treatment times examined were increased by two minutes. The setup reported here is a more physiologically relevant setup and now allows for testing of dual-frequency US *in vivo*, which was not previously possible. Aside from the increased treatment time required in this study, the general trend of LTR enhancement as a result of treatment with 20 kHz + 1 MHz compared to 20 kHz alone is in good agreement with that presented previously [11].

Next, the flux of 4 kDa dextran and theoretical pore sizes of treated skin were determined for treatment times of six and eight minutes. Fluxes are shown in Figure 3-2B and pore sizes in Table 3-1.

Table 3-1: Pore radius estimates using the aqueous porous pathway model. The average, lower, and upper limits on pore size are based on the average and 95% confidence interval for *C* in Eq. 3-3.

Treatment Time (min)	r_{pore} (Å)					
	20 kHz			20 kHz + 1 MHz		
	Lower	Average	Upper	Lower	Average	Upper
6	69.07	80.57	95.2	> 870	> 870	> 870
8	55.57	64.67	75.9	> 870	> 870	> 870

A statistically significant increase in the flux of 4 kDa dextran was observed by using 20 kHz + 1 MHz as opposed to 20 kHz alone (P = 0.0012 and 1.25×10^{-6} for six and eight minute treatments, respectively). Again, there was a statistical difference between the flux observed for samples treated with 20 kHz + 1 MHz for six or eight minutes (P = 0.009), but no increase in flux with treatment time for the use of 20 kHz alone. Interestingly, the enhancement in flux at both treatment times using 20 kHz + 1 MHz was greater than that which would be expected based on the increase in LTR sizes alone at each treatment time. The dextran flux was 3.5- and 7.1-fold greater using 20 kHz + 1 MHz at six and eight minutes, respectively, compared to the use of 20 kHz alone, while LTR area increased 2.5- and 6-fold respectively. Specifically, regression slope analysis of plots of permeability (from Eq. 3-1) vs. LTR area demonstrated a greater increase in permeability per increase in LTR area through the use of 20 kHz + 1 MHz at both six and eight minute treatment times. Moreover, at each treatment time, the 95% confidence interval of the regression slopes do not overlap. This would suggest that LTRs generated by 20 kHz + 1 MHz are more permeable than those generated with 20 kHz alone.

This result is further supported by the pore size estimates utilizing the aqueous porous pathway model (Table 3-1). While the average theoretical pore size generated in samples treated with 20 kHz US was less than 81 Å, even the lower estimate of the pore sizes generated in samples treated with 20 kHz + 1 MHz was larger than the limit of detection (870 Å). These theoretical pore sizes can be attributed to the LTRs because the pore sizes of non-LTRs have

previously been shown to be nearly identical to those found in untreated skin [23]. Because this previous result was found using a smaller permeant (calcein), a larger distribution of skin pores could be sampled by the permeant (on account of its smaller size), which would result in larger pore size estimates. As a result, it is reasonable to assume that the majority of the 4 kDa dextran would diffuse through the LTRs and therefore, the pore sizes calculated would more greatly reflect pore sizes within the LTRs. Further, there was no statistical difference between the pore sizes found as a result of six or eight minute treatments with 20 kHz alone (two-tailed Student's T-test).

The finding that the enhancement in permeability is greater than that observed in LTR size is a new and surprising result not previously explored using steady-state permeation studies. Indeed, the opposite result was previously reported, demonstrating a greater enhancement in LTR formation than in the delivery of model permeants [11]. This previous finding was hypothesized to be a result of larger molecules only having the capacity to "sample" pores large enough to diffuse through, with 20 kHz + 1 MHz treatment having no effect on the size of pores generated in the skin. This finding could potentially have been due to the artificial enhancement in permeability stemming from the experimental setup employed masking the true enhancement in permeability gained through the use of 20 kHz + 1 MHz US. Regardless of the reason, the data reported here unequivocally demonstrate that treatment with 20 kHz + 1 MHz does in fact increase pore size, resulting in a greater enhancement in permeability than in LTR size.

Further exploring the increase in pore size as a result of treatment with 20 kHz + 1 MHz US, the diffusion of 3, 10, and 70 kDa dextran labeled with Texas red was visualized by microscopy (Figure 3-3). Qualitatively, examination of skin samples treated with 20 kHz + 1 MHz showed greater penetration of 3, 10, and even 70 kDa dextran compared to skin treated with 20 kHz alone. As expected, there was negligible penetration of any molecule into untreated skin. Discernable diffusion of macromolecules into skin in a relatively short diffusion time is exciting and could potentially allow for a broader range of therapeutics to be administered transdermally.

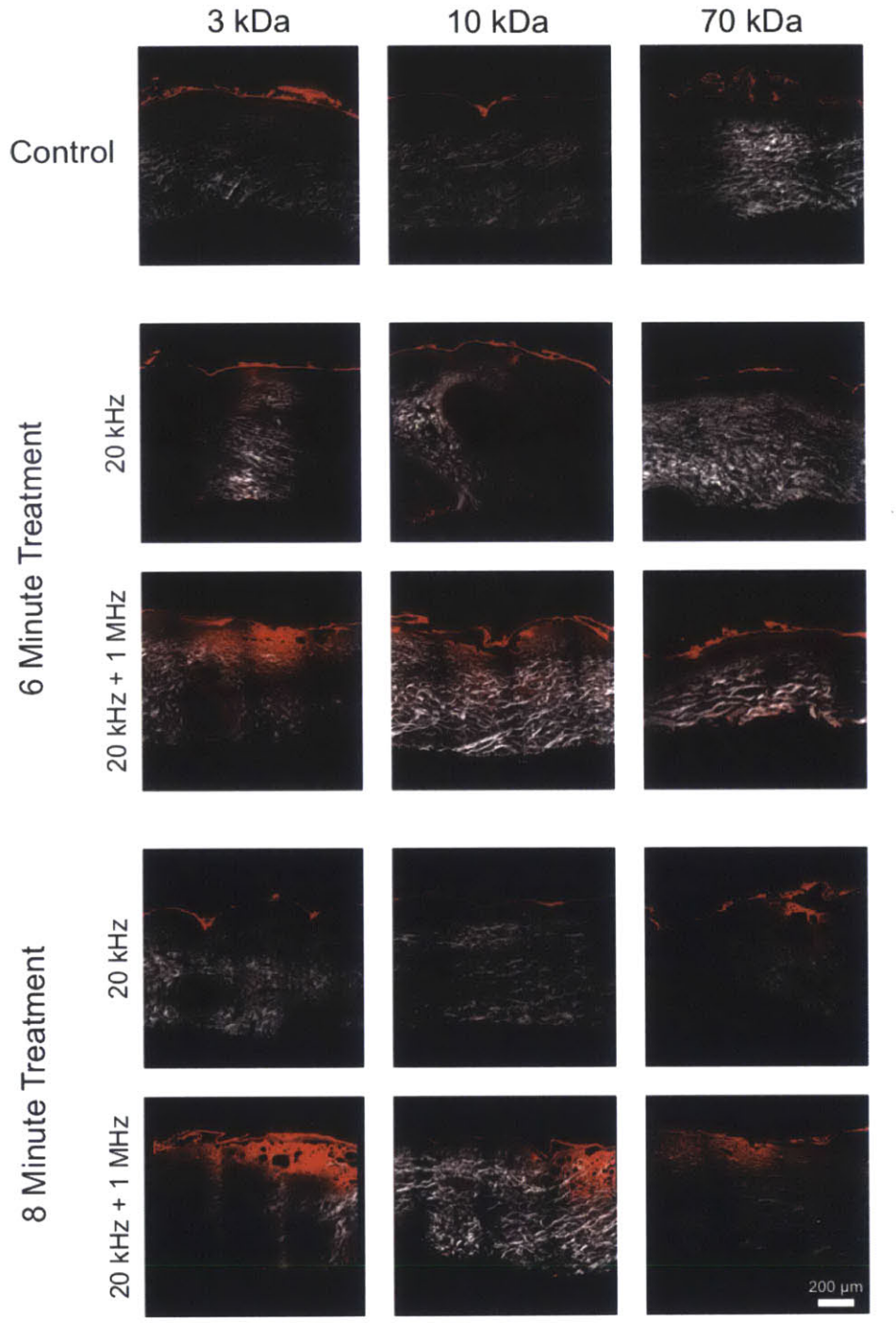

Figure 3-3: Representative images of the red channel and second harmonic showing diffusion of dextrans of various sizes labeled with Texas red into skin treated with 20 kHz or 20 kHz + 1 MHz US for six or eight minutes. Untreated skin is included as a control.

In addition to the permeability enhancement capabilities of the simultaneous use of 20 kHz + 1 MHz US, the safety of this method was also assessed through histological examination of treated skin. All histology samples were examined by a pathologist in a blinded fashion to assess the location, extent, and severity of any disruption to normal tissue architecture. Representative skin histology images are shown in Figure 3-4.

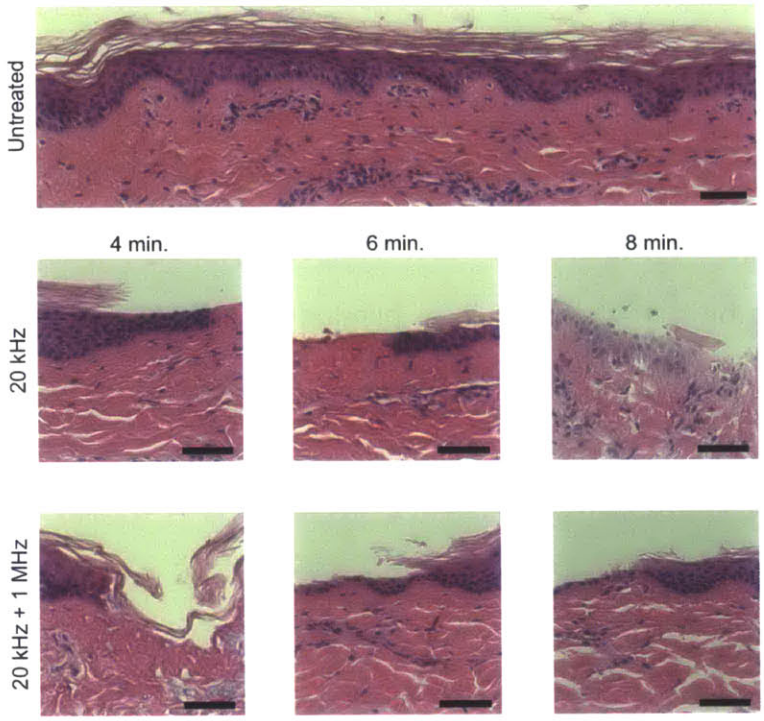

Figure 3-4: Representative images of the histological view of *in vitro*-treated porcine skin. Skin that was dermatomed and then immediately fixed in formalin is shown as the Control. The scale bar in all images is 50 μm.

As expected, histological damage was noted to scale with treatment time regardless of the frequencies employed. Ablation of the SC was noted in all samples in discrete, sporadic areas. At treatment times of six and eight minutes, there were ablative effects noted in the viable epidermis, and superficial dermis in a localized manner. This was determined by the observation of minor coagulation of collagen in the superficial layer of the dermis making distinction of individual fibers impossible. This was observed in both samples treated with 20 kHz and 20 kHz + 1 MHz US. Further, samples treated for six and eight minutes showed evidence of vacuole formation in the epidermis and dermis and minor coagulative necrosis was observed sporadically throughout the dermis. These observations have previously been noted in the literature [26]. Importantly, there was no quantifiable difference in extent or severity of tissue disruption between samples treated with 20 kHz and those treated with 20 kHz + 1 MHz at each treatment time considered. The fact that 20 kHz + 1 MHz US results in similar skin disruption as that resulting from treatment with 20 kHz alone, is reassuring, considering that the latter is an FDA-approved modality for the delivery of lidocaine [27].

3.3.2. In Vivo Results

Based on the significant enhancement observed at treatment times of six and eight minutes *in vitro* and the likely safety of this method, this new treatment regimen was translated to *in vivo* testing in Yorkshire pigs. LTR formation and histological examination was performed to ascertain if the enhancement

observed *in vitro* would persist in an *in vivo* system. The sizes of LTRs as a result of treatment are shown in Figure 3-5.

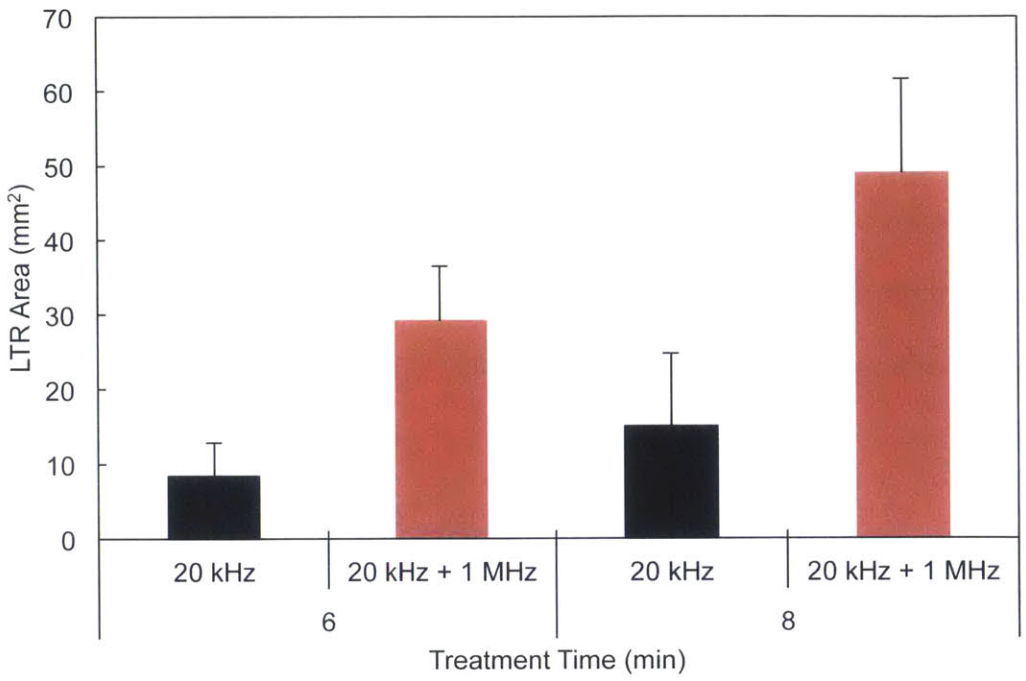

Figure 3-5: *In vivo* LTR sizes as a result of treatment with either 20 kHz US or 20 kHz + 1 MHz US. Each condition represents n = 4 biological repeats. Averages and standard deviations are presented.

The trends in LTR formation observed *in vivo* are in good agreement with those found *in vitro*. Treatment with 20 kHz + 1 MHz US resulted in statistically larger LTRs compared to those generated with the use of 20 kHz alone at both treatment times tested ($P \leq 0.032$). Moreover, similar to the *in vitro* results, the size of LTRs generated with 20 kHz US alone at six and eight minutes were not statistically different ($P = 0.73$). Additionally, LTR formation using 20 kHz + 1 MHz US for six minutes was again larger, on average, than that resulting from eight minutes of treatment using 20 kHz alone. This further confirms the fact that 20 kHz + 1 MHz US enables the reduction of treatment times to achieve comparable LTR sizes. Reducing the required treatment time will make US-assisted transdermal drug delivery more convenient, potentially enabling broader clinical use.

Clinical monitoring of the pigs over the period of a week post treatment showed the animals to be free of distress. Further, the area of the skin that was treated appeared healthy and uninfected. The treated area was undistinguishable from the surrounding tissue within four days post treatment and identification of the treated area at earlier times post treatment was only possible because of the presence of the Allura red dye staining the LTRs (see Figure 3-6). Histological examination of the skin demonstrated sporadic ablation of the SC, epidermis and dermis in addition to minor vacuole formation and coagulative necrosis sporadically thought the upper layers of the dermis (see Figure 3-7). The extent of skin injury was comparable to that observed in tissue treated *in vitro*. Finally, the extent and severity of tissue injury again could not be

differentiated between those samples treated with 20 kHz or 20 kHz + 1 MHz US. Based on histological examination, treatments should likely be less than eight minutes so that the treatment minimizes disruption to the dermis.

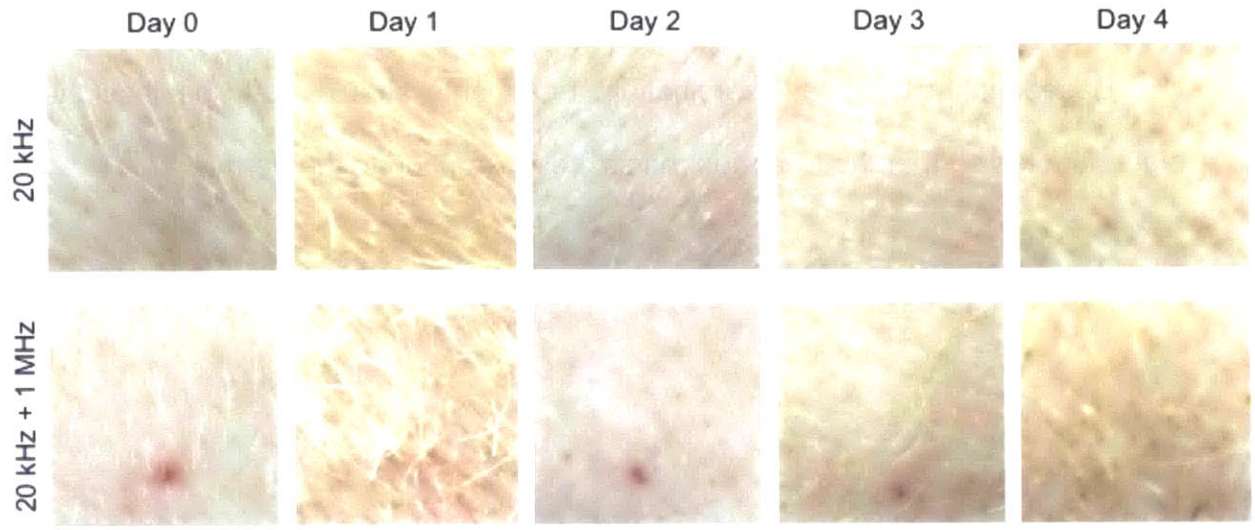

Figure 3-6: Images of the sites of US treatment *in vivo* over time. Images on Day 0 were taken immediately after US treatment. Image brightness has been adjusted to account for differences in lighting on subsequent days. Each image is 15 x 15 mm.

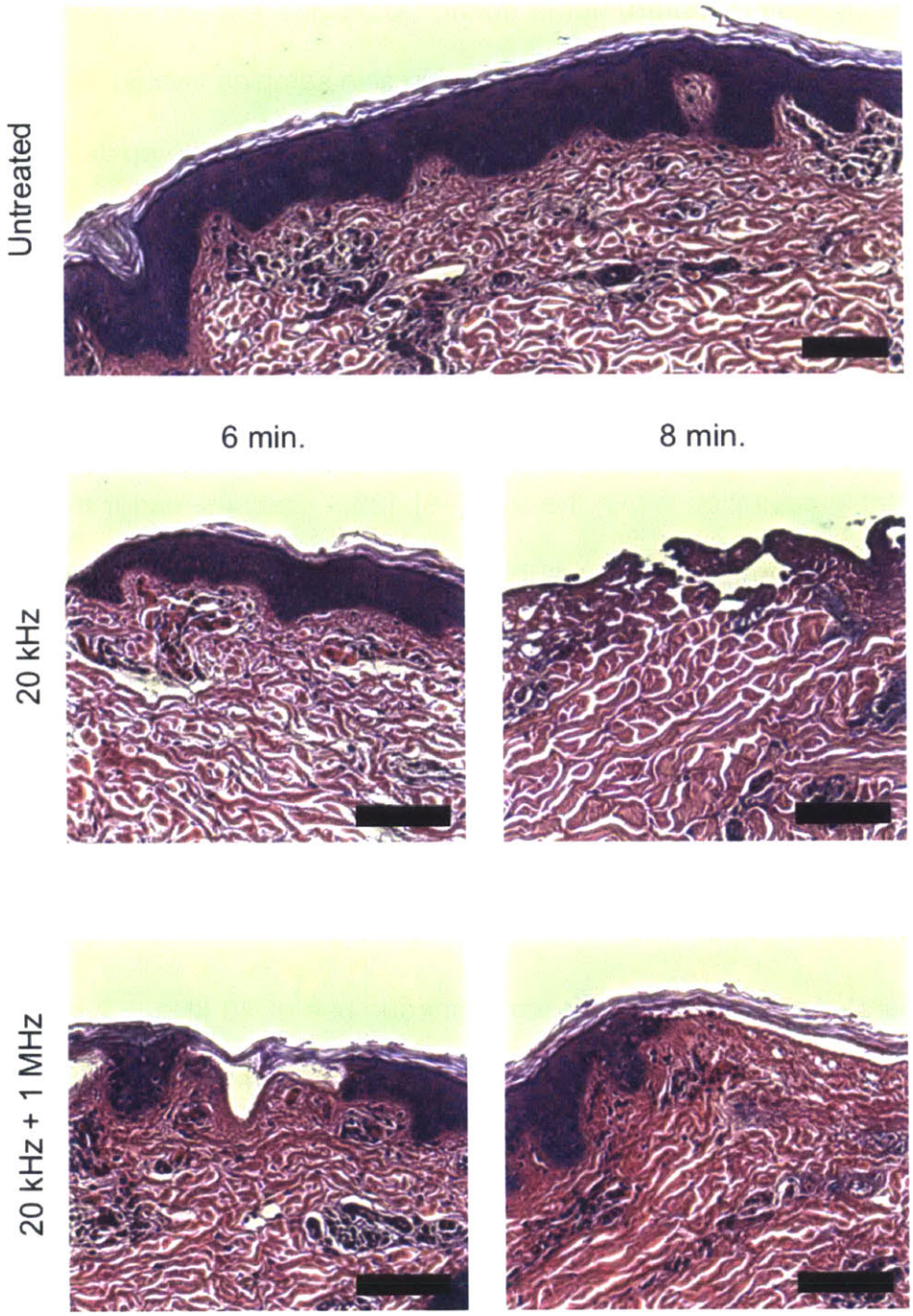

Figure 3-7: Representative images of the histological view of *in vivo*-treated porcine skin. The scale bar in all images is 100 μm.

One interesting feature noted during histological examination of the tissue was the pattern of tissue ablation observed in skin samples treated with 20 kHz + 1 MHz US. As it can be seen in Figure 3-7, portions of viable epidermis appear to have been ablated without ablation of the SC in samples treated with 20 kHz + 1 MHz US. This might suggest that transient cavitation is occurring within the skin. Cavitation within the skin has previously been hypothesized to play a significant role in low-frequency US and high-frequency US has been shown to produce stable cavitation within the skin [18], [28]. Perhaps, under the influence of the 20 kHz horn, cavitation bubbles within the skin are now growing to unstable sizes, resulting in transient cavitation within the skin. This would be an interesting new area of study and would present a new phenomenon in US-mediated transdermal drug delivery.

3.4. Conclusions

This study investigated the simultaneous use of 20 kHz + 1 MHz US for the purpose of transdermal drug delivery *in vitro* and *in vivo* in Yorkshire pigs. LTR formation as a result of 20 kHz + 1 MHz was found to be enhanced compared to 20 kHz alone at treatment times of six and eight minutes. It was further found that utilizing 20 kHz + 1 MHz could decrease the required treatment time to achieve a certain LTR size. Additionally, LTRs formed as a result of treatment with 20 kHz + 1 MHz US were found to be more permeable than those formed with 20 kHz US alone. This was hypothesized to be due to enhanced cavitational activity, resulting in the estimation of larger pore sizes present in skin

treated with 20 kHz + 1 MHz utilizing hindered-transport theory. Despite this greater permeability, histological examination of skin treated with 20 kHz + 1 MHz US *in vitro* and *in vivo* showed no greater disruption of viable tissues compared to the use of 20 kHz US alone, an FDA approved modality. Animals treated with 20 kHz + 1 MHz showed no clinical signs of distress and the treated area remained free of infection. The significant improvement in performance utilizing dual-frequency US should motivate further investigation into this method.

3.5. References

[1] M. R. Prausnitz and R. Langer, "Transdermal drug delivery," *Nat Biotechnol*, vol. 26, no. 11, pp. 1261–1268, Nov. 2008.

[2] C. M. Schoellhammer, D. Blankschtein, and R. Langer, "Skin permeabilization for transdermal drug delivery: recent advances and future prospects.," *Expert Opin. Drug Deliv.*, vol. 11, no. 3, pp. 393–407, Jan. 2014.

[3] A. C. Watkinson, "A Commentary on Transdermal Drug Delivery Systems in Clinical Trials," *Journal of Pharmaceutical Sciences*, vol. 102, no. 9, pp. 3082–3088, Sep. 2013.

[4] M. R. Prausnitz, S. Mitragotri, and R. Langer, "Current status and future potential of transdermal drug delivery," *Nature Reviews Drug Discovery*, vol. 3, no. 2, pp. 115–124, Feb. 2004.

[5] B. E. Polat, D. Hart, R. Langer, and D. Blankschtein, "Ultrasound-mediated transdermal drug delivery: Mechanisms, scope, and emerging

trends," *Journal of Controlled Release*, vol. 152, no. 3, pp. 330–348, Jun. 2011.

[6] N. B. Smith, "Perspectives on transdermal ultrasound mediated drug delivery," *International Journal of Nanomedicine*, vol. 2, no. 4, pp. 585–594, Apr. 2009.

[7] M. Ogura, S. Paliwal, and S. Mitragotri, "Low-frequency sonophoresis: Current status and future prospects," *Advanced drug delivery reviews*, vol. 60, no. 10, pp. 1218–1223, Jun. 2008.

[8] Y. Sunny, C. R. Bawiec, A. T. Nguyen, and J. A. Samuels, "Optimization of un-tethered, low voltage, 20-100 kHz flexural transducers for biomedical ultrasonics applications," *Ultrasonics*, 2012.

[9] E.-J. Park, J. Werner, J. Beebe, S. Chan, and N. B. Smith, "Noninvasive Ultrasonic Glucose Sensing with Large Pigs (~200 Pounds) Using a Lightweight Cymbal Transducer Array and Biosensors," *Journal of Diabetes Science and Technology*, vol. 3, no. 3, pp. 517–523, Apr. 2009.

[10] C. R. Bawiec, Y. Sunny, A. T. Nguyen, and J. A. Samuels, "Finite element static displacement optimization of 20–100kHz flexural transducers for fully portable ultrasound applicator," *Ultrasonics*, 2012.

[11] C. M. Schoellhammer, B. E. Polat, J. Mendenhall, R. Maa, B. Jones, D. P. Hart, R. Langer, and D. Blankschtein, "Rapid skin permeabilization by the simultaneous application of dual-frequency, high-intensity ultrasound," *Journal of Controlled Release*, vol. 163, no. 2, pp. 154–160, 2012.

[12] S. Debeer, J.-B. Le Luduec, D. Kaiserlian, P. Laurent, J.-F. Nicolas, B.

Dubois, and J. Kanitakis, "Comparative histology and immunohistochemistry of porcine versus human skin," *European Journal of Dermatology*, vol. 23, no. 4, pp. 456–466, 2013.

[13] J. E. Seto, B. E. Polat, R. F. V. Lopez, D. Blankschtein, and R. Langer, "Effects of ultrasound and sodium lauryl sulfate on the transdermal delivery of hydrophilic permeants: Comparative in vitro studies with full-thickness and split-thickness pig and human skin," *Journal of Controlled Release*, vol. 145, no. 1, pp. 26–32, Jul. 2010.

[14] T. Terahara, S. Mitragotri, J. Kost, and R. Langer, "Dependence of low-frequency sonophoresis on ultrasound parameters; distance of the horn and intensity," *International Journal of Pharmaceutics*, vol. 235, pp. 35–42.

[15] B. E. Polat, J. E. Seto, D. Blankschtein, and R. Langer, "Application of the aqueous porous pathway model to quantify the effect of sodium lauryl sulfate on ultrasound-induced skin structural perturbation," *Journal of Pharmaceutical Sciences*, vol. 100, no. 4, pp. 1387–1397, Oct. 2010.

[16] B. E. Polat, W. M. Deen, R. Langer, and D. Blankschtein, "A physical mechanism to explain the delivery of chemical penetration enhancers into skin during transdermal sonophoresis — Insight into the observed synergism," *Journal of Controlled Release*, vol. 158, no. 2, pp. 250–260, Mar. 2012.

[17] J. Kushner, D. Blankschtein, and R. Langer, "Evaluation of hydrophilic permeant transport parameters in the localized and non-localized

transport regions of skin treated simultaneously with low-frequency ultrasound and sodium lauryl sulfate," *Journal of Pharmaceutical Sciences*, vol. 97, no. 2, pp. 906–918, 2007.

[18] S. Mitragotri, D. A. Edwards, D. Blankschtein, and R. Langer, "A mechanistic study of ultrasonically-enhanced transdermal drug delivery," *Journal of Pharmaceutical Sciences*, vol. 84, no. 6, pp. 697–706, Jun. 1995.

[19] G. B. Kasting and L. A. Bowman, "DC Electrical-Properties of Frozen, Excised Human Skin," *Pharm Res*, vol. 7, no. 2, pp. 134–143, Feb. 1990.

[20] S. Mitragotri, J. Farrell, H. Tang, T. Terahara, J. Kost, and R. Langer, "Determination of threshold energy dose for ultrasound-induced transdermal drug transport," *Journal of Controlled Release*, vol. 63, no. 1, pp. 41–52, 2000.

[21] J. Kushner, D. Blankschtein, and R. Langer, "Experimental demonstration of the existence of highly permeable localized transport regions in low-frequency sonophoresis," *Journal of Pharmaceutical Sciences*, vol. 93, no. 11, pp. 2733–2745, 2004.

[22] H. Tang, S. Mitragotri, and D. Blankschtein, "Theoretical description of transdermal transport of hydrophilic permeants: Application to low-frequency sonophoresis - Tang - 2001 - Journal of Pharmaceutical Sciences - Wiley Online Library," *Journal of Pharmaceutical Sciences*, 2001.

[23] B. E. Polat, P. L. Figueroa, D. Blankschtein, and R. Langer, "Transport

pathways and enhancement mechanisms within localized and non-localized transport regions in skin treated with low-frequency sonophoresis and sodium lauryl sulfate," *Journal of Pharmaceutical Sciences*, vol. 100, no. 2, pp. 512–529, Aug. 2010.

[24] P. Dechadilok and W. M. Deen, "Hindrance factors for diffusion and convection in pores," *Industrial & Engineering Chemistry Research*, vol. 45, no. 21, pp. 6953–6959, 2006.

[25] W. Yuan, Y. Lv, M. Zeng, and B. M. Fu, "Non-invasive measurement of solute permeability in cerebral microvessels of the rat," *Microvascular Research*, vol. 77, no. 2, pp. 166–173, Mar. 2009.

[26] D. Miller, N. Smith, M. Bailey, G. Czarnota, K. Hynynen, I. Makin, American Institute of Ultrasound in Medicine Bioeffects Committee, "Overview of Therapeutic Ultrasound Applications and Safety Considerations," *Journal of ultrasound in medicine : official journal of the American Institute of Ultrasound in Medicine*, vol. 31, no. 4, pp. 623–634, Apr. 2012.

[27] B. E. Polat, D. Blankschtein, and R. Langer, "Low-frequency sonophoresis: application to the transdermal delivery of macromolecules and hydrophilic drugs," *Expert Opin. Drug Deliv.*, vol. 7, no. 12, pp. 1415–1432, Dec. 2010.

[28] I. Lavon, N. Grossman, J. Kost, E. Kimmel, and G. Enden, "Bubble growth within the skin by rectified diffusion might play a significant role in sonophoresis," *Journal of Controlled Release*, vol. 117, no. 2, pp. 246–

255, Feb. 2007.

Chapter 4

Microneedles for Drug Delivery via the Gastrointestinal Tract

4.1. Introduction

Oral drug administration remains the preferred method particularly when compared to parenteral routes [1], [2]. Oral drug delivery, however, is limited by poor drug absorption and drug degradation. This is of particular concern for the biologic class of drugs (such as insulin, monoclonal antibodies and nucleic acids), which are susceptible to proteases, endonucleases, bacteria, and the extremes in pH encountered in the GI tract [3]. As a result, biologics are not currently orally administrable and require delivery through injection. Several approaches have been pursued in an attempt to enable oral administration of biologics, including co-administration with enzyme inhibitors, chemical modification of the drug, polymeric micro- and nano- carriers, liposome carriers, as well as targeted nanoparticles [4]-[6]. However, these approaches require reformulation of the active pharmaceutical ingredient (API) to ensure both compatibility with the specific technique and that the activity of the API is maintained. Physical methods of administration provide an alternative means of delivery, requiring minimal reformulation of the drug, providing a potentially broad delivery platform. Similarly, these methods have the potential to deliver macromolecules. Microneedle-based technology has been extensively evaluated for transdermal drug and vaccine delivery [7] to many parts of the body, including the perianal skin area for the treatment of fecal incontinence [8]. Unlike the skin,

the GI tract is insensate and therefore provides a unique opportunity for the use of needle-based delivery systems. Moreover the likelihood of efficacy and safety of delivery across the GI barrier with needles is supported by the extensive gastroenterological experience with GI mucosal injection as well as by the literature on the ingestion of foreign objects. Epinephrine injections in the GI tract are part of the standard of care with respect to the treatment of bleeding ulcers as well as polypectomy-induced GI bleeding [9]. Despite being used for localized vasoconstriction of bleeding vessels at ulcer sites, a common observation during these procedures is a near immediate tachycardic response in the patient [9], supporting the systemic bioavailability of epinephrine when administered via the GI mucosa [10]. With regards to safety, inadvertent or purposeful ingestion of sharp and foreign objects has helped establish clinical guidelines with respect to object characteristics and object length for risk stratification of clinical complications and therefore guidance for clinical management [11]. Surprisingly, the overwhelming majority of foreign objects, including sharp objects, are capable of being passed via the GI tract without complications [12]. A large case series of 542 patients reporting the ingestion of foreign bodies noted that in those patients where foreign bodies were retained and surgical removal was required, the size range of the objects was large; approximately 3-16cm [13] well above the size range of needles used in the proposed ingestible devices. Taken together, these prior observations would suggest that drug delivery may be possible from a capsule containing needles in a safe manner. Specifically, one could imagine an ingestible capsule containing radially-protruding microneedles

that could be used as a platform for the oral delivery of a broad range of therapeutics currently limited to injection (Figure 4-1). This presents a highly novel and unexplored route of drug administration. However, this technology would only warrant further study if such a device could be safely passed, and if the bioavailability of drugs administered in this way were comparable to that achieved through subcutaneous injection. To address these two questions, here we investigate the safety and passage of such a device and explore the impact of direct injection in the GI tract on the bioavailability of a model biologic. To this end, here we report a series of experiments to establish the use of needle-based delivery of a model biologic macromolecule (insulin) via the GI tract. First, we establish the kinetics of delivery in the different portions of the GI tract and compare them to the kinetics achieved through traditional subcutaneous injection. We then examine the safety and feasibility of passing a model device, as well as its approximate retention time, for the purpose of guiding the design of subsequent microneedle-based GI drug delivery systems.

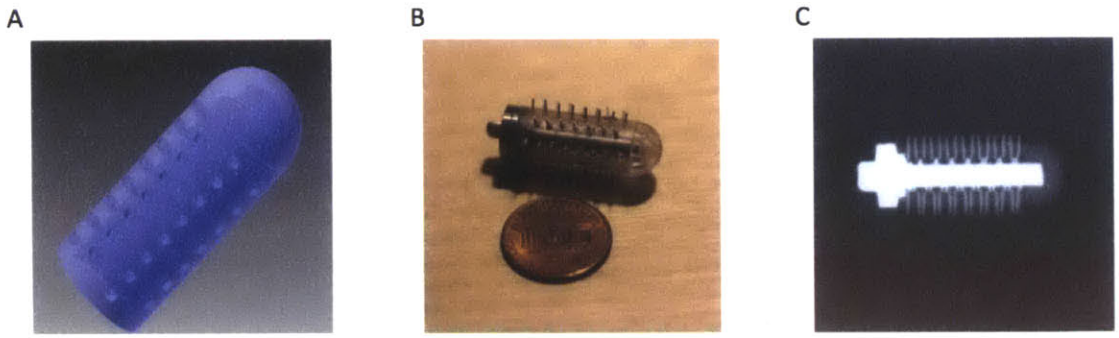

Figure 4-1: A cylindrical microneedle pill for the oral administration of biologic drugs. (A) Computer-aided design of the radial prototype housing used for *in vivo* safety evaluation. (B) Finished prototype used for *in vivo* safety showing the metal endcap and pin. (C) Radiography of the prototype in (B). Pill length 2cm, diameter 1cm, needle gauge – 25G.

4.2. Materials and Methods

4.2.1. Device Design and Construction

Computer aided design software (Solidworks, Dassault Systemes, Waltham MA) was utilized for the design of the prototype for safety evaluation (Figure 4-1A). This was fabricated from clear acrylic and 25G needles protruding 5mm from the surface were fitted manually into the orifices. The device was 2cm in length and 1cm in diameter. A central metallic core was included for increasing the radio-opacity for rapid radiographic detection of the device.

4.2.2. *In Vivo* Insulin Delivery

All procedures were conducted in accordance with protocols approved by the Massachusetts Institute of Technology Committee on Animal Care. Insulin was chosen as a model biologic because it is recognized to have negligible oral bioavailability. It also induces a rapid physiological response (reduction of blood glucose), which can be readily monitored and quantified in real-time. *In vivo* porcine studies were performed on 3 Yorkshire pigs weighing approximately 75-80kg. Prior to the procedures, the animals were fasted overnight. On the day of the procedure, the morning feed was withheld and the animal was sedated. Following induction of anesthesia with intramuscular injection of Telazol (tiletamine/zolazepam) 5mg/kg, xylazine 2mg/kg, and atropine 0.05 mg/kg, the pigs were intubated and maintained on isoflurane (1-3% inhaled). After sedation, a catheter was placed in the femoral vein using the Seldinger technique to allow for frequent blood sampling. Prior to administration of insulin, 4mL blood

samples were taken from the catheter in the femoral vein to quantify the animal's starting blood-glucose levels. A real-time readout was achieved using a TRUEtrack® blood glucose meter (Nipro Diagnostics Inc., Fort Lauderdale, FL) and the remainder of the blood sample was saved in a blood collection tube with sodium fluoride and EDTA to minimize further glucose metabolism (Beckton Dickinson, Franklin Lakes, NJ). All data shown represents the blood-glucose values quantified from the blood collection tubes.

Following baseline blood collections to establish an initial blood-glucose level, 10 units of rapid acting insulin aspart (NovoLog, Novonordisk, Bagsværd, Denmark) in 1ml of 0.9% saline was administered using a 25G Carr-Locke Needle (US Endoscopy, Mentor, OH). Injections were performed in triplicate on separate experimental days in the stomach, duodenum, colon and skin. A submucosal injection was confirmed via direct endoscopic visualization of a submucosal expansion. Colonic injection was preceded by a tap water enema to facilitate tissue visualization. Subcutaneous injections were performed using a 25G needle in the anterior abdominal wall of the animal. It should be noted that only one injection in one tissue area was administered to an animal on a given day. Upon injection, blood was sampled from the catheter approximately every two minutes and analyzed as described above. The animal's blood-glucose was monitored in this way until no further drop occurred or until a blood-glucose concentration of 40mg/dL was achieved in order not to harm the animal. Persistent hypoglycemia under 40mg/dL was corrected with intravenous boluses of 50% dextrose. Blood-glucose values presented are normalized by the animal's

initial value, defined as the last blood-glucose value observed before injection of insulin.

4.2.3. Evaluation of Device Passage and Safety Assessment

To place the prototype shown in Figure 4-1B, the animal was first sedated and intubated as described above. Then, an overtube (US Endoscopy, Mentor, Ohio) was placed in the esophagus. The microneedle pill was deployed in the stomach under direct endoscopic visualization. Placement was further confirmed radiographically. The animals were evaluated clinically twice daily for any evidence of obstruction including abdominal distension, lack of fecal material in the cage and vomiting while evidence of the device remained radiographically visible. Radiographs were performed every 48-72 hours. The retention time of the device was estimated based on when it was no longer visible on radiographs. Post mortem inspection of the entire GI tract confirmed passage of the device. The GI tissue was evaluated for any macroscopic evidence of damage. Furthermore, sections were taken from the pylorus, ileocecal valve and anal canal, representing the three points of constriction distal to the stomach, and evaluated for any evidence of macroscopic and microscopic damage through analysis of hematoxylin and eosin-stained tissue sections.

4.2.4. Statistical Analysis

The time necessary to observe a drop in the animal's blood-glucose as a result of insulin administration was defined as a drop in initial blood-glucose ≥

5%. Insulin administration in each tissue was repeated on separate days at least three times.

Statistical significance was assessed by one-way ANOVA. Statistical significance is defined as $P < 0.05$. All calculations were performed using MatLab R2014a (MathWorks, Natick, MA).

4.3. Results

4.3.1. Systemic Delivery of Insulin

The ability for systemic delivery of insulin was evaluated through serial injections via the gastric, duodenal and colonic mucosa of approximately 75-80kg Yorkshire pigs. Subcutaneous insulin administration was used as a comparator (Figure 4-2A). The induction of hypoglycemia was monitored following the administration of insulin, and the time to hypoglycemic onset (defined as a drop in the initial blood-glucose ≥ 5%) was used for comparison across the varying anatomic sites (Figure 4-2B-D). Hypoglycemic onset following the injection of 10 units of rapid acting insulin was observed at 23.08 +/- 7.00, 6.28 +/- 4.48, 6.66 +/- 1.65 and 16.91 +/- 6.39 minutes for subcutaneous, gastric, duodenal and colonic administration, respectively. The onset time was significantly diminished when insulin was administered via the GI tract as compared to traditional subcutaneous administration (Figure 4-2B-D). While the average onset time via the colon was shorter than that observed via the skin, the difference was not statistically significant. However, administration via the gastric and duodenal mucosa

demonstrated a significant reduction in the onset time compared to subcutaneous administration ($P < 0.008$).

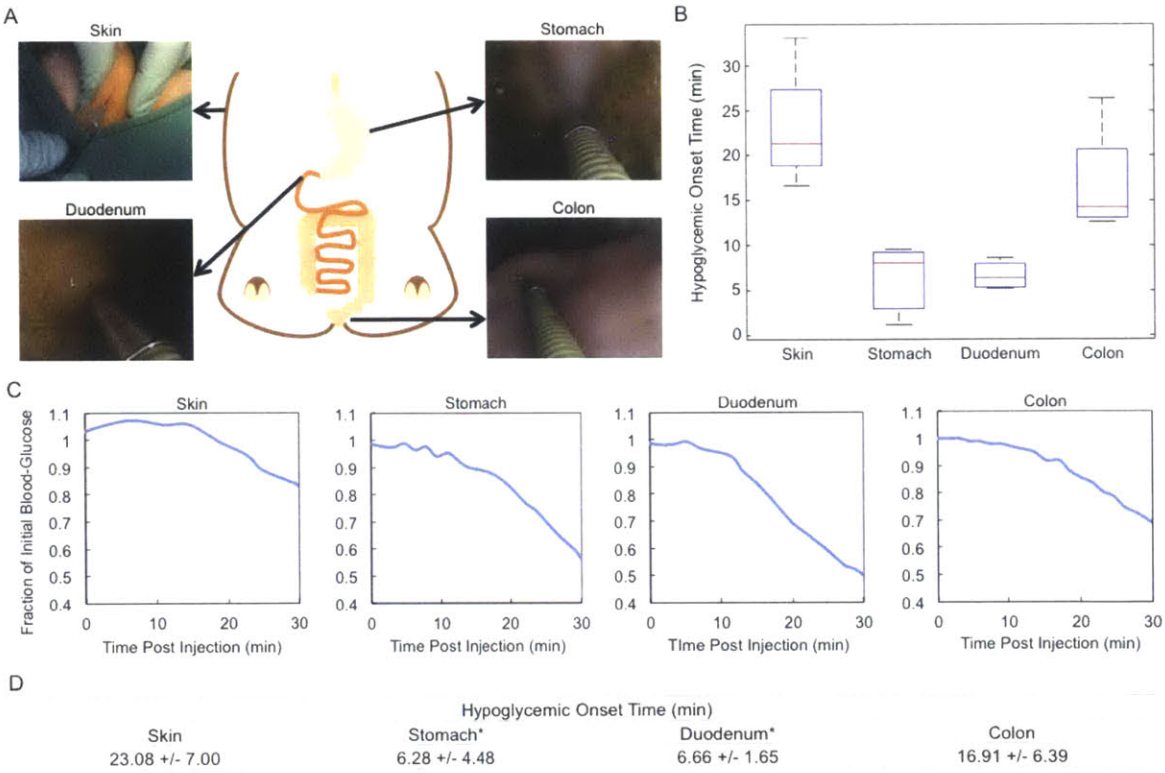

Figure 4-2: (A) Images of insulin injection in three different regions of the GI tract compared to subcutaneous administration. Clockwise from upper left: skin, stomach, colon, and duodenum. Representative images of the injections are shown. (B) Time in minutes to observe a drop in blood-glucose as a result of injection of insulin in the various GI tissue and skin. The median, 25th, and 75th percentiles are given. The whiskers indicate the most extreme data points. (C) Representative plots of normalized blood-glucose with time as a result of insulin injection subcutaneously, or through the stomach, duodenum, or colon. (D) Time in minutes to observe a drop in blood-glucose as a result of injection of insulin in the various GI tissue and skin. Averages and standard deviations are given. (*) indicates statistical significance compared to skin based on a multiple comparisons test from the ANOVA ($P < 0.008$).

4.3.2. Safety Evaluation of a Microneedle Prototype in the Gastrointestinal Tract

The safety and ability for natural passage of a microneedle-containing device via the GI tract was investigated. Safety and passage time was estimated using the custom-built device shown in Figure 4-1B. The dimensions of this prototype were modeled around those of FDA-approved ingestible devices, such as the video capsule endoscope [14]. The microneedles were placed radially around the device to ensure maximal apposition of the needles with the GI mucosa. A metal core was added to aid in the visualization of the pill on radiographs (Figure 4-1C).

The device was endoscopically deployed in the stomach of three animals as shown in Figure 4-3A. The animals were monitored daily and radiographs were taken to track the pill movement and to monitor for any evidence of intestinal obstruction or perforation (Figure 4-3B). Throughout the transit time of the prototype, all animals remained free of clinical signs of obstruction. Furthermore, radiographs remained free of evidence of intestinal obstruction or perforation. Loss of a detectable radiopaque device on the radiographs was used to determine the approximate transit time of the prototypes. The passage time of the device in three different animals was 7, 19, and 56 days. Upon loss of the radiopaque device, the animals were euthanized, and the entire GI tract was examined and found to be macroscopically normal. Further, the three sites of constriction in the GI tract distal to the site of prototype deployment (pylorus,

ileocecal valve, and anal canal) were examined and appeared normal (Figure 4-3C-E). Additionally, these three points were also fixed in formalin for histological examination (Figure 4-3C-E). Histological examination was notable for normal appearing tissue at all three sites of constriction in the GI tract in the three animals.

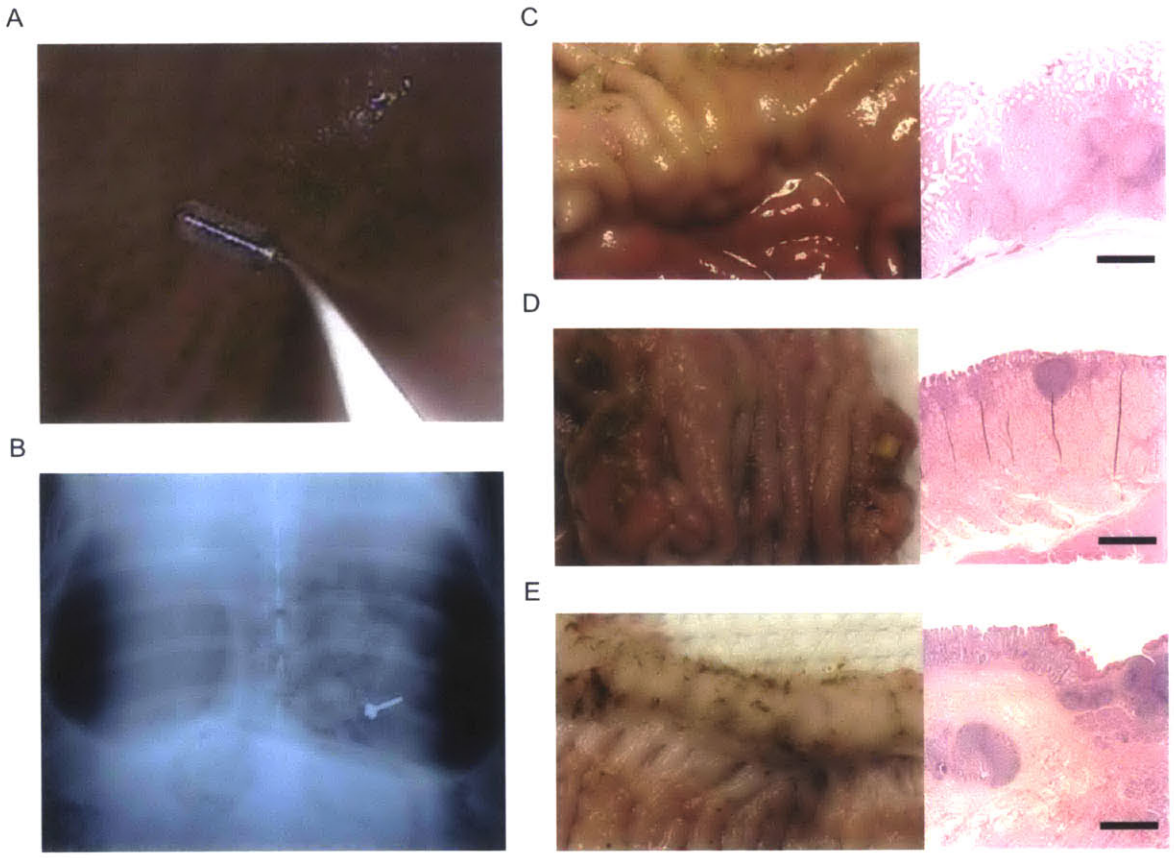

Figure 4-3: Safety assessment surrounding passage of the microneedle pill. (A) Endoscopic deployment of the device in the stomach. (B) X-rays are taken to monitor the progression of the pill. Representative gross and histological images of the (C) pylorus, (D) ileocecal valve, and (E) anal valve after natural passage of the device. The scale bar in the histology images represents 1 mm.

4.4. Discussion

Here we report *in vivo* proof-of-concept experiments supporting the feasibility and safety of microneedle-based trans-GI delivery of a macromolecule. With regards to bioavailability, delivery was found to be more effective than subcutaneous administration. Specifically, GI-based delivery afforded improved pharmacokinetics and a more robust hypoglycemic effect. Because of the extensive investigation into the use of microneedles for transdermal delivery, we compared these results to recent literature reports of microneedle-based transdermal delivery of insulin [15]-[17]. To compare delivery routes, the subcutaneous administration of insulin included in each study was used as a control. Then, the efficacy of each route relative to its respective subcutaneous control was assessed and compared qualitatively. This was done to account for differences in experimental methods across studies. In the transdermal studies, subcutaneous administration always afforded a faster hypoglycemic onset time compared to microneedle-based transdermal delivery of insulin. Even when multiple techniques were employed transdermally (microneedles and iontophoresis), subcutaneous administration afforded a faster onset time. This should be contrasted with the findings presented here, where microneedle-based trans-GI delivery affords faster onset compared to subcutaneous injection. Not having to use multiple techniques also greatly simplifies administration [15]-[17]. While the bioavailability presented here is likely to be higher than that from a fully-integrated microneedle capsule, it was critical to first demonstrate the bioavailability of therapeutics administered in this way to confirm that it is

adequate. There are many possible avenues of exploration surrounding the bioavailability achieved from a stand-alone device. For example, solid, drug-containing microneedles could be fabricated from biocompatible polymer. These could then detach from the capsule and get lodged in the GI tissue, where they could slowly release their payload (Figure 4-4). Additionally, the peristaltic motion in the GI tract could be utilized to compress the capsule, leading to release of drug only when the tissue was in intimate contact with the needles.

In addition to the bioavailability of compounds administered in this way, the safety and natural passage of such a device is paramount to further investigation. To this end, safety evaluation in the swine model confirmed the absence of any intestinal obstruction or GI mucosal damage and demonstrated the ability to pass such a device. Additionally, histological examination was notable for normal GI mucosa at the three distal points of constriction, which are at greatest risk for damage. It should be noted that 25 gauge needles were purposefully used for the device shown in Figure 4-1B. These needles have an outer diameter exceeding 500 μm, increasing the likelihood of perforation. The safe passage of this particular prototype, therefore, is reassuring and further indicative of the potential for this new method of macromolecule delivery to be safe.

With respect to retention time, typical GI retention times in pigs have previously been reported to range from 2 to 33 days [18], [19]. The large range in observed retention times of the device in this study may be attributed to the increased interaction between the microneedles and the GI mucosa but may also

reflect the transient gastric retention of the device. Specifically, the retention time of objects in the stomach of pigs has previously been estimated to range from 1 to 28 days [19]. This could be due to the quadrupedal nature. It has also been noted that gastric retention scales with object size [20]. As a result, the geometry and design of the microneedles would be another interesting area of investigation for their effect on retention time. The safety and tolerability of this device over an extended period of time, however, is encouraging and raises the possibility of using derivatives of this device for extended release oral formulations of both small molecule therapeutics as well as biologics. Taken together, this work will serve as the catalyst for a significant change in the development of oral delivery systems for macromolecules enabling the bypassing of the harsh GI mucosal environment.

4.5. Conclusions

The oral route of drug administration is the most convenient route for patients [1], [2]. However, the hostile environment present in the GI tract limits oral delivery to small molecules. As a result, the biologic class of drugs is mainly limited to needle-based administration. Physical delivery methods, such as microneedles, might enable a platform technology for the oral delivery of a broad range of substances. To this end, here we present a proof-of-concept study involving the use of microneedles for the delivery of biologics via the GI tract for the first time. The blood-glucose response kinetics of a model macromolecule, insulin, was significantly improved compared to the subcutaneous route when

administered via the GI tract, demonstrating that the bioavailability of a model compound is still adequate when administered via injection in the GI tract. To investigate the potential tolerability of such a device, results surrounding the safe passage of such a device were presented. Specifically, a model device having exposed radially-protruding microneedles was safely passed via the GI tract without any evidence of tissue damage. With additional injvestigation, we anticipate multiple variations of devices enabling the oral administration of therapeutics from capsules containing microneedles. These include utilizing the peristaltic motion of the GI tract to stimulate microinjection using hollow microneedles, or needle dislodgement where the needles are fabricated of drug-loaded polymers (Figure 4-4). By demonstrating the potential safety and efficacy of this method, this study provides the basis for further development of integrated microneedle devices for oral macromolecule delivery.

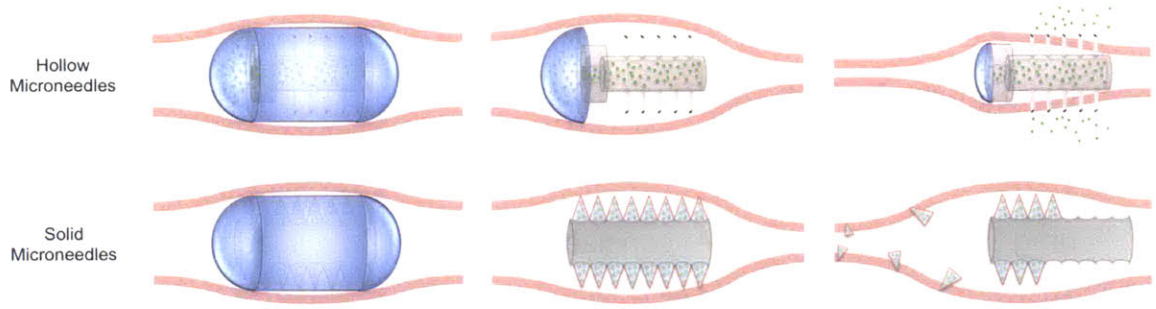

Figure 4-4: Therapeutic use concept of the microneedle pill. Both hollow and solid microneedles could be used. In both cases, the pill's needles are initially coated by a pH-responsive coating to aid in ingestion (left). When the pill has reached the desired location in the GI tract, the coating dissolves, revealing the microneedles (middle). In the case of hollow microneedles (top right), the drug reservoir is compressed through peristalsis, releasing the drug through the needles. In the case of solid microneedles (bottom right), the drug is formulated into the microneedles. The microneedles penetrate the tissue and break off of the pill, leaving the needle to release the drug in a controlled manner, based on the needle formulation.

4.6. References

[1] S. Mignani, S. El Kazzouli, M. Bousmina, and J.-P. Majoral, "Expand classical drug administration ways by emerging routes using dendrimer drug delivery systems: A concise overview," *Advanced drug delivery reviews*, vol. 65, no. 10, pp. 1316–1330, Oct. 2013.

[2] M. M. Borner, P. Schoffski, R. de Wit, F. Caponigro, G. Comella, A. Sulkes, G. Greim, G. J. Peters, K. van der Born, J. Wanders, R. F. de Boer, C. Martin, and P. Fumoleau, "Patient preference and pharmacokinetics of oral modulated UFT versus intravenous fluorouracil and leucovorin: a randomised crossover trial in advanced colorectal cancer.," *Eur J Cancer*, vol. 38, no. 3, pp. 349–358, Feb. 2002.

[3] Y. Aoki, M. Morishita, K. Asai, B. Akikusa, S. Hosoda, and K. Takayama, "Region-Dependent Role of the Mucous/Glycocalyx Layers in Insulin Permeation Across Rat Small Intestinal Membrane," *Pharm Res*, vol. 22, no. 11, pp. 1854–1862, Jul. 2005.

[4] K. Chaturvedi, K. Ganguly, M. N. Nadagouda, and T. M. Aminabhavi, "Polymeric hydrogels for oral insulin delivery.," *Journal of controlled release : official journal of the Controlled Release Society*, vol. 165, no. 2, pp. 129–138, Jan. 2013.

[5] M. A. Radwant and H. Y. Aboul-Enein, "The effect of oral absorption enhancers on the in vivo performance of insulin-loaded poly(ethylcyanoacrylate) nanospheres in diabetic rats.," *Journal of Microencapsulation*, vol. 19, no. 2, pp. 225–235, Mar. 2002.

[6] "Folate-decorated PLGA nanoparticles as a rationally designed vehicle for the oral delivery of insulin," Sep. 2012.

[7] "Microneedles for drug and vaccine delivery," vol. 64, no. 14, pp. 1547–1568, Nov. 2012.

[8] C. Baek, M. Han, J. Min, M. R. Prausnitz, J.-H. Park, and J. Park, "Local transdermal delivery of phenylephrine to the anal sphincter muscle using microneedles," *Journal of Controlled Release*, pp. 1–10, May 2011.

[9] "Gastroenterological endoscopy," Stuttgart [Germany] ; New York : Thieme, 2010.

[10] "Ventricular tachycardia after endoscopic injection of epinephrine for bleeding ulcer," vol. 95, p. 2618, Aug. 2000.

[11] "Management of ingested foreign bodies and food impactions," vol. 73, no. 6, pp. 1085–1091, Jun. 2011.

[12] "Management of swallowed razor blades-retrieve or wait and see?," vol. 53, no. 4, pp. 477, 486, Apr. 2004.

[13] "Ingested foreign bodies of the gastrointestinal tract: retrospective analysis of 542 cases," vol. 20, no. 8, pp. 1001–1005, Oct. 1996.

[14] "Wireless capsule endoscopy.," vol. 405, no. 6785, p. 417, May 2000.

[15] "The development and characteristics of novel microneedle arrays fabricated from hyaluronic acid, and their application in the transdermal delivery of insulin.," vol. 161, no. 3, pp. 933–941, Aug. 2012.

[16] "Transdermal delivery of insulin using microneedle rollers in vivo.," vol. 392, no. 1, pp. 127–133, Jun. 2010.

[17] "Iontophoresis-driven penetration of nanovesicles through microneedle-induced skin microchannels for enhancing transdermal delivery of insulin.," vol. 139, no. 1, pp. 63–72, Oct. 2009.

[18] V. Snoeck, N. Huyghebaert, E. Cox, A. Vermeire, J. Saunders, J. P. Remon, F. Verschooten, and B. M. Goddeeris, "Gastrointestinal transit time of nondisintegrating radio-opaque pellets in suckling and recently weaned piglets.," *J Control Release*, vol. 94, no. 1, pp. 143–153, Jan. 2004.

[19] M. Hossain, W. Abramowitz, B. J. Watrous, G. J. Szpunar, and J. W. Ayres, "Gastrointestinal transit of nondisintegrating, nonerodible oral dosage forms in pigs.," *Pharm Res*, vol. 7, no. 11, pp. 1163–1166, Nov. 1990.

[20] "Gastric emptying of tablets and granules in humans, dogs, pigs, and stomach-emptying-controlled rabbits.," vol. 81, no. 12, pp. 1170–1174, Dec. 1992.

Chapter 5

Ultrasound-Mediated Gastrointestinal Drug Delivery

5.1. Introduction

The delivery of macromolecules across the gastrointestinal (GI) tract is one of the most highly investigated areas of research in drug delivery. Delivery via the GI tract, however, is still limited to small molecules [1]. Even delivery of small molecules can be challenging, with most drugs often requiring specialized formulations to stabilize the active pharmaceutical ingredient and provide optimal absorption in the GI tract. Therefore, a platform that could allow for the delivery of a broad range of therapeutics without the need for time-consuming and costly reformulation could present a paradigm shift in delivery science and have wide clinical impact. Physical methods of drug delivery, such as ultrasound, may be capable of delivering macromolecules while circumventing the need for extensive formulation development. Despite being investigated for other uses, ultrasound has never been studied for drug delivery in the GI tract to the best of our knowledge.

Ultrasound is a longitudinal pressure wave with frequencies above the audible range (> 20 kHz). Clinically, ultrasound is utilized in a variety of settings, including ultrasonography, tumor ablation, and lithotripsy [2]-[4]. These applications mainly utilize high-frequency ultrasound (> 1 MHz). At low frequencies (< 100 kHz), however, ultrasound has unique properties including the

ability to transiently permeabilize, and propel therapeutic substances into, tissue by a phenomenon known as transient cavitation [5]. Transient cavitation can be induced using a variety of ultrasound probe configurations, including axial and radial emission. Furthermore, the optimal ultrasound configuration could be adjusted depending on the condition being treated, maximizing the potential generalizability of this modality.

Using a physical delivery modality such as ultrasound to maximize drug delivery to the GI tract could have broad clinical utility. Inflammatory bowel disease represents one set of conditions that may be amenable to ultrasound assisted drug administration. These are a debilitating set of conditions associated with high morbidity and a negative impact on quality-of-life [6]. The most common subtype is ulcerative colitis [6]. First line therapy for ulcerative colitis includes aminosalicylates administered via the oral and rectal routes, with the latter being recognized as more efficacious, particularly with mild to moderate disease activity [6]-[9]. However, rectal (enema) treatment efficacy is directly dependent on retention time and tissue drug absorption [8], [10], which is challenging for patients suffering from diarrhea and frequent bowel movements. Therefore, the use of ultrasound to maximize local mucosal concentrations of aminosalicylates in the rectum, while reducing the necessary retention time of the enema, could be one potential application of this technology with significant clinical impact and benefit for patients who must currently self-administer medicated enemas.

In addition to therapeutic delivery to the rectum locally, a physical delivery modality could also allow for the systemic delivery of a wide-range of compounds, shifting the way in which diseases are targeted and treated. Therefore, we hypothesized that the use of ultrasound as a physical delivery platform would enable a significantly greater amount of drug to be delivered in all segments of the GI tract. As an initial proof-of-concept, we first evaluate the delivery of model therapeutics across a broad range of molecular weights in all portions of the GI tract *ex vivo.* Specifically recognizing the potential impact of the use of this platform technology in the rectum, we then focused our studies on the delivery of topical therapeutics currently used for the management of inflammatory bowel disease. The current standard of care is the self-administration of medicated enemas. As a result, the simultaneous application of an ultrasonic probe that also administered the medicated enema would not present a hurdle to adoption for these patients. Additionally, higher mucosal concentrations of these agents have previously been shown to correlate with decreased disease activity [8], [11]. Moreover, we show the capacity for ultrasound-mediated gastrointestinal delivery (UMGID) in varying probe configurations (axial and radial) in the rectum in both small and large animal models, thereby demonstrating adaptability to varying clinical and research scenarios.

5.2. In Vitro Methods

5.2.1. Chemicals

Phosphate buffered saline (PBS), hydrocortisone, mesalamine, and inulin from Dahlia Tubers (5,000 Da), and deuterated dimethyl sulfoxide (DMSO) were obtained from Sigma-Aldrich (Saint Louis, Missouri). Granular D-glucose was obtained from Mallinckrodt Chemicals (Phillipsburg, New Jersey). Lysine-fixable 3 and 70 kDa dextrans labeled with Texas Red were purchased from Invitrogen (Carlsbad, California). All radiolabeled chemicals were obtained from American Radiolabeled Chemicals, Inc. (St. Louis, Missouri) and included ^{3}H-labeled glucose and hydrocortisone ,^{14}C-labeled mesalamine and 5,000 Da inulin. The tissue solubilizer Soluene-350 and scintillation cocktail Hionic-Fluor were obtained from Perkin-Elmer (Waltham, Massachusetts). Solutions of the four compounds at a concentration of 1 mg/mL were prepared with a radiolabel content ranging between 0.001–2.5% depending on the stock solution's radiolabel content.

5.2.2. Tissue Preparation

The MIT Committee on Animal Care approved all animal-related research aspects of this study. GI tissue from Yorkshire pigs was procured within 20 minutes of animal euthanization and stored at 4°C. Drug delivery testing took place within 6 hours of euthanization. All tissue was obtained from Research 87, Inc. (Boylston, Massachusetts). Upon delivery, tissue was washed with PBS and excess fat was carefully dissected away. With the exception of tongue tissue,

the full thickness of the tissue was used for testing. The tissue was sectioned into approximately 2 cm by 2 cm pieces and kept hydrated with PBS. The receiver chambers of Franz diffusion cells (15 mm-diameter, PermeGear, Hellertown, Pennsylvania) were filled with PBS and the tissue placed on top with the luminal side up. These diffusion cells result in an exposed area of 1.77 cm^2. Unless otherwise noted, delivered quantities represent the total amount of permeant delivered over this area. A donor chamber was placed on top of the tissue and the entire assembly clamped tightly together. The donor chamber was then filled with PBS to keep the tissue hydrated before treatment. The variability in thickness of tongue tissue prevented mounting of the entire thickness in the diffusion chambers. Instead, the top surface was isolated with an electric dermatome (Zimmer Orthopedic Surgical Products, Dover, Ohio) to a thickness of 700 μm and then dissected into sections approximately 1 inch square. After all the required tissue had been dissected and mounted in Franz diffusion cells, the cells were randomly assigned to the various experimental groups.

5.2.3. Ultrasound Treatment

Immediately prior to ultrasound treatment, the PBS solution in the donor chamber was discarded and replaced with a 1 mg/mL solution containing radiolabeled material. Ultrasonic frequencies of 20, 40, and 60kHz were generated using three separate ultrasound generators (Sonics and Materials,

Inc., Newtown, Connecticut), the VCX 500, VCX 130, and a custom order probe, respectively. The probes provide axial emission of ultrasound.

Each horn has a 13 mm diameter tip. Three separate powers at each frequency were tested and each calibrated by calorimetry using an unlined dewar. Calorimetry was employed because this specific method is commonly used in the literature to estimate ultrasonic power [12]. The three powers at 20 kHz were 2.5, 5, and 7.5 W/cm^2. At 40 kHz they were 7.3, 10.5, and 13.4 W/cm^2. At 60 kHz the powers were 9.6, 11.5, and 12.4 W/cm^2. The difference in powers tested at each frequency were due to the sensitivities and efficiency of each ultrasound generator. Regardless of frequency or power, all treatments lasted for a total of 1 minute of ultrasound exposure using a 50% duty cycle (5s on, 5s off) with the ultrasound horn tip 3 mm away from the surface of the tissue.

Immediately after treatment, the donor solution was discarded and the donor compartment washed with PBS to remove any residual radiolabeled material not delivered into the tissue. The receiver solution was collected through the sampling port of the diffusion cell using a 15-mL transfer pipet (VWR, Radnor, Pennsylvania) and placed in a scintillation vial. The portion of the tissue exposed to the compound of interest was cut away and also placed in a scintillation vial, with any remaining tissue being discarded. The number of repeats ranged from 3 to 10 for every treatment condition. In general, untreated tissue required more repeats (n = 6). Esophagus also required more repeats due to the macroscopic non-uniformity of the tissue.

5.2.4. Quantifying Radiolabeled Material Delivered

Depending on the tissue type, either 5 (tongue, and intestine) or 10 mL (all other tissue) of Soluene-350 were added to the sample to solubilize the tissue. This mixture was heated and allowed to sit until the tissue was completely dissolved. Regardless of the tissue, 5 mL of the Soluene-tissue mixture were aliquoted into a second scintillation vial for radiometric analysis.

The collected receiver solutions were thoroughly mixed and then a 0.5 mL sample was aliquoted into a second scintillation vial. 15 mL of Hionic-Fluor scintillation cocktail was then added to both the receiver solution and soluene-tissue aliquot samples and allowed to sit for 1 h for the signal to equilibrate. The samples were evaluated on a Tri-Carb Liquid Scintillation Counter (Perkin Elmer, Waltham, Massachusetts).

5.2.5. Mixing Studies

Tissue samples were mounted in Franz diffusion cells as detailed above. A 1 mg/mL solution of glucose spiked with 2 μCi/mL tritiated glucose was used as the model permeant. Immediately before treatment, the donor cell was filled with 1.5 mL of the glucose solution and a 5 mm magnetic stir bar was added. The donor cell was then capped and an inverted stir plate was placed on top of the cells ensuring stirring of the donor solution without the stir bar directly agitating the tissue. A Bell-Ennium 9-position magnetic Stirrer was used to stir the receiver chamber at 500 RPM. The donor chambers were agitated for two minutes total and then immediately removed. The diffusion cell was then

disassembled and the receiver solution and tissue sampled for radiometric analysis according to the procedure described above. The agitated samples were compared to samples treated with the same glucose solution and 20 kHz ultrasound at 2.5 W/cm^2 according to the same treatment conditions detailed above. A third control group was also tested which received neither ultrasound nor stirring. Each study group utilized 6 repeats.

5.2.6. Temperature Enhancement Studies

In order to better understand the role of thermal effects in the delivery enhancement, intestinal tissue was treated *ex vivo* and the temperature monitored remotely over the course of the treatment. Specifically, tissue was mounted in 15 mm-diameter Franz diffusion cells as described previously. The tissue was then treated for two minutes with 20 kHz ultrasound set to an intensity of 7.5 W/cm^2 at a duty cycle of 50% (1 minute of ultrasound). During the treatment, the temperature of the donor chamber was monitored remotely using a thermal imaging camera (FLIR E50, FLIR systems, Inc., Belgium). Immediately after treatment the coupling solution was discarded and the tissue surface was also imaged with the thermal camera to quantify the tissue temperature. Three biological replicates were performed. The measured temperature was noted to be below 40 $^{\circ}$C.

The temperatures noted above during ultrasound treatment were then used to test whether heating tissue could enhance delivery. Specifically, separate tissue samples were mounted in 15 mm-diameter Franz diffusion cells.

Heat treatment was applied using a circulating water bath (VWR, Radnor, Pennsylvania). Specifically, tubing with an outer diameter of 7 mm was fitted to the inlet and outlet of the water bath and insulated. This tubing was then placed in the donor chamber of diffusion cell in an orientation ensuring the donor chamber would fill and maintain a fixed level of fluid. The water bath was filled with deionized water and set to a temperature of 40 $^{\circ}C$ using the digital temperature controller and confirmed via thermometer. Treatment consisted of either two- or five-minutes of continuous flow of the heated water over the tissue. To control for any tissue disruption as a result of the flowing water, separate diffusion cells were also treated similarly with room temperature water. Immediately after treatment, the donor chamber was filled with a 1 mg/mL solution containing tritiated glucose. This solution was allowed to diffuse for two minutes maintaining constant the permeant contact time across experiments. After exposure, the tissue and receiver chamber were collected and sampled for radiometric content as described previously. Three biological repeats were performed for each water bath treatment.

5.2.7. High-Frequency Ultrasound Enhancement Studies

To characterize the contributions of transient cavitation and acoustic streaming to the mechanism of enhancement, 1 MHz ultrasound was evaluated. 1 MHz was chosen because the threshold for transient cavitation is recognized to be well above intensities achievable clinically [13]. Therefore, any enhancement would be a result of acoustic streaming or stable cavitation. The larger diameter

of commercially available high-frequency ultrasound probes necessitated the use of a larger diffusion cell. Specifically, 29 mm-diameter diffusion cells with a receiver chamber volume of 29 mL were utilized. These diffusion cells result in an exposed area of 6.6 cm^2. Tissue was mounted as described previously. The donor chamber was filled with a 1 mg/mL solution containing tritiated glucose. 1 MHz ultrasound was generated using a Dynatron D125 ultrasound probe digitally programmed to an intensity of 2 W/cm^2 (determined to be 5.22 W via calorimetry) and continuous operation (Dynatronics, Salt Lake City, Utah). Because of the reduced power, treatment was carried out for longer than two minutes. Specifically, tissue was exposed so as to keep constant the total ultrasonic power delivered to the tissue at the highest intensity tested (40 kHz at 13.4 W/cm^2). The resulting treatment time, therefore, was 3.4 min. Post treatment, the donor solution was discarded and the tissue washed and sectioned as described previously. Each treatment condition (1 MHz ultrasound or no ultrasound) was repeated three times. As a result of the differences in glucose exposure time and tissue area exposed, results are presented as the ratio of glucose delivered to treated and untreated tissue.

5.2.8. Aluminum Foil Pitting Experiments

To assess whether transient cavitation is occurring, pits resulting from ultrasound treatment were quantified in aluminum foil as has been done previously in the literature [14]. Sheets of aluminum foil (Reynolds, Richmond, Virginia) were cut into inch-square pieces, avoiding wrinkling. Using vacuum

grease, the aluminum foil squares were mounted on the receiver compartment of 15 mm diameter Franz diffusion cell. The vacuum grease enabled the aluminum foil to adhere to the receiver compartment of the diffusion cells. The receiver chamber was then filled with PBS and the cell submerged in PBS. The samples were treated with either 20, 40, or 60 kHz ultrasound at the highest intensity considered for each frequency for 2 seconds. The horn tip was positioned 1 cm above the surface of the aluminum foil. This ensured that the number of discrete pits were not too numerous to quantify. After treatment, the samples were gently peeled from the receiver chambers and mounted on heavy card stock paper. These were then scanned using a Canon CanoScan 8800F at 1200 dpi in grayscale mode and saved in the BMP file format. Pits were then counted manually from these images.

5.2.9. Pore-Size Study

The permeability (P_i) was determined using the following method. Side-by-side diffusion cells (PermeGear, Hellertown, Pennsylvania) with an inner diameter of 9 mm were used for the experiment. Tissue was placed between the two compartments and clamped together with the luminal side facing the donor chamber. Stir bars were added to both the donor and receiver chambers and agitated using a Bell-Ennium 9 position magnetic Stirrer.

The donor solution consisted of 2 μCi/mL ^{3}H-glucose and 2 μCi/mL ^{14}C-labeled inulin. Each donor cell was filled with 3 mL of this solution and the receiver solution was filled with 3 mL fresh PBS. 100 μL samples were taken

from the receiver chamber at 10-minute intervals and replaced with an equal volume of fresh PBS over the course of an hour. 15 mL of Hionic Fluor were then added to these samples and analyzed for tritiated decomposition and ^{14}C decomposition. Seven repeats were performed for the Control, and 17 for the Treated. The need for more repeats for the ultrasound-treated group was as a result of the heterogeneous nature of the permeabilization.

5.2.10. Dextran Permeation Study

In order to visualize the permeation of molecules as a result of simultaneous ultrasound treatment, colonic tissue was treated *in vitro* with dextran labeled with Texas red in the donor chamber. Specifically, porcine tissue was mounted in 15 mm-diameter Franz diffusion cells as described previously. Skin was treated with 20 kHz ultrasound at the highest power considered as described previously. The coupling solution contained either 3 or 70 kDa dextran at a concentration of 1 mg/mL. Immediately after treatment, the coupling solution was discarded and the tissue washed thoroughly with PBS to remove any residual dextran. The diffusion cell was then disassembled and the tissue exposed to dextran carefully dissected and fixed in 10% formalin. The tissue sections were then mounted in paraffin blocks. Two, 8 µm-thick sections separated by a 200 µm step were then mounted to glass microscope slides for subsequent imaging of the tissue. Tissue samples not treated with ultrasound were also exposed to dextran keeping the permeant contact time constant (2 minutes). These samples were subsequently processed similarly.

Resulting histology slides were imaged by the microscopy core facility in the Swanson Biotechnology Center. Imaging was performed with an Olympus FV-1000MP multiphoton microscope with a 25x, 1.05 N.A. objective. Samples were excited at 860 nm using a Ti-Sapphire pulsed laser (Spectra-Physics, Santa Clara, CA). Emission was collected with a 607/70 nm band-pass filter and collagen was imaged by second harmonic generation at 430 nm. Individual image channels were combined in ImageJ.

5.2.11. Effect of Sonication on Therapeutic Compound Structure

Mesalamine and hydrocortisone samples at a concentration of 4 mg/mL were prepared in deuterated DMSO. 1.5 mL samples were sonicated with 20 kHz ultrasound at the highest intensity considered as described above. Three biological replicates were performed. Unsonicated samples were used as the control. ^{1}H NMR spectra were recorded on a Varian 500 (^{1}H, 500 MHz) spectrometer and processed using Mnova (MestraLab, Santiago de Compostela, Spain). ^{1}H NMR spectra were referenced with residual non-deuterated solvent shifts (DMSO-d5 = 2.5 ppm). All shifts are reported in ppm.

The effect of sonication on insulin was also tested. 200 units of rapid-acting insulin aspart was formulated in 10 mL of PBS. This sample was then sonicated with 20 kHz ultrasound at the highest intensity considered as described above. Three biological repeats were performed for both sonicated and unsonicated groups. Insulin structure was analyzed by reversed phase analytical HPLC using an Agilent ZORBAX Eclipse Plus C18 column (4.6 x 100

mm, 3.5 μm), with a mobile phase gradient from 95% to 5% of acetic acid (1.5%) in H_2O in acetonitrile over 15 minutes.

5.3. *In Vivo* Methods

5.3.1. Porcine Model

Both female and male Yorkshire pigs between 70-80 kg in weight were used for this study based on the availability of sex from the vendor. Before every experiment, the animal was fasted overnight. Sedation was induced with intramuscular injection of Telazol 5 mg/kg, xylazine 2 mg/kg, and atropine 0.04 mg/kg. The animal was then intubated and sedation maintained with isoflurane (1-3% inhaled). The rectum was cleared with a tap water enema. A clean rectum was confirmed by colonoscopy prior to treatment. Control and Treatment tests were performed on separate days. A PBS solution of mesalamine at the same volume (60 mL) and concentration (66.6 mg/mL) used clinically was prepared. The ultrasound treatment was applied using a 20 kHz horn for 2 minutes at a 50% duty cycle at an intensity of 7.5 W/cm^2. Colonic areas treated with ultrasound were then biopsied using endoscopic biopsy forceps (US Endoscopy, Mentor, Ohio) for drug delivery evaluation as well as histological analysis (n = 13). For Control samples, the ultrasound probe was inserted into the colon, but not turned on (n = 16). All procedures were conducted in accordance with protocols approved by the Massachusetts Institute of Technology Committee on Animal Care.

5.3.2. Drug Mass Evaluation from Colonic Biopsies

This work was performed by MPI Research Inc., (State College, Pennsylvania) in a blinded fashion. Briefly, tissue was ground and mixed with phosphate buffered saline and precipitated with 10% trichloroacetic acid. The resulting supernatant was extracted with ethyl acetate. This extract was dried with anhydrous sodium sulfate, transferred to a glass tube, and evaporated to dryness under nitrogen. Then, the sample was reconstituted with toluene and derivatized with BSTFA + TMCS(99:1) (Sigma Aldrich, Saint Louis, Missouri) and heated at 60˚C for 30 min. Finally, the sample was allowed to cool to room temperature and analyzed by GC/MS. An Agilent 5973 MSD/6890 Gas Chromatograph with a Rtx-5, 30 m x 0.25 mm x 0.1 µm column (Restek Corporation, Bellefonte, Pennsylvania) was used for the analysis.

5.3.3. Insulin Delivery

In addition to the preparation noted above, a central venous catheter was placed in the femoral vein using the Seldinger technique to allow for frequent blood sampling. Before administration of insulin, 4 mL blood samples were drawn from the femoral vein to quantify the animal's initial blood-glucose levels. A real-time readout was achieved using a TRUEtrack® blood glucose meter (Nipro Diagnostics Inc., Fort Lauderdale, Florida). The remaining blood sample was saved in a blood collection tube with sodium fluoride and EDTA to minimize further glucose metabolism (Beckton Dickinson, Franklin Lakes, New Jersey). All

data shown represents the blood-glucose values quantified from the blood collection tubes, which was evaluated in a blinded fashion.

Once the rectum was cleared and the animal's base-line blood-glucose quantified, a 10 mL enema containing 100 units of rapid-acting insulin aspart (NovoLog, Novonordisk, Bagsværd, Denmark) was instilled in the colon and blood samples taken at approximately 2-minute intervals. The ultrasound treatment regimen was unchanged from that used for mesalamine testing. The blood-glucose was monitored for at least 40 min, depending on the experiment's effect on blood-glucose. When necessary, hypoglycemia was corrected with intravenous boluses of 50% dextrose (only needed when ultrasound treatment took place). The presented blood-glucose values are normalized by the animal's starting value, defined as the last blood-glucose value observed before administration of insulin. Each treatment regimen was repeated three times.

5.3.4. Dextran Sodium Sulfate-Induced Murine Colitis Model

15-week old, female C57BL/6 mice were purchased from Charles River Laboratories (Wilmington, Massachusetts) for the induction and treatment of dextran sodium sulfate (DSS)-induced Colitis. Five animals were utilized per group. This was based on power calculations utilizing our results in pigs demonstrating an order-of-magnitude increase in drug delivery using ultrasound. Therefore, a similar improvement in stool score to that seen in prior experiments in rats with mesalamine administered at 3% and 30% were conservatively expected [1], [10]. Using a significance level of 0.05, a sample size of 5 animals

per group achieves 90% power to detect the predicted difference of 4 in the stool score based on previously published results [2]-[4], [10] and given the expected order-of-magnitude improvement in mesalamine delivery observed in the pig model. A sample size of 5 per group has also been suggested in previously published protocols [5], [15], [16]. Each cage (group) was used as it was received and randomly assigned to experimental groups by the researchers performing the work. On day 1, blood was drawn from all mice and an initial weight of each animal was taken. Colitis was induced according to previously published protocols, with slight modifications [6], [15]. Specifically, colitis was induced with 40-50 kDa DSS (Affymetrix Inc., Santa Clara, California). Starting on day 1, a 3% w/w DSS solution was administered in drinking water *ad libitum.* On days 3 and 5, the drinking solution was replaced with fresh DSS solution. On day 7, the DSS solution was removed and replaced with normal drinking water.

Treatment was administered starting on day 2. Treatment consisted of either a mesalamine enema alone or in combination with ultrasound. The enema consisted of mesalamine (66.6 mg/mL) in a 0.5% w/w carboxymethyl cellulose (Sigma-Aldrich Saint Louis, Missouri) solution in PBS. Here, a custom-designed 40 kHz probe was fabricated to allow for insertion into the colon (Sonics and Materials, Inc., Newtown, Connecticut). The shaft was 2 mm in diameter and contained two, 3 mm diameter protrusions at half-wavelength intervals to achieve radial ultrasound emission. The power of ultrasound treatment was calibrated to 4.0 W by calorimetry. The probe was inserted into the rectum and turned on for 0.5 seconds. The animals were monitored daily for weight, fecal consistency,

and for the presence of fecal occult blood using Hemoccult cards (Beckman Coulter, Pasadena, California).

Fecal consistency and the presence of blood was scored based on previously published protocols [6], [10], [17]. Specifically, stool consistency was scored as follows: (1) normal pellet-like feces, (2) pellet of stool easily crushed, (3) soft, watery stool with granules present, or (4) diarrhea. The presence of blood was confirmed by hemoccult testing daily. Animals with negative hemoccult results were scored (1). Positive hemoccult results were further stratified as follows: (2) feces with discrete blood speckles on the surface, (3) feces stained with blood, or (4) feces completely covered with blood or the presence of blood staining around the anus. The total fecal score was the summation of the consistency and blood score. Therefore, the total fecal score ranged from 2-8. If feces could not be collected on an individual day, that animal was assigned a total fecal score of 8.

On day 14, a final weight was taken and fecal score assessed. Blood was taken, and the animal euthanized. Immediately after euthanasia, the colon was dissected out and imaged macroscopically. It was then fixed in 10% formalin. Once fixed, the colon was sectioned into 2-6 pieces and mounted in paraffin. Two, 8 μm sections were taken from each paraffin block separated by a 200 μm step. The sections were stained with hematoxylin and eosin and mounted on glass microscope slides.

Histological examination was performed by a clinical pathologist at the Massachusetts General Hospital in a single-blinded fashion. Scores were

determined according to previously published protocols [6]-[9], [15], [17] with slight modification as follows: Score 0: Normal colonic mucosa with preservation of normal crypt architecture. Score 1: Shortening of the crypts with moderate chronic inflammatory infiltrate above the muscularis mucosae. Score 2: Base of the mucosa effaced but residual surface epithelium and upper portion of the crypt preserved. Score 3: Complete effacement of the mucosa with chronic inflammation of the lamina propria and only residual surface epithelium present. Score 4: Complete effacement and erosion of the mucosal surface with fibrinopurulent debris present. Each tissue cross-section present on the microscope slide (n = 2-6) was scored individually between 0-4 with a corresponding percentage involvement (rounded to the nearest quartile). The resulting score for each cross section examined for every animal in a given study group was then averaged to determine the histology score for that study group.

A separate cohort of animals that did not have disease induced were used to test the safety and tolerability of ultrasound in the rectum. Insertion of the probe into the rectum (n = 5), and insertion of the probe followed by sonication (n = 5) were tested in healthy animals using the same QD treatment regimen detailed above. These groups were compared to a control group that received no treatment (n = 5). The total fecal score was assessed daily and hematocrit and hemoglobin were quantified on day 1 and day 14. On day 14, the animals were euthanized and the liver, spleen, pancreas, kidney, small intestine, and colon were carefully dissected, fixed in formalin, mounted in paraffin, and sectioned and stained as described above. Additionally, a separate colonic

tissue sample was saved and immediately frozen at -80 °C for cytokine determination.

These tissue samples were processed to extract RNA. RNA was isolated using an Ambion Purelink RNA Mini Kit following the manufacturer's protocol. Concentration and quality of the resulting RNA were determined using a NanoDrop 2000 Spectrophotometer (Thermo Scientific, Waltham, Massachusetts). Cytokine mRNA was quantified using the Mouse Inflammatory Panel from nanoString Technologies (Seattle, Washington) following the manufacturer's protocol. Results were normalized using internal negative and positive controls.

5.3.5. Statistical Analysis

Statistical analysis for the *in vitro* and *in vivo* porcine work was performed using two-tailed Student's *t*-tests to determine statistical significance. Statistical analysis for the *in vivo* mouse work was performed using one-way analysis-of-variance (ANOVA) tests with multiple comparisons. No samples were excluded from analysis in this study. Statistical significance was defined throughout as $P < 0.05$. All calculations were performed in MatLab R2014a (MathWorks, Natick, MA).

5.4. Results

5.4.1. Proof-of-Concept Use of Ultrasound for Drug Delivery *Ex Vivo*

To understand whether ultrasound could safely permeabilize GI tissue to allow for enhanced drug delivery and to identify the optimal conditions for UMGID, we developed an *ex vivo* platform utilizing fresh porcine GI tissue mounted in Franz diffusion cells (see Figure 5-1a). We focused on the use of low-frequency (< 100 kHz) ultrasound given prior data supporting increased cavitational activity at typical intensities compared to high-frequency (> 1 MHz) ultrasound at the same intensities [8], [10], [18]. First, we evaluated the transport of tritiated glucose as a model permeant comparing its delivery to all major segments of the GI tract. 20 kHz ultrasound was utilized and calibrated to an intensity of 7.5 W/cm^2. This intensity was selected based on calorimetry measurements demonstrating a negligible increase in the temperature of the coupling solution, thereby minimizing thermal effects. We found that the mass of glucose delivered to GI tissue was enhanced by as much as an order-of-magnitude when delivery was combined with one minute of ultrasound treatment (two-tailed Student's t-test, $P < 0.03$) (see Figure 5-1b). To further understand the frequency and intensity dependencies and identify the optimal parameters of UMGID, glucose delivery was tested using three distinct frequencies, 20, 40, and 60 kHz at 3 separate intensities for each frequency in all tissue-types of the GI tract. Because transient cavitation was hypothesized to be the dominant mechanism, these frequencies were chosen to ensure the cavitation threshold could be exceeded. To assess the effect of analyte molecular weight and

because glucose is actively absorbed across the GI tract by glucose transporters, this same survey was carried out using inulin (5,000 Da). Inulin was chosen for its lack of recognized active absorption via the GI epithelium [8], [11], [19]. As a result of this test, delivery was found to be more greatly enhanced at frequencies of 20 and 40 kHz compared to 60 kHz (see Supplementary Figure 5-1). Delivery was relatively insensitive to the intensity at all frequencies. To characterize the tissue distribution of ultrasound-mediated analyte delivery, we evaluated the distribution of 3 and 70 kDa dextran labeled with Texas red. Without ultrasound, there was no visible permeation of 3 or 70 kDa dextran into colonic tissue (Figure 5-1f). This is to be contrasted with the use of 20 kHz ultrasound, which enabled significant penetration of both 3 and 70 kDa dextran into the tissue. Dextran was observed throughout the entire thickness of the colonic tissue when ultrasound was utilized. This suggests that ultrasound enables drug to rapidly permeate the tissue. This was further confirmed by analyzing the distribution of radiolabeled compounds between the tissue and receiver chamber. The permeant content in the tissue was significantly greater than that present in the receiver chamber as a result of ultrasound treatment. Inulin delivery to colonic tissue, for example, resulted in 90-fold more inulin in the tissue compared to that in the receiver chamber on average.

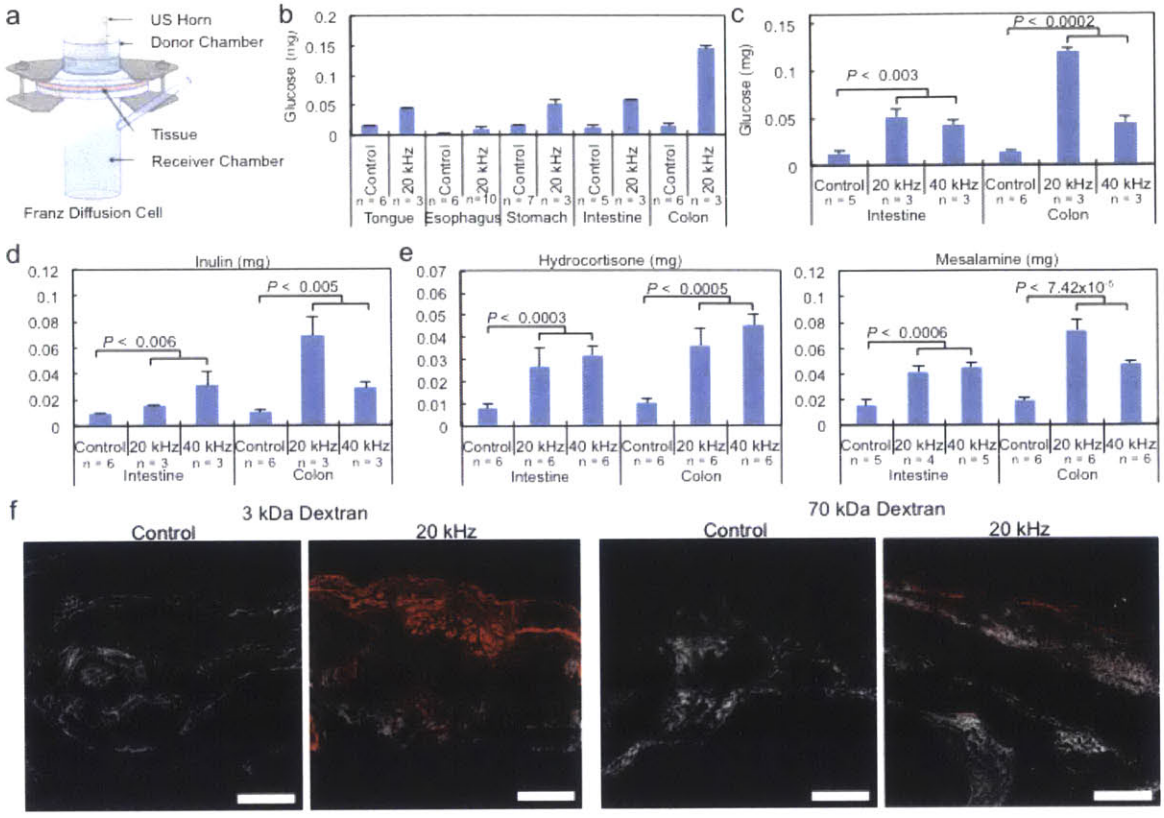

Figure 5-1: (a) *In vitro* experimental setup, the Franz diffusion cell. The receiver chamber is first filled with PBS. A section of fresh GI tissue is then placed over the receiver chamber, and a donor chamber is placed on top of the tissue. The entire assembly is then clamped together to prevent leakage. The receiver chamber is inspected to ensure that there are no air bubbles present in the PBS. Immediately before treatment, the donor chamber is filled with a solution containing the permeant of interest and an ultrasound horn (either 20, 40, or 60 kHz) is submerged in the permeant solution. (b) Comparison of the amount of glucose delivered to various tissues of the GI tract with (20 kHz) and without (Control) ultrasound. The treatment utilized a 20 kHz ultrasound horn calibrated calorimetrically to 7.5 W/cm^2. The duration of treatment was two minutes with the horn set to pulse (50% duty cycle 5 s on, 5 s off, resulting in one minute of

ultrasound exposure). Delivery utilizing ultrasound was significantly greater than passive delivery (two-tailed Student's t-test, $P < 0.03$). (c) Survey of glucose delivery to intestine and colon using 20 and 40 kHz ultrasound at the lowest intensity considered for each frequency. A solution of 1 mg/mL glucose was utilized in the donor chamber. Treatment duration was again two minutes at 50% duty cycle, as described above. Treatment using ultrasound resulted in significantly greater delivery in both tissues. (d) The same survey described in (c) was also performed using 5,000 Da inulin at a concentration of 1 mg/mL in the donor cell. Again, delivery was greater when ultrasound was used. (e) The same survey described in (c) and (d) was then carried out using the clinically relevant compounds hydrocortisone and mesalamine. Both molecules were loaded in the donor chamber at a concentration of 1 mg/mL. (f) Multiphoton microscopic images of cross-sections of colonic tissue exposed to dextrans labeled with Texas red with and without treatment with 20 kHz ultrasound. The red channel and second harmonic are shown. The scale bar represents 500 μm. All graphs represent averages and standard deviations. Sample sizes indicated are biological replicates. Each individual experiment was replicated once. Because not all experiments could be performed from one organ, controls were run for each additional organ procured to account for potential inter-tissue variability. All *P*-values shown represent two-tailed Student's t-tests.

Having shown that ultrasound can enhance delivery for all tissue types encountered in the GI tract *ex vivo* and identified optimal treatment conditions with this novel GI delivery modality, we focused our studies on the delivery of topical therapeutics currently used for the management of inflammatory bowel disease utilizing 20 and 40 kHz axial emission. Higher mucosal concentrations of these agents have previously been shown to correlate with decreased disease activity [8], [11], [20]-[22]. Radiolabeled mesalamine (5-aminosalicylic acid) and hydrocortisone, both recognized topical treatments for inflammatory bowel disease, were evaluated with UMGID. Mesalamine was evaluated in the small and large intestine where it is used clinically. Hydrocortisone was evaluated throughout the GI tract in keeping with its broader clinical application. All treatment times were maintained at 1 minute of total ultrasound exposure, ensuring a practical treatment regimen compatible with the high-throughput nature of clinical endoscopy as well as patient self-administered enemas. Mesalamine delivery to the intestine was 14.97 ± 5.10, 41.52 ± 4.45, and 44.43 ± 3.67 μg without ultrasound (control), and with 20 and 40 kHz, respectively. Delivery to the colon was 18.40 ± 2.73, 73.70 ± 8.39, and 47.37 ± 3.05 μg for the control, 20, and 40 kHz, respectively. Hydrocortisone delivery was enhanced 2-5 fold throughout the GI tract also using 20 and 40 kHz ultrasound (see Figure 5-1e and Supplementary Figure 5-1).

5.4.2. Transient Cavitation is Responsible for Permeabilization

Based on prior studies evaluating phenomena associated with ultrasound transmission through liquids, we postulated that three mechanisms could be contributing to the observed enhancement: 1) transient cavitation, 2) acoustic streaming, and 3) thermal effects [13], [18], [23], [24]. To elucidate which mechanism was dominant, we evaluated the delivery of tritiated glucose to the small intestine under the isolated effects of heating the tissue, stirring the donor chamber (to mimic general agitation which would reduce the diffusive boundary layer), as well as sonication with 1 MHz ultrasound at an intensity below the threshold for cavitation to isolate the effect of acoustic streaming. These regimens were compared to delivery using 20 and 40 kHz ultrasound. Treatment of tissue *ex vivo* mounted in Franz diffusion cells using 20 kHz ultrasound at 7.5 W/cm^2 was found to raise the donor chamber temperature to 40 $^{\circ}C$ at the end of treatment (Figure 5-2a). There was no difference between the donor chamber temperature and the probe temperature at the end of treatment. Therefore, the enhancement in delivery as a result of heating tissue to 40 $^{\circ}C$ was tested. Heating of small intestine tissue *ex vivo* to 40 $^{\circ}C$ for two or five minutes provided no enhancement in delivery compared to the control (Figure 5-2a,b). The impact of acoustic streaming and agitation was then assessed (Figure 5-2c). Tissue was sonicated with 1 MHz ultrasound to achieve the same energy delivered to the tissue as that delivered using the highest intensity considered in this study (40 kHz at an intensity of at 13.4 W/cm^2). This treatment resulted in no enhancement in glucose delivery. Stirring of the donor chamber was also

considered. Stirring did enhance delivery by a factor of 2.10 compared to the control. However, that enhancement and the absolute amount of glucose was significantly less than that achieved with 40 kHz ultrasound. The fact that heating the tissue does not provide an enhancement in delivery suggests that thermal effects do not contribute significantly to the delivery observed using low-frequency ultrasound for the time intervals noted. Acoustic streaming, similarly, would seem to not contribute significantly to the mechanism of enhancement based on the use of 1 MHz ultrasound not enabling any enhancement in delivery. Taken together, these results suggest that UMGID is facilitated primarily by transient cavitation.

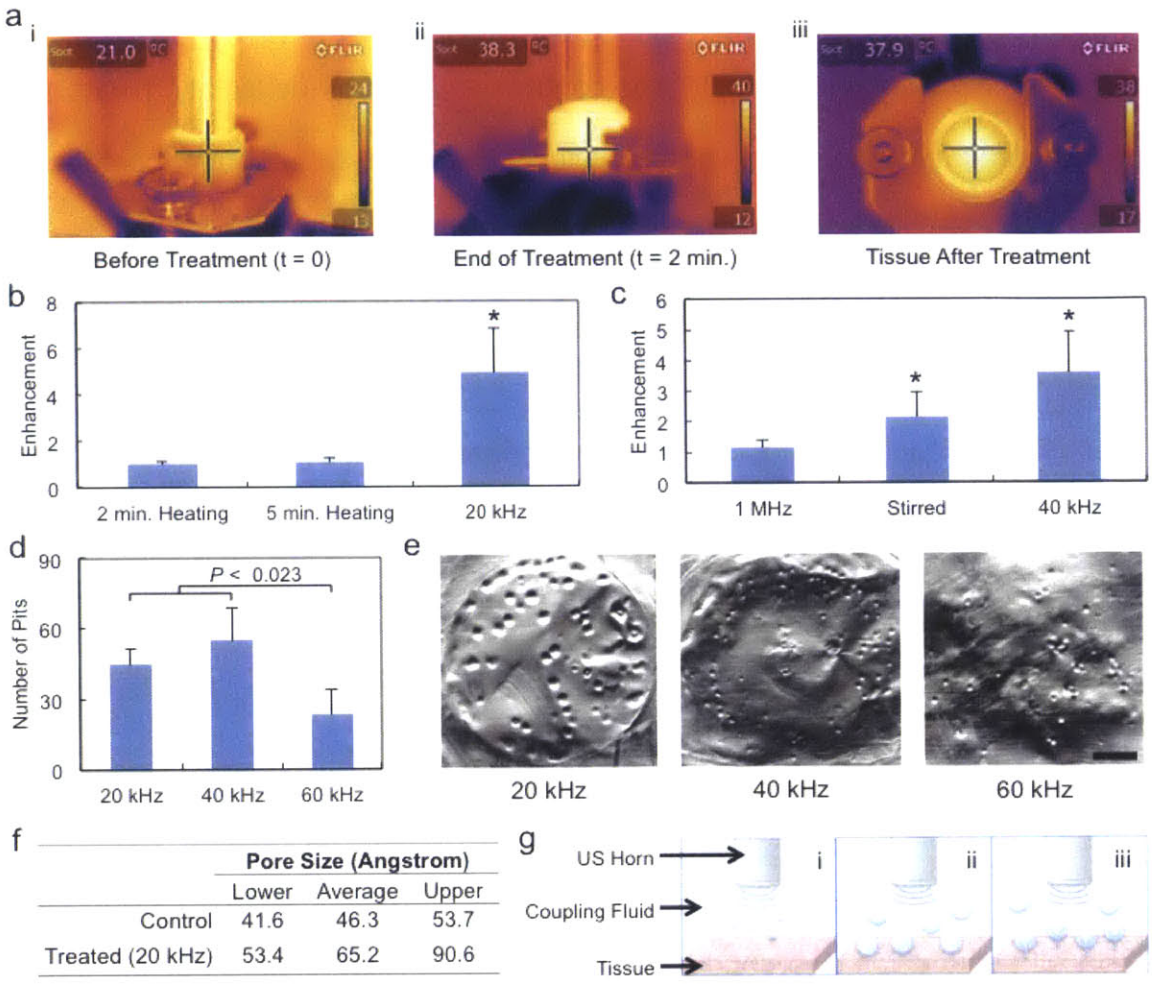

Figure 5-2: (a) Representative infrared heat maps of intestinal tissue treated *ex vivo* with 20 kHz ultrasound set to an intensity of 7.5 W/cm^2 at a duty cycle of 50% for 2 minutes total (i) before treatment has started, (ii) at the end of the ultrasound treatment, and (iii) the tissue surface immediately after having discarded the coupling solution post treatment. The lower- and upper-bounds of temperature in the field of view are shown on the right side of each image. The temperature displayed in the upper-left of each image is the temperature at the crosshairs. The highest temperature observed was 40 °C. (b) Relative enhancement in glucose delivery to small intestine as a result of exposing the

tissue to water maintained at 40 °C using a circulating water bath for two or five minutes (n = 3 for each treatment). The control consisted of recirculating water at room temperature two or five minutes. This is compared to the enhancement in delivery using 20 kHz ultrasound set to an intensity of 7.5 W/cm^2 at a duty cycle of 50% for 2 minutes total (control n = 5, ultrasound n = 3). (*) indicates a statistical difference between the treatment and its respective control determined by a two-tailed Student's t-test. (c) Relative enhancement in glucose delivery to small intestine as a result treatment with 1 MHz ultrasound set to 2 W/cm^2 (5.22 W actual) for 3.4 min (n = 3), stirring of the donor chamber (control n = 5, stirring n = 6), and 40 kHz ultrasound set to an intensity of 13.4 W/cm^2 (control n = 5, ultrasound n = 3). (*) indicates a statistical difference between the treatment and its respective control determined by a two-tailed Student's t-test. (d) Number of pits observed in aluminum foil pitting experiments when treated using 20, 40, or 60 kHz ultrasound for 2 seconds at the highest intensity considered for each frequency (n = 5 for each frequency). (e) Representative images of pitted aluminum foil samples treated with either 20, 40, or 60 kHz ultrasound. The scale bar represents 3 mm. (f) Estimation of pore size radius created in small intestine tissue as a result of ultrasound exposure using the Aqueous Porous Pathway Model. (g) Diagram of the hypothesized mechanism of ultrasound-enhanced GI delivery. Ultrasound emission results in the formation of cavitation bubbles in the fluid (i). As treatment continues, the number of nucleated bubbles increases and the bubbles move around chaotically and grow in size through a process known as rectified diffusion (ii). Finally, some of the bubbles reach a

threshold size above which they are no longer stable. These bubbles implode, creating a jet of fluid, referred to as a microjet, which impinges against the tissue and drives drug in (iii). All graphs represent averages and standard deviations. Sample sizes indicated are biological replicates. Each individual experiment was replicated once. Because not all experiments could be performed from one organ, controls were run for each additional organ procured to account for potential inter-tissue variability.

To confirm the generation of transient cavitation by the application of the various low-frequency ultrasound probes tested in this study, aluminum foil pitting experiments were carried out. Pitting of aluminum foil has been previously validated as an assay for transient cavitation [14], [25]. The number of pits generated with 20 and 40 kHz was found to be statistically greater than the number of pits generated with 60 kHz ultrasound (one-way ANOVA with multiple comparisons, $P < 0.023$, Figure 5-2d,e). Conversely, no pitting was visible when 1 MHz ultrasound was applied.

Lastly, because these results suggest that transient cavitation is occurring, theoretical pore sizes generated in the small intestine as a result of treatment with 20 kHz ultrasound were calculated utilizing hindered-transport theory with radiolabeled glucose and inulin as the model permeants [26]. The permeability of each molecule in tissue not treated with ultrasound was found to be $1.28 \times 10^{-4} \pm 5.05 \times 10^{-5}$ and $1.36 \times 10^{-5} \pm 6.77 \times 10^{-6}$ cm/min respectively. In ultrasound treated samples, the average permeability of glucose and inulin was $1.95 \times 10^{-4} \pm 4.84 \times 10^{-5}$ and $2.94 \times 10^{-5} \pm 1.36 \times 10^{-5}$ cm/min respectively. Ultrasound was found to result in a statistically higher permeability for both glucose and inulin (two-tailed Student's t-test, $P \leq 0.008$). These values were then used to calculate the theoretical pore sizes. The upper limit on the calculated theoretical pore radii in untreated intestine was found to be 53 Å, compared to an upper limit of 90 Å in treated samples (Figure 5-2f, Supplementary Equations 5-1 through 4, Supplementary Figure 5-2, Supplementary Table 5-1).

5.4.3. *In Vivo* Delivery using Axial UMGID in Swine

Given the efficacy of UMGID that we observed *in vitro*, as well as prior observations that drug delivery by traditional methods is generally greater *in vivo* than *in vitro*, we hypothesized that this technology would translate into even greater degrees of drug delivery enhancement *in vivo* [27]. Further, two different configurations of UMGID were tested *in vivo* for delivery efficacy: axial emission in swine and radial emission in mice (described below). Both hand-held devices were lightweight and had dimensions amenable to insertion into the rectum. *In vivo* evaluation was first performed utilizing axial emission of 20 kHz ultrasound in Yorkshire pigs. The size of the probe tip that was inserted is comparable to the size of a standard colonoscope. Safety evaluations were performed through the insertion of the 20 kHz probe into the rectum (Figure 5-3a) followed by biopsies of the treated site and an adjacent, untreated area of the colonic mucosa. Gross and histological views of the tissue pre- and post-ultrasound treatment are shown in Figure 5-3b. Clinical monitoring of the animals demonstrated overall initial safety. Histological examination demonstrated only minor epithelial disruption in < 5% of the treated area examined as determined by a clinical pathologist. Specifically, there was minor cellular disarray in the control samples, which was determined to be an artifact due to the fixation procedure. In the samples treated with ultrasound, patchy saponification of the adipose tissue was noted. Further, minimal congestion of intramucosal capillary vessels located in the superficial submucosa was noted. There was no evidence of epithelial damage and mucosal integrity was maintained. The efficacy of mesalamine

delivery was then assessed with the same 1 minute treatment regimen used in the *in vitro* testing. A mesalamine enema at the concentration and volume used clinically (Rowasa® (mesalamine) 4 g in 60 mL suspension [28]) was instilled in the swine rectum immediately followed by UMGID. GC/MS-based quantification of mesalamine in tissue biopsies taken immediately following UMGID demonstrated a 22.4-fold increase in delivery using ultrasound compared to colonic tissue not treated with ultrasound ($P = 4.06 \times 10^{-4}$) (Figure 5-3c). It should be further noted that one-half of the untreated samples were found to have a drug content below the limit of detection (50 ng/g tissue). ^{1}H NMR spectroscopy was used to confirm the chemical stability of mesalamine after treatment with ultrasound (Supplementary Figure 5-3). In addition to the delivery of mesalamine, insulin, a model biologic, was evaluated to determine the potential of UMGID to deliver larger, biologically active molecules. The same 1-minute ultrasound treatment with an insulin enema resulted in a robust hypoglycemic response (Figure 5-3d). Sonication of insulin was similarly found to have no impact on its active protein structure (Supplementary Figure 5-4). Successful delivery of drugs varying in molecular weight by an order of magnitude supports the likely broad applicability of UMGID.

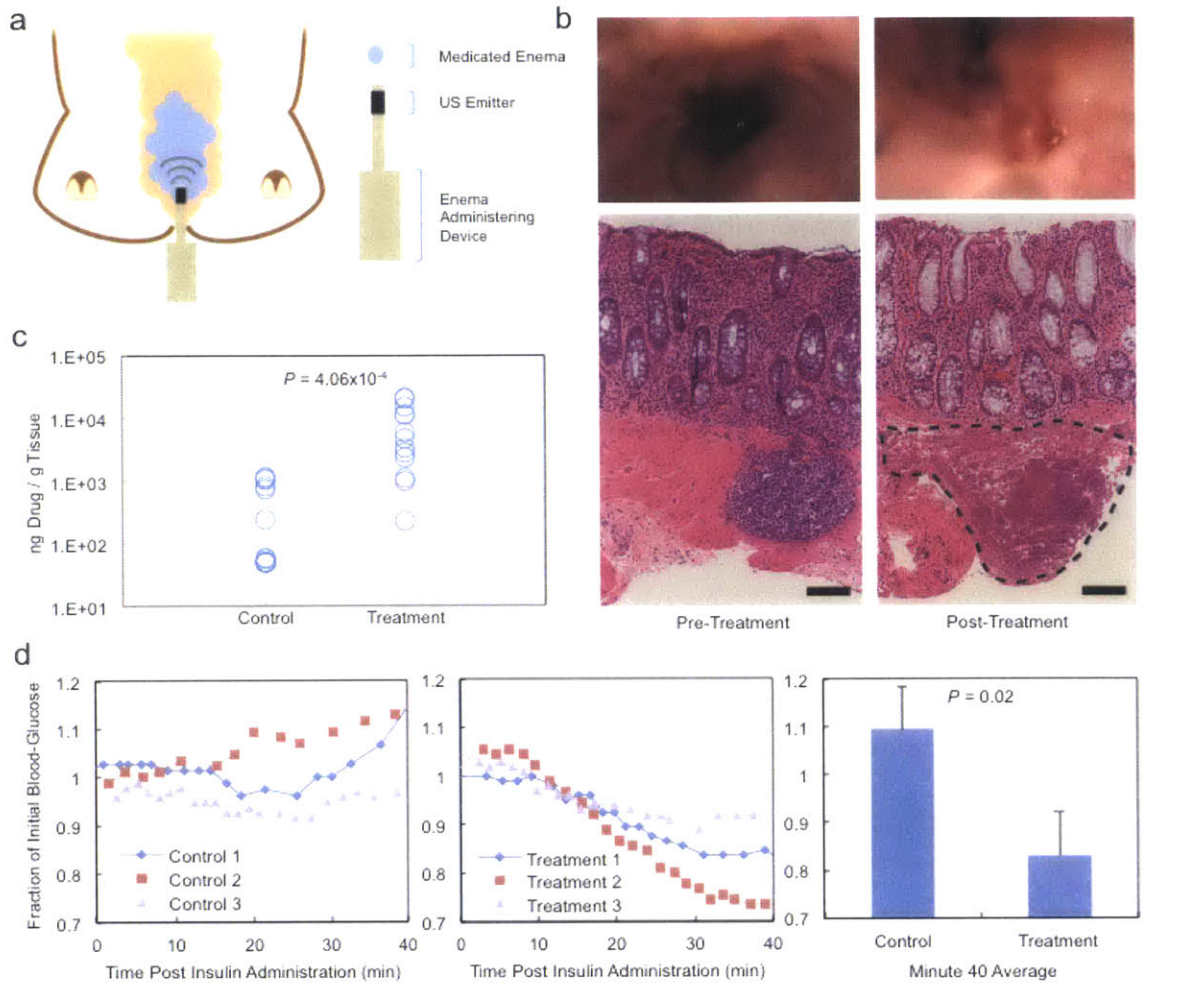

Figure 5-3: (a) Experimental setup showing placement of a medicated enema and insertion of the 20 kHz ultrasound probe in the rectum. (b) Macroscopic (top) and histological (bottom) view of the rectum pre- and post-ultrasound treatment. The outlined area indicates minor localized saponification of the muscularis in < 5% of the treated area examined. The scale bar represents 100 μm (c) Mesalamine drug content in tissue biopsies normalized by the mass of the tissue biopsy as a result of placement of a mesalamine enema in the colon without (Control) and with (Treatment) 20 kHz ultrasound. Each point represents one biological replicate (n = 16 for Control, n = 13 for Treatment). The *P*-value

represents a two-tailed Student's t-test. (d) The animal's blood-glucose normalized to its starting value as a result of placement of an enema containing 100U insulin without (left) or with (middle) simultaneous 20 kHz ultrasound treatment. Each individual curve is a biological repeat. The bar graph (right) represents the average and standard deviation after 40 minutes of monitoring. The *P*-value represents a two-tailed Student's t-test.

5.4.4. Radial UMGID Significantly Improves Colitis Activity in Mice

Finally, the clinical relevance of the enhancement in mesalamine delivery was analyzed in a murine model of dextran sodium sulfate (DSS)-induced acute colitis (Figure 5-4a). This murine model was chosen because it is recognized to not benefit from topical mesalamine administration [29], [30]. Therefore, improvement in disease indices in this model as a result of ultrasound treatment would underscore the impact of UMGID. Given the colonic anatomy and the often circumferential nature of colitis involvement, it was hypothesized that radial UMGID would be most beneficial so as to direct the treatment over the largest area of inflamed tissue. Radial emission was achieved using a custom-designed miniature ultrasound probe with dimensions amenable to insertion directly into the mouse colon (probe diameter ≤ 3 mm, see Figure 5-4b). This device was found to result in no measurable temperature increase as a result of the short treatment time and the formation of pits was confirmed in aluminum foil samples.

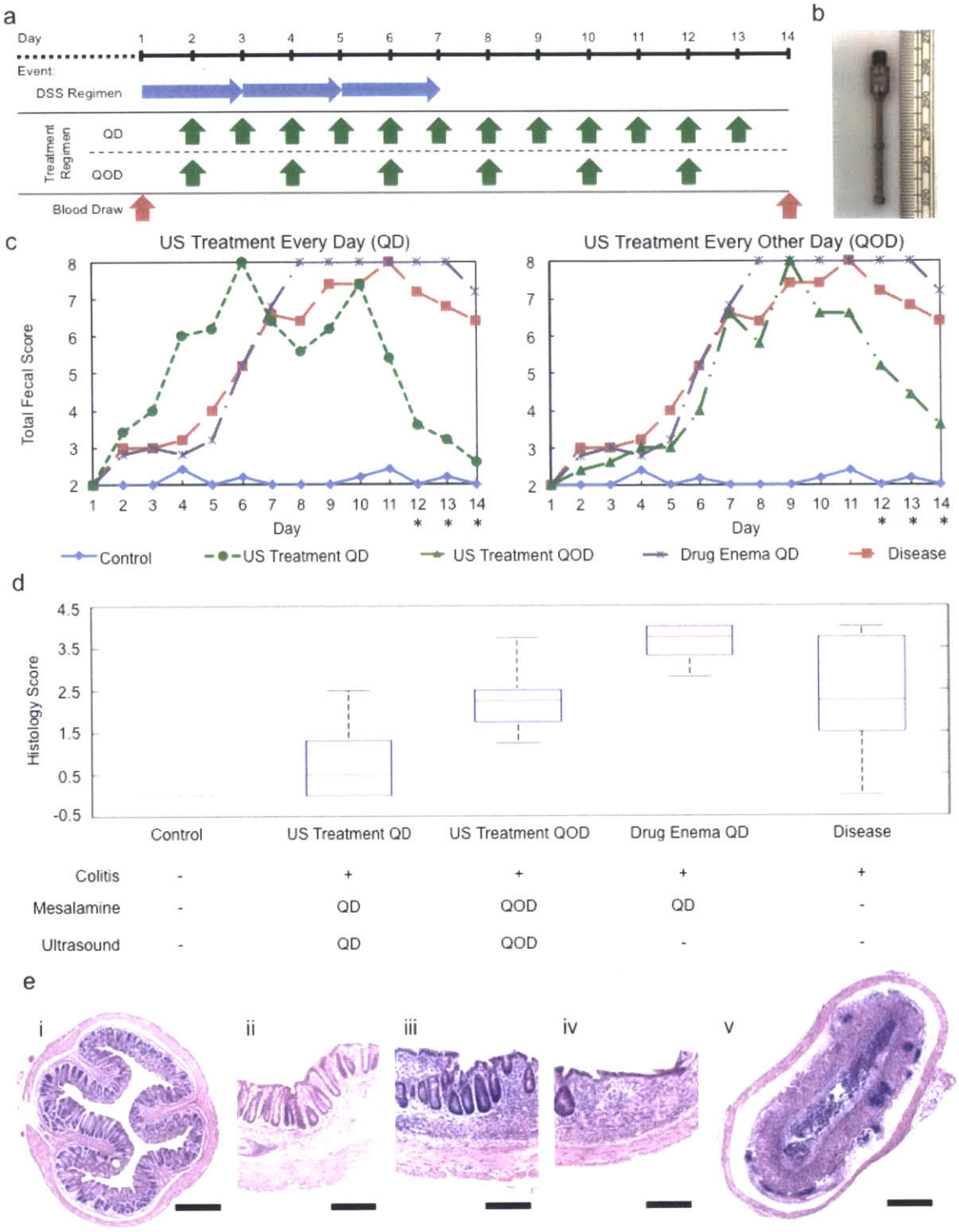

Figure 5-4: (a) Colitis induction and treatment schedule. (b) The custom-designed ultrasound probe tip with a shaft diameter of 2 mm. The two bumps shown have a diameter of 3 mm and enhance radial ultrasound emission. (c)

Total Fecal Score for healthy animals (Control) and animals with DSS-induced colitis: receiving no treatment (Disease), receiving mesalamine enema daily (Drug Enema QD), receiving mesalamine enema with ultrasound treatment daily (US Treatment QD), and receiving mesalamine enema with ultrasound treatment every other day (US Treatment QOD). All groups were comprised of 5 animals. The * indicates a statistical difference between the ultrasound Treatment groups and those groups receiving no treatment or mesalamine enema alone (one-way analysis of variance testing with multiple comparisons, $P < 0.047$). (d) Histology score of tissue sections at Day 14. The median, 25^{th}, and 75^{th} percentiles are shown. The whiskers indicate the most extreme data points. ** Indicates a statistical difference between the ultrasound QD group and all other colitis groups (one-way analysis of variance testing with multiple comparisons, $P < 2.9 \times 10^{-4}$). (e) Histological images of colonic tissue at Day 14. Representative images of tissue score: i) Score 0 (healthy tissue), ii) Score 1, iii) Score 2, iv) Score 3, and v) Score 4. The scale bar for i) and v) represents 500 μm. The scale bar for ii), iii), and iv) represents 200 μm.

The tolerability of this device was first tested in healthy animals in the absence of colitis (Supplementary Figures 5-5 and 5-6). Specifically, the effect of insertion of the probe alone and of probe insertion followed by sonication were tested. These results were compared to a control group that received no treatment. Treatment followed the daily (QD) regimen presented in Figure 5-4a. Treatment was found to be well tolerated and all animals were free of clinical signs of distress over the 14 day period. Additionally, there was no statistical difference in the animals' hematocrit or hemoglobin as a result of treatment compared to controls, suggesting that the device does not induce gross bleeding (Supplementary Figure 5-6). The histology score for colonic tissue for these animals was statistically better than the score observed for any group that had colitis induced. In addition, the liver, spleen, pancreas, kidney, and small intestine were examined for any injury as a result of treatment (Supplementary Figure 5-5). On gross examination, the organs appeared normal without any ecchymoses noted over the organs. Histologically, the organs had preservation of normal architecture with no cytologic abnormalities. Finally, cytokine levels known to be enhanced as a result of acute inflammation were profiled from colonic tissue [31]. To further evaluate potential toxicity from UMGID, cytokine expression including TNF-α, IFN-γ, IL-6, and IL-17 was performed from colonic tissue from all three groups. No difference was observed (one-way analysis of variance testing with multiple comparisons). The minimal toxicity as evaluated through the absence of anemia, low fecal score, low histology scores, and

normal cytokine levels supports the likely safety of this drug delivery modality in the GI tract.

Colitis was induced with 3% w/w DSS given *ad libitum* for seven days with concurrent treatment administration starting on day 2 (see Figure 5-4a). Administration of mesalamine in combination with QD ultrasound treatments, as well as every other day (QOD), enabled significantly faster recovery from colitis symptoms compared to daily administration of a mesalamine enema alone (the current standard-of-care), as assessed by the total fecal score (Figure 5-4c). Specifically, both groups receiving ultrasound treatments demonstrated improved total fecal scores when compared to the disease group and enema group from day 12 on (one-way ANOVA with multiple comparisons, $P < 0.047$) and demonstrated total fecal scores below 4 on day 14. This is in contrast to both disease groups receiving no treatment and those receiving mesalamine enemas alone QD, which still demonstrated significantly elevated total fecal scores on day 14. In addition to the total fecal score, colonic tissue was evaluated histologically at the end of the trial in a blinded fashion. The average histology score for each study group is shown in Figure 5-4d and histological images representing tissue graded scores 0-4 are shown in Figure 5-4e. The ultrasound Treatment QD group had a statistically lower histology score than any other treatment regimen and the disease group. The tissue in the ultrasound treatment QD group appeared to have significantly less erosion of the epithelium and only minor shortening of the crypts when compared to the other colitis groups.

5.5. Discussion

This study presents to the best of our knowledge, the use of ultrasound as an active drug delivery modality throughout the GI tract for the first time. It was found that ultrasound was able to effectively enhance the delivery of model compounds with a wide range of molecular weights in all parts of the GI tract *ex vivo*. More surprisingly was the relatively short treatment time required for this (one minute of total ultrasound exposure). Investigation into the method of enhancement supports that transient cavitation provides a significant contribution to the delivery enhancement. Indeed, thermal effects and sonication with 1 MHz ultrasound were both found to elicit no enhancement in delivery. Further, the generation of pits on aluminum foil samples as a result of sonication with 20, 40, or 60 kHz ultrasound supports the occurrence of transient cavitation. The effect of 20 kHz ultrasound on theoretical pore sizes generated in the tissue were also quantified and found to increase significantly as a result of ultrasound treatment. Even further enhancement in delivery could be achieved with additional investigation into the treatment regimen and device implementation.

Translating our current understanding and optimization of UMGID *ex vivo*, we tested two configurations *in vivo*: axial and radial ultrasound emission in the rectum. The ability to generate ultrasound in multiple configurations in small, portable form factors amenable to at-home self-administration supports the generalizability of UMGID and its tunability. This is paramount for broad clinical and research applicability. In the immediate use-case of rectal delivery for diseases such as inflammatory bowel disease where enemas are already

established as the standard-of-care treatment, patients may utilize a small, hand-held device that emits ultrasound radially to achieve a high degree of circumferential tissue permeability, increasing drug delivery. Continued improvement in ultrasound miniaturization could allow for a variety of different operating formats to enable convenient ultrasound exposure to all parts of the GI tract, including ingestible ultrasound-emitting capsules to facilitate systemic delivery in a convenient manner [32].

Axial emission in swine was demonstrated to be safe based on histological examination of the tissue and clinical monitoring of the animal. Ultrasound was also shown to significantly enhance delivery of mesalamine by an order-of-magnitude. The fact that this level of delivery is achievable with only one-minute of ultrasound application is indicative of the potential power of UMGID. Further, the delivery of insulin as a model biologic highlights the ability of axial emission to achieve systemic delivery of larger molecules through the rectum and potentially through the varying segments of the GI tract. It should be noted that while insulin was chosen for experimental convenience, its successful delivery is illustrative of the ability to deliver biologics locally to the rectum while retaining their function. Local delivery of biologics has the potential to be useful in a variety of diseases. For ulcerative colitis, for example, the local delivery of monoclonal antibodies targeting TNF could be beneficial to downregulate proinflammatory processes [33]. This technology in its present form could also be beneficial in the local delivery of chemotherapeutics and biologics in the rectum for the treatment of colorectal cancer [34]. Indeed, current strategies to

achieve local delivery of these agents largely rely on formulation techniques, which suffer from low loading efficiencies and lack broad applicability to deliver many drugs [35], [36].

In addition to axial emission, radial emission was tested in a clinically relevant murine colitis model. The most efficacious treatment of mild to moderate colitis is rectal administration [7], [9]. However, active disease can make retention of the medication difficult. For example, the current procedure for the rectal administration of Rowasa® for the treatment of inflammatory bowel disease requires patients to first empty their bowels. They are then instructed to lay on their left side. The patient then must insert an applicator tip into the rectum and gently infuse the drug. Patients are instructed to remain in this position for at least 30 minutes and to retain the enema overnight [37], [38]. This creates a precarious and uncomfortable experience that must be endured nightly. This is particularly challenging for patients with active colitis who are experiencing urgency with frequent bowel movements. Even when this regimen is strictly adhered to, disease relapse rates are high [39]. To test whether UMGID had the capacity to promote rapid delivery of mesalamine and thereby enhance treatment efficacy, an ultrasound probe with radial emission was used for its ability to permeabilize a larger area of tissue. The use of a custom-designed ultrasound probe with a shaft diameter ≤ 3 mm is indicative of the ability to significantly miniaturize this technology. Ultrasound in combination with a medicated enema was found to significantly improve disease indices. The trend towards improved clinical outcome in the QOD group suggests that ultrasound

treatment QOD may be useful in less severe cases of colitis and in patients with suboptimal adherence to medication. The superior disease outcomes, both clinically and histologically, of ultrasound treatment QD compared to the current standard-of-care is exciting and suggests that UMGID could enable remission to be achieved with shorter treatment regimens. Moreover, it provides a solution for accelerated drug delivery in clinical settings where rapid disease-associated GI transit time limits the absorption of therapeutics. As a result, this technology may eliminate the need for extended enema retention.

5.6. Conclusion

UMGID has many potential applications ranging from localized site-specific treatment with anti-inflammatories to the more broad delivery of macromolecules. With further work, this technology could be miniaturized to dimensions compatible with ingestion, allowing for ingestible ultrasound-emitting capsules for systemic delivery. Based on the studies described here, ultrasound technology has the potential to deliver substances such as nanoparticles, monoclonal antibodies, or vaccines to modulate mucosal immune responses [40], [41]. Additionally, ultrasound could potentially enable the delivery of new classes of therapeutics such as DNA and RNA-based therapeutics, where delivery requires overcoming several biological barriers [42], [43]. With further study, this technology could prove invaluable in both clinical and research settings, enabling improved therapies and expansion of research techniques applied to the GI tract as well as new medical devices to enable local rectal delivery and, eventually, oral administration using ingestible devices.

5.7. Supplementary Information

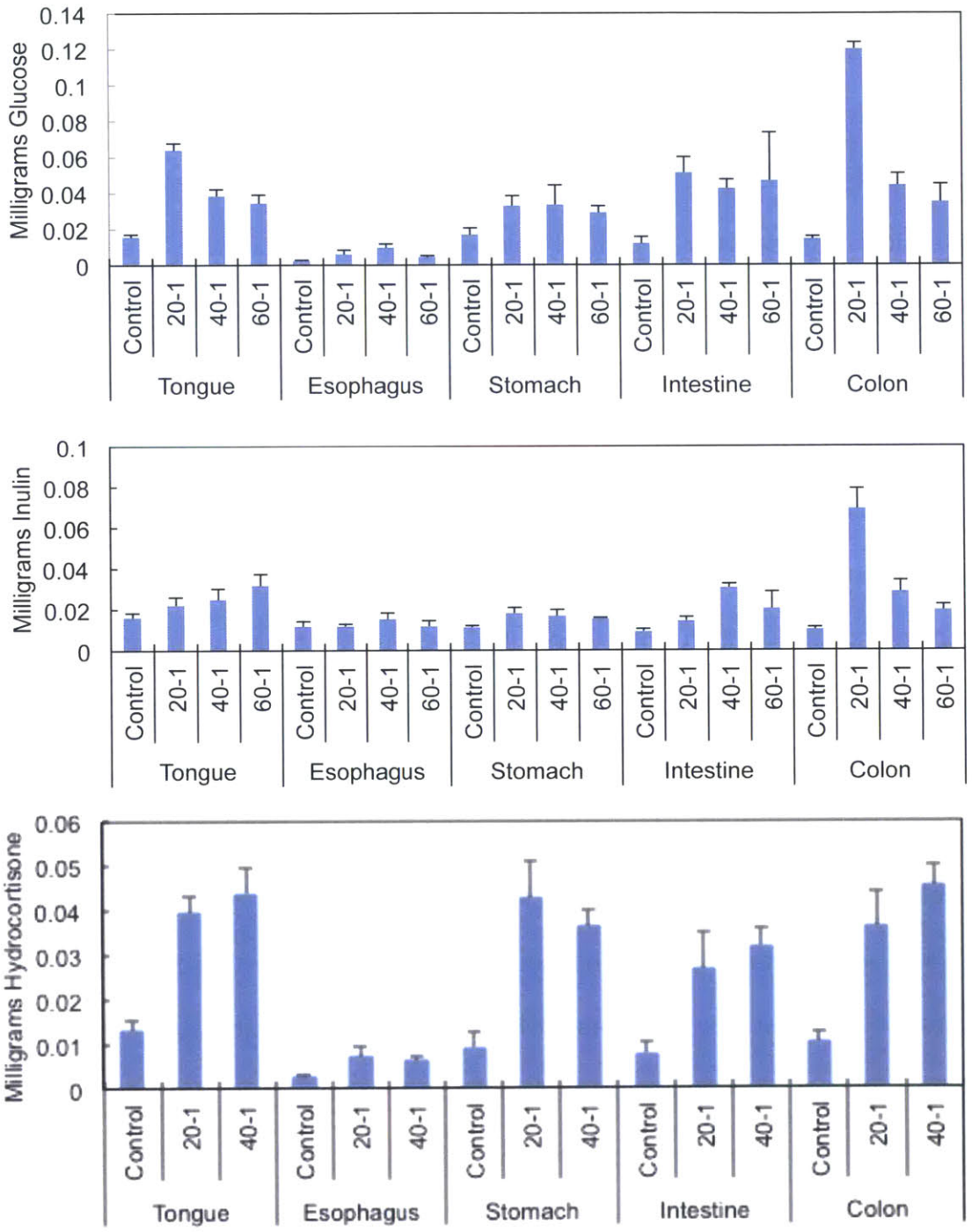

Figure 5-5: *In vitro* survey of glucose delivery (n = 3-7) (top), inulin (n = 3-9) (middle), and hydrocortisone (n = 6) (bottom) as a result of a one-minute

exposure to ultrasound at either 20, 40, or 60 kHz (glucose and inulin only) at an intensity of 2.5, 7.3, and 9.6 W/cm^2 respectively. Error bars represent one standard deviation. Ultrasound treatment significantly enhances the amount of material delivered to the tissue. Delivery of all three molecules was shown to be relatively insensitive to both the frequency and intensity the tissue was exposed to.

5.7.1. Pore Size Determination

To further elucidate the mechanism of enhancement of UMGID, theoretical pore-size estimates were made using hindered-transport theory, which has previously been utilized to model diffusion across membranes [44]. The permeability, *P*, of a molecule traversing a porous membrane can be expressed as follows:

$$P = CDF(\lambda) \tag{5-1}$$

where *C* is a constant depending solely on properties of the membrane, *D* is the free diffusion coefficient of the molecule in solution, and $F(\lambda)$ is known as the hindrance factor which depends on λ, the ratio of the hydrodynamic radius of the molecule and the membrane pore radius [26]. The most advanced expression of $F(\lambda)$ is [44]:

$$F(\lambda) = 1 + \frac{9}{8}\lambda ln(\lambda) - 1.56034\lambda + 0.528155\lambda^2 + 1.91521\lambda^3 - 2.81903\lambda^4 + 0.270788\lambda^5 + 1.10115\lambda^6 - 0.435933\lambda^7 \tag{5-2}$$

Because both *C* and the membrane pore size (embedded in λ) in Supplementary Equation 5-1 are unknown, one can make use of two permeant molecules to eliminate C as follows:

$$\frac{P_x}{P_y} = \frac{D_x F(\lambda_x)}{D_y F(\lambda_y)} = K \tag{5-3}$$

Note that the only unknown in Supplementary Equation 5-3 is the pore size in λ. Therefore, *P* may be determined experimentally for each permeant to estimate the membrane pore size. The permeability can be found using the following expression:

$$P_i = \frac{1}{AC_i}\frac{dQ_i}{dt} \tag{5-4}$$

where *A* is the area of the membrane exposed to the permeant, C_i is the concentration of the permeant in the donor cell, and $\frac{dQ_i}{dt}$ is the slope of the plot of the permeant quantity in the receiver chamber vs. time after the lag-phase.

This data along with the diffusion coefficients and hydrodynamic radii of glucose and inulin were used in Supplementary Equations 5-1 through 4 to estimate the pore size generated when porcine small intestine was treated with 20 kHz for 2 minutes at a 50% duty cycle [16], [45]-[47].

5.7.2. Validity of the Aqueous Porous Pathway Theory

From Supplementary Equation 5-3 above, it can be seen that a plot of $log(P_x)$ vs. $log(P_y)$ should yield a linear curve with a slope of one and a y-intercept of $log(K)$. Therefore, we fitted linear regressions to both the control, and treated, plots of $log(P_{glucose})$ vs. $log(P_{inulin})$, and required that the 95% confidence interval of the slope contain the theoretical value of one.

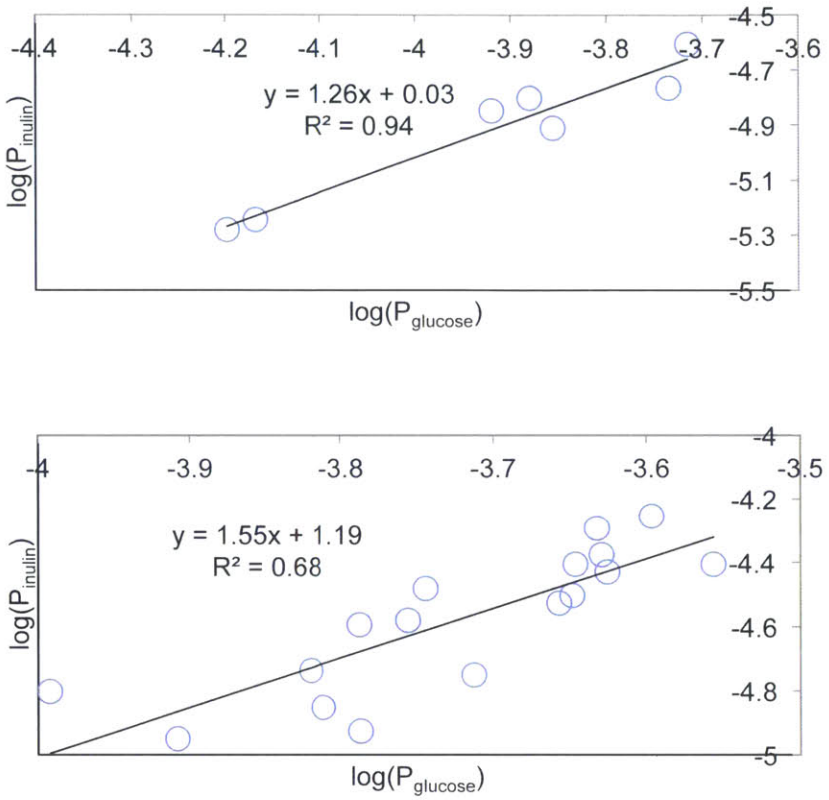

Figure 5-6: Plots of $\boldsymbol{log(P_{glucose})}$ vs. $\boldsymbol{log(P_{inulin})}$ for native small intestine (above) and small intestine treated with 20 kHz ultrasound for two minutes (one minute total of ultrasound exposure) (below).

Table 5-1: Number of samples performed, 95% confidence interval of the regression slope, and the r^2 value of the linear regression for the control and treated samples.

	n	Slope	r^2
Control	7	1.26 ± 0.38	0.94
Treated (20 kHz)	17	1.55 ± 0.64	0.68

The fact that the theoretical slope of one is contained in the 95% confidence interval of both experimental groups supports the validity of this analysis, and therefore, it is reasonable to deduce pore sizes using Supplementary Equations 5-2 and 5-3.

Values of K were calculated for every sample using Supplementary Equation 5-3 above. The average, and lower and upper pore size estimates are based on the average value of K and the 95% confidence interval for K.

5.7.3. Effect of Sonication on Drug Activity

The effect of sonication on the molecular structure of mesalamine and hydrocortisone was investigated by analyzing the molecules after sonication using NMR (Supplementary Figure 5-3). Note the disappearance of the volatile internal TMS standard after ultrasound treatment, which was carried out in an uncapped vial.

Deuterium exchange occurs as labile protons on the analyte exchange with the deuterated solvent it is dissolved in. This exchange is catalyzed during the ultrasound reaction and is apparent in the post ultrasound samples (Supplementary Figure 5-4ai, bi). Replacement of protons by deuterium results in loss of signal, shown either as a reduction in the integration fractions or disappearance of the peak altogether. Other indications of deuterium exchange include a slight broadening of peak shape, a shift in peak location, and slight change in J coupling values. These changes reflect the natural equilibrium of

labile protons in solution and do not reflect changes in the overall molecular structure.

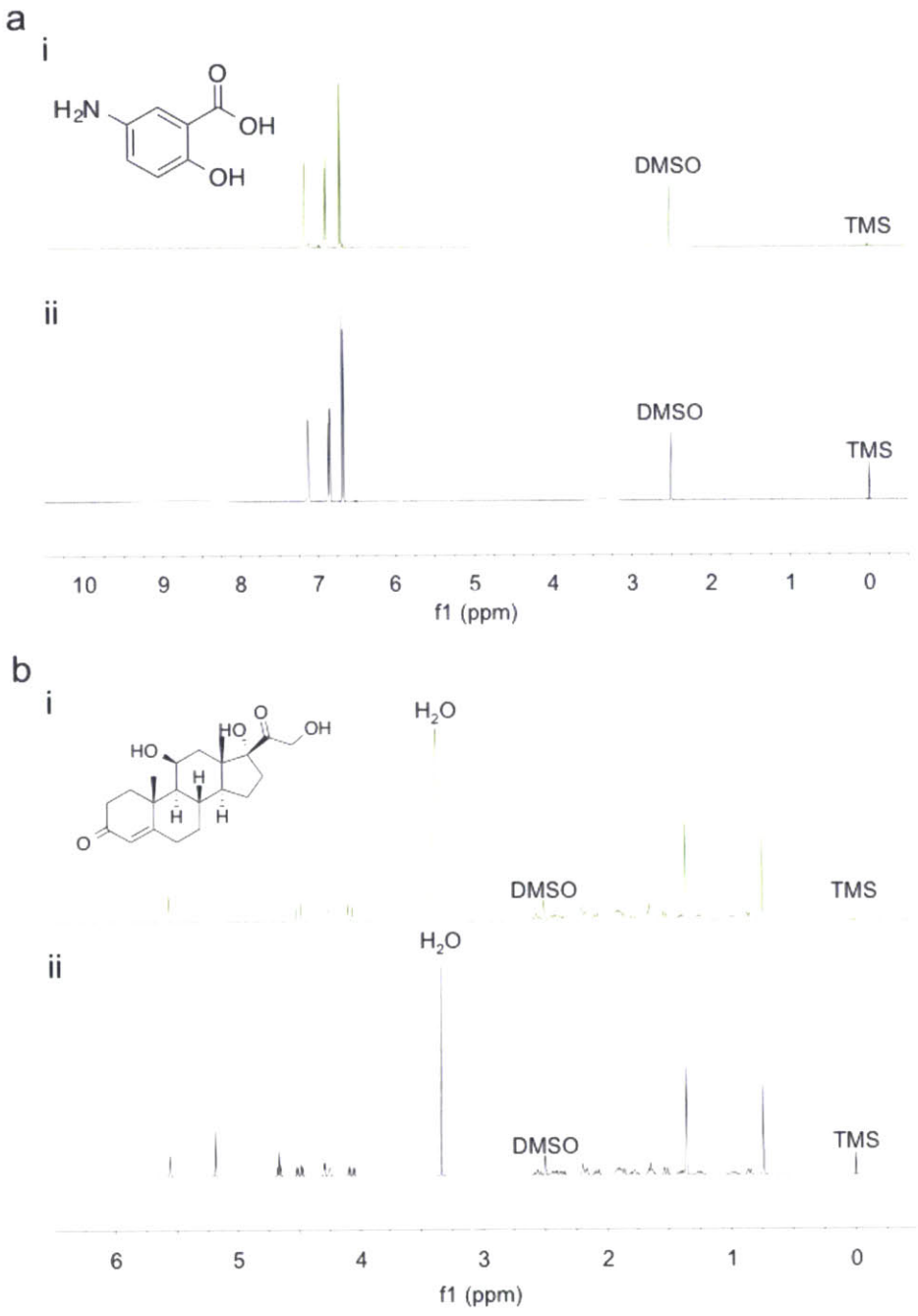

Figure 5-7: (a) Representative NMR spectra of mesalamine after sonication (top) and before sonication (bottom). (i) ^{1}H NMR (500 MHz, DMSO) δ Majority: 7.16 (1H, d, *J* = 2.8 Hz); 6.90-6.87 (1H, dd, *J* = 2.8, 8.8 Hz); 6.70 (1H, d, *J* = 8.8 Hz). Minority: 7.10 (1H, d, *J* = 3.1 Hz); 6.98-6.96 (1H, dd, *J* = 3.1, 8.9 Hz); 6.67 (1H, d, *J* = 8.9 Hz). (ii) ^{1}H NMR (500 MHz, DMSO) δ 7.12 (1H, d, *J* = 2.8 Hz); 6.87-6.84

(1H, dd, J = 2.8, 8.8 Hz); 6.68 (1H, d, J = 8.8 Hz). (b) Representative NMR spectra of hydrocortisone after sonication (top) and before sonication (bottom). (i) ^{1}H NMR (500 MHz, DMSO) δ 5.56 (1H, s); 5.19 (1H, s); 4.52-4.47 (1H, d, J = 19.1 Hz); 4.30 (1H, bm); 4.25 (1H, bm); 4.09-4.05 (1H, d, J = 19.1 Hz); 2.56 (1H, m); 2.40 (2H, m); 2.20 (2H, m); 2.07 (1H, m); 1.90 (3H, m); 1.78 (1H, m); 1.65 (2H, m); 1.54 (1H, m); 1.40 (1H, m); 1.36 (3H, s); 1.26 (1H, m); 0.99 (1H, m); 0.85 (1H, m); 0.74 (3H, s). (ii) ^{1}H NMR (500 MHz, DMSO) δ 5.56 (1H, s); 5.19 (1H, s); 4.67 (1H, m); 4.52-4.47 (1H, dd, J = 5.9, 19.1 Hz); 4.29 (1H, d, J = 3.32); 4.25 (1H, p, J = 3.32); 4.10-4.05 (1H, dd, J = 5.9, 19.1 Hz); 2.56 (1H, m); 2.40 (2H, m); 2.20 (2H, m); 2.07 (1H, m); 1.92 (3H, m); 1.78 (1H, m); 1.65 (2H, m); 1.54 (1H, m); 1.40 (1H, m); 1.36 (3H, s); 1.26 (1H, m); 0.99 (1H, m); 0.85 (1H, m); 0.74 (3H, s). Three biological replicates were performed for both sonicated and unsonicated samples. No change in the molecular structure was found as a result of sonication.

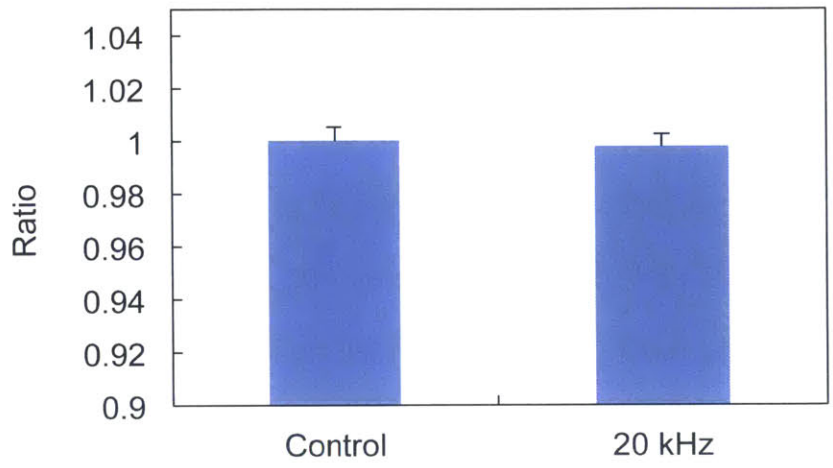

Figure 5-8: Impact of sonication on insulin function determined by HPLC. No statistical difference was found on the concentration of active insulin as a result of sonication with 20 kHz set to an intensity of 7.5 W/cm^2 (two-tailed Student's t-test, $P = 0.48$). Three biological repeats were tested for each group. The averages and standard deviations are shown.

5.7.4. Tolerability of Rectal Ultrasound in Healthy Mice

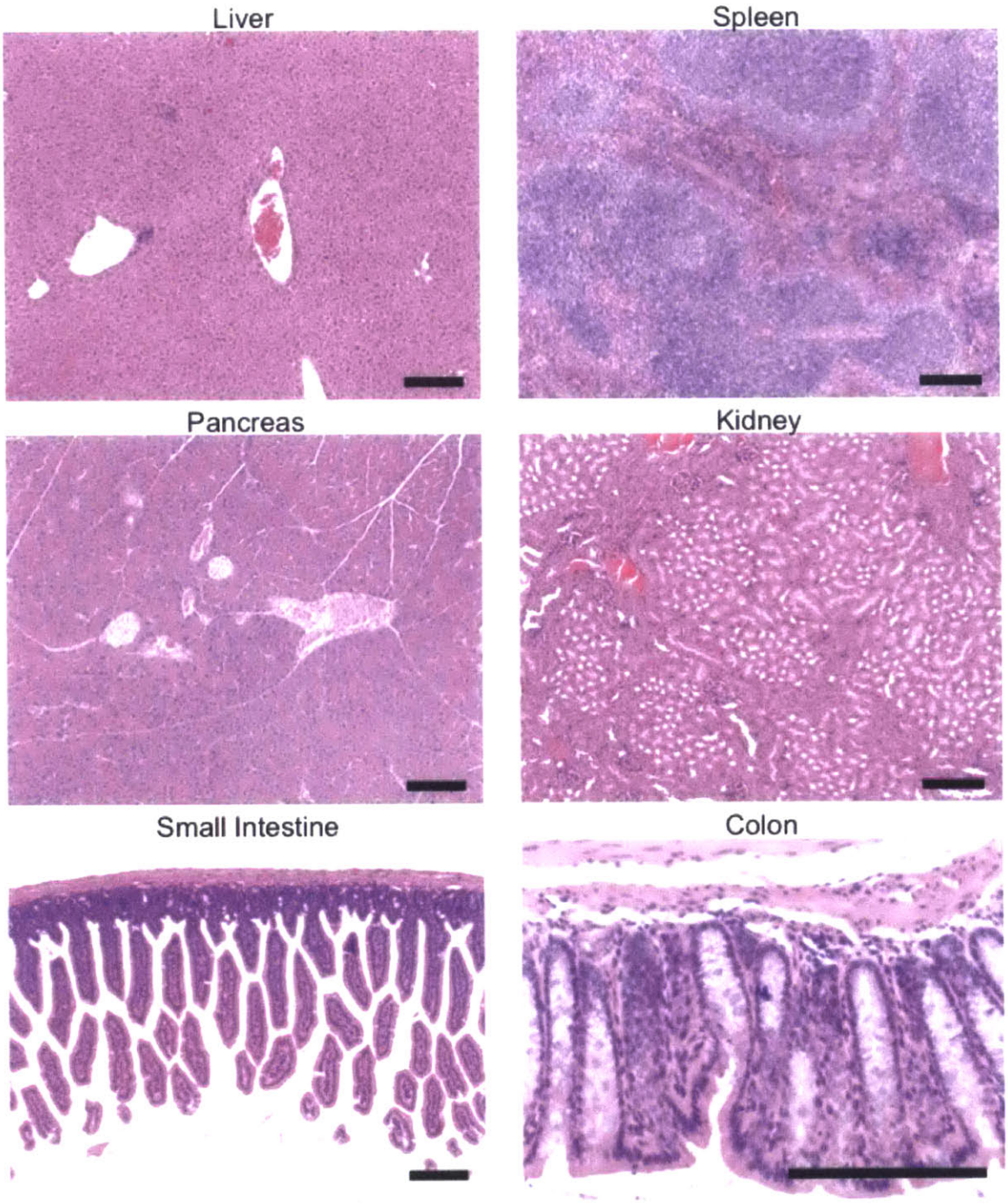

Figure 5-9: Representative histological images of mouse liver, spleen, pancreas, kidney, small intestine, and colon after a 14 day treatment regimen of either no

treatment (n = 5), insertion of the probe without turning it on (n = 5), or insertion of the probe and sonication (n = 5). Blinded evaluation of the histology by a clinical pathologist determined the tissue beyond the colon to be of normal architecture with no cytologic abnormality in all groups. Only in the group receiving insertion of the probe and sonication was there minor disruption of the colon only, as described in the manuscript. The scale bar represents 200 μm.

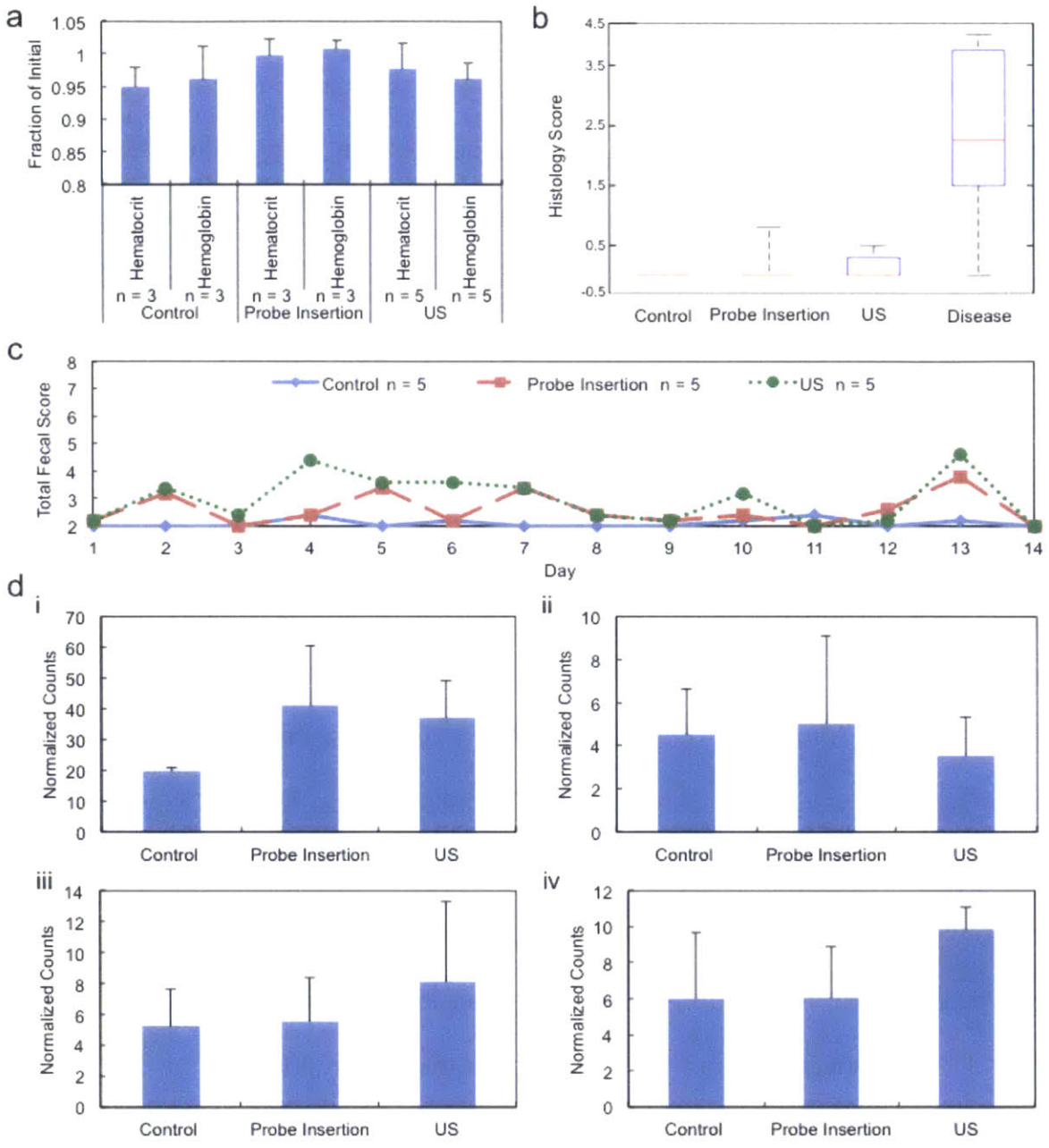

Figure 5-10: (a) To determine whether ultrasound probe insertion and ultrasound treatment in the colon of mice induced significant trauma leading to rectal bleeding or inflammation, we evaluated mice pre- and post- probe insertion with and without ultrasound. Hematocrit and hemoglobin normalized to day 1 for healthy animals (Control), healthy animals receiving daily probe insertion (Probe

Insertion), and healthy animals receiving daily ultrasound sonication (US). A one-way analysis-of-variance showed there to be no statistical difference between any group's final normalized hematocrit or hemoglobin, suggesting that probe insertion and sonication does not induce significant blood loss and is well tolerated. While five animals were used in each group, some blood samples from day 1 and day 14 clotted, resulting in fewer than five values for some groups. (b) Histology score of tissue sections at Day 14. The median, 25^{th}, and 75^{th} percentiles are shown. The whiskers indicate the most extreme data points. The Disease group is shown for comparison. Both the Probe Insertion and US groups had statistically better histology scores than any other group that had disease induced (one-way analysis of variance testing with multiple comparisons, $P < 0.015$). (c) Total fecal score for all three groups over the 14-day period was determined to evaluate for the presence of inflammation leading to worsening fecal scores. A paired, two-tailed t-test between the Probe Insertion and ultrasound groups showed no significant difference between their scores on any day. The largest standard deviation observed in the Total Fecal Score for the Control, Probe Insertion, and US groups over the 14-day trial is 0.54, 2.68, and 3.28, respectively. The average standard deviation for each group over the 14-day trial is 0.17, 0.99, and 1.56, respectively. (d) Cytokine levels of TNF-α (i), IFN-γ (ii) IL-6 (iii), and IL-17 (iv). n = 4 biological repeats for all groups. No statistical difference was found between treatment groups for any cytokine (one-way analysis of variance testing with multiple comparisons). All graphs represent averages and standard deviations. Sample sizes indicated are biological

replicates. Toxicity as evaluated through the absence of anemia, low fecal score, low histology scores, and normal cytokine levels supports the likely safety of this drug delivery modality in the GI tract.

5.8. References

[1] L. M. Ensign, R. Cone, and J. Hanes, "Oral drug delivery with polymeric nanoparticles: The gastrointestinal mucus barriers," *Advanced drug delivery reviews*, vol. 64, no. 6, pp. 557–570, 2012.

[2] C. J. Pavlin, K. Harasiewicz, M. D. Sherar, and F. S. Foster, "Clinical Use of Ultrasound Biomicroscopy," *Ophthalmology*, vol. 98, no. 3, pp. 287–295, 1991.

[3] A. J. Coleman, E. Draguioti, R. Tiptaf, N. Shotri, and J. E. Saunders, "Acoustic performance and clinical use of a fibreoptic hydrophone," *Ultrasound in Medicine & Biology*, vol. 24, no. 1, pp. 143–151, Jan. 1998.

[4] J. E. Kennedy, "Innovation: High-intensity focused ultrasound in the treatment of solid tumours," *Nat Rev Cancer*, vol. 5, no. 4, pp. 321–327, Mar. 2005.

[5] C. K. Holland, "Thresholds for transient cavitation produced by pulsed ultrasound in a controlled nuclei environment," *J. Acoust. Soc. Am.*, vol. 88, no. 5, pp. 2059–2069, 1990.

[6] M. F. Neurath, "Cytokines in inflammatory bowel disease," *Nature Reviews Immunology*, vol. 14, no. 5, pp. 329–342, May 2014.

[7] S. Danese and C. Fiocchi, "Ulcerative Colitis," *N Engl J Med*, vol. 365, no. 18, pp. 1713–1725, 2011.

[8] G. Frieri, R. Giacomelli, M. Pimpo, G. Palumbo, A. Passacantando, G. Pantaleoni, and R. Caprilli, "Mucosal 5-aminosalicylic acid concentration inversely correlates with severity of colonic inflammation in patients with

ulcerative colitis," *Gut*, vol. 47, pp. 410–414.

[9] F. Seibold, N. Fournier, C. Beglinger, C. Mottet, V. Pittet, and G. Rogler, "Topical therapy is underused in patients with ulcerative colitis," *Journal of Crohn's and Colitis JA* -, vol. 8, no. 1. pp. 56–63 PB –, 01-Jan-2014.

[10] T. Nakashima, T. Maeda, H. Nagamoto, T. Kumakura, M. Takai, and T. Mori, "Rebamipide Enema is Effective for Treatment of Experimental Dextran Sulfate Sodium Induced Colitis in Rats," *Dig Dis Sci*, vol. 50, no. 1, pp. S124–S131, Oct. 2005.

[11] M. Naganuma, Y. Iwao, H. Ogata, N. Inoue, S. Funakoshi, S. Yamamoto, Y. Nakamura, H. Ishii, and T. Hibi, "Measurement of Colonic Mucosal Concentrations of 5-Aminosalicylic Acid Is Useful for Estimating Its Therapeutic Efficacy in Distal Ulcerative Colitis: Comparison of Orally Administered Mesalamine and Sulfasalazine," *Inflammatory Bowel Diseases*, vol. 7, no. 3, pp. 221–225, Aug. 2001.

[12] Y. Liu, H. Miyoshi, and M. Nakamura, "Encapsulated ultrasound microbubbles: Therapeutic application in drug/gene delivery," *Journal of Controlled Release*, vol. 114, no. 1, pp. 89–99, Aug. 2006.

[13] T. Li, H. Chen, T. Khokhlova, Y.-N. Wang, W. Kreider, X. He, and J. H. Hwang, "Passive Cavitation Detection during Pulsed HIFU Exposures of Ex Vivo Tissues and In Vivo Mouse Pancreatic Tumors," *Ultrasound in Medicine & Biology*, vol. 40, no. 7, pp. 1523–1534, Jul. 2014.

[14] L. Wolloch and J. Kost, "The importance of microjet vs shock wave formation in sonophoresis," *Journal of Controlled Release*, vol. 148, no. 2,

pp. 204–211.

[15] S. Wirtz, C. Neufert, B. Weigmann, and M. F. Neurath, "Chemically induced mouse models of intestinal inflammation," *Nature Protocols*, vol. 2, pp. 541–546.

[16] A. Tezel, A. Sens, and S. Mitragotri, "Description of transdermal transport of hydrophilic solutes during low-frequency sonophoresis based on a modified porous pathway model," *Journal of Pharmaceutical Sciences*, vol. 92, no. 2, pp. 381–393, Jan. 2003.

[17] C. HS, M. SN, S. RS, and S. DJ, "Clinicopathologic study of dextran sulfate sodium experimental murine colitis.," *Lab Invest*, vol. 69, no. 2, pp. 238–249, Aug. 1993.

[18] T. G. Leighton, *The Acoustic Bubble*. Academic Press, 1997.

[19] G. Veereman, "Pediatric Applications of Inulin and Oligofructose," *The Journal of nutrition*, vol. 137, pp. 2585S–2589S, 2007.

[20] J. Liu, T. N. Lewis, and M. R. Prausnitz, "Non-invasive assessment and control of ultrasound-mediated membrane permeabilization.," *Pharm Res*, vol. 15, no. 6, pp. 918–924, Jun. 1998.

[21] H.-Y. Lin and J. L. Thomas, "PEG−Lipids and Oligo(ethylene glycol) Surfactants Enhance the Ultrasonic Permeabilizability of Liposomes," *Langmuir*, vol. 19, no. 4, pp. 1098–1105, Feb. 2003.

[22] H.-Y. Lin and J. L. Thomas, "Factors Affecting Responsivity of Unilamellar Liposomes to 20 kHz Ultrasound," *Langmuir*, vol. 20, no. 15, pp. 6100–6106, Jul. 2004.

[23] A. Brotchie, F. Grieser, and M. Ashokkumar, "Characterization of Acoustic Cavitation Bubbles in Different Sound Fields," *J. Phys. Chem. B*, vol. 114, no. 34, pp. 11010–11016, Sep. 2010.

[24] N. A. PELEKASIS, A. GAKI, A. DOINIKOV, and J. A. TSAMOPOULOS, "Secondary Bjerknes forces between two bubbles and the phenomenon of acoustic streamers," *J. Fluid Mech.*, vol. 500, pp. 313–347, 1999.

[25] P. Prentice, A. Cuschieri, K. Dholakia, M. Prausnitz, and P. Campbell, "Membrane disruption by optically controlled microbubble cavitation," *Nat Phys*, vol. 1, no. 2, pp. 107–110, Oct. 2005.

[26] K. D. Peck, A.-H. Ghanem, and W. Higuchi, "Hindered Diffusion of Polar Molecules Through and Effective Pore Radii Estimates of Intact and Ethanol Treated Human Epidermal Membrane," *Pharm Res*, vol. 11, no. 9, pp. 1306–1314, 1994.

[27] W. H. Barr and S. Riegelman, "Intestinal drug absorption and metabolism I: Comparison of methods and models to study physiological factors of in vitro and in vivo intestinal absorption," *Journal of Pharmaceutical Sciences*, vol. 59, no. 2, pp. 154–163, Feb. 1970.

[28] J. K. Marshall and E. J. Irvine, "Putting rectal 5-aminosalicylic acid in its place: The role in distal ulcerative colitis," *American Journal of Gastroenterology*, vol. 95, no. 7, pp. 1628–1636, Jul. 2000.

[29] L. B. Vong, T. Tomita, T. Yoshitomi, H. Matsui, and Y. Nagasaki, "An Orally Administered Redox Nanoparticle That Accumulates in the Colonic Mucosa and Reduces Colitis in Mice," *Gastroenterology*, vol. 143, no. 4,

pp. 1027–1036.e3, 2012.

[30] H. Sann, J. V. Erichsen, M. Hessmann, A. Pahl, and A. Hoffmeyer, "Efficacy of drugs used in the treatment of IBD and combinations thereof in acute DSS-induced colitis in mice," *Life Sciences*, vol. 92, no. 12, pp. 708–718, Apr. 2013.

[31] P. Alex, N. C. Zachos, T. Nguyen, L. Gonzales, T.-E. Chen, L. S. Conklin, M. Centola, and X. Li, "Distinct cytokine patterns identified from multiplex profiles of murine DSS and TNBS-induced colitis.," *Inflammatory Bowel Diseases*, vol. 15, no. 3, pp. 341–352, Mar. 2009.

[32] Y. Sunny, C. R. Bawiec, A. T. Nguyen, and J. A. Samuels, "Optimization of un-tethered, low voltage, 20-100 kHz flexural transducers for biomedical ultrasonics applications," *Ultrasonics*, 2012.

[33] M. F. Neurath, "New targets for mucosal healing and therapy in inflammatory bowel diseases," *Mucosal Immunol*, vol. 7, no. 1, pp. 6–19.

[34] P. Karaca-Mandic, J. S. McCullough, M. A. Siddiqui, H. Van Houten, and N. D. Shah, "Impact of New Drugs and Biologics on Colorectal Cancer Treatment and Costs," *Journal of Oncology Practice*, vol. 7, no. 3, pp. e30s–e37s, May 2011.

[35] N. A. Capurso and T. M. Fahmy, "Development of a pH-Responsive Particulate Drug Delivery Vehicle for Localized Biologic Therapy in Inflammatory Bowel Disease," *The Yale Journal of Biology and Medicine*, vol. 84, no. 3, pp. 285–288, Sep. 2011.

[36] N. Škalko-Basnet, "Biologics: the role of delivery systems in improved

therapy," *Biologics : Targets & Therapy*, vol. 8, pp. 107–114, 2014.

[37] J. M. Wolf and B. A. Lashner, "Inflammatory bowel disease: sorting out the treatment options.," *Cleveland Clinic Journal of Medicine*, vol. 69, no. 8, pp. 621–626, Aug. 2002.

[38] C. A. CIARLEGLIO and M. L. Swartz, "Rowasa Suspension Enema (Mesalamine, USP).," *Gastroenterology Nursing KW* -, vol. 12, no. 2, 1989.

[39] R. D. C. Prashant Kedia, "Once-daily MMX mesalamine for the treatment of mild-to-moderate ulcerative colitis," *Therapeutics and Clinical Risk Management*, vol. 3, no. 5, pp. 919–927, Oct. 2007.

[40] A. Cerutti, "Location, location, location: B-cell differentiation in the gut lamina propria," *Mucosal Immunol*, vol. 1, no. 1, pp. 8–10, Jan. 2008.

[41] Q. Zhu, J. Talton, G. Zhang, T. Cunningham, Z. Wang, R. C. Waters, J. Kirk, B. A. R. Eppler, D. M. Klinman, Y. Sui, S. Gagnon, I. M. Belyakov, R. J. Mumper, and J. A. Berzofsky, "Large intestine-targeted, nanoparticle-releasing oral vaccine to control genitorectal viral infection," *Nature Publishing Group*, pp. 1–7, Jul. 2012.

[42] C. V. Pecot, G. A. Calin, R. L. Coleman, G. Lopez-Berestein, and A. K. Sood, "RNA interference in the clinic: challenges and future directions," *Nat Rev Cancer*, vol. 11, no. 1, pp. 59–67, Jan. 2011.

[43] M. P. Morrow and D. B. Weiner, "DNA Drugs Come of Age," *Scientific American*, vol. 303, no. 1, pp. 48–53, Jul. 2010.

[44] P. Dechadilok and W. M. Deen, "Hindrance factors for diffusion and

convection in pores," *Industrial & Engineering Chemistry Research*, vol. 45, no. 21, pp. 6953–6959, 2006.

[45] W. D. Stein, *Channels, Carriers, and Pumps: An Introduction to Membrane Transport*. Elsevier Science, 2012.

[46] L. C. M. Samuel B Horowitz, "The Nuclear Permeability, Intracellular Distribution, and DIffusion of Inulin in the Amphibian Oocyte," *The Journal of Cell Biology*, vol. 60, no. 2, p. 405, Feb. 1974.

[47] S. G. Schultz and A. K. Solomon, "Determination of the Effective Hydrodynamic Radii of Small Molecules by Viscometry," *The Journal of General Physiology*, vol. 44, no. 6, p. 1189, Jul. 1961.

Chapter 6

Thesis Summary and Future Research Directions

6.1. Thesis Summary

The primary focus of this thesis was to broaden the utility of US-assisted transdermal drug delivery, and to expand the use of physical enhancers, specifically exploring the use of ultrasound and microneedles in the GI tract for the first time. With regards to transdermal delivery, this thesis focused on the development of a new treatment regimen utilizing low- and high-frequency US simultaneously, presented in Chapters 2 and 3. This treatment regimen was tested to elucidate the mechanism of enhancement relative to traditional low-frequency US and to quantify the level of enhancement. The safety and tolerability of the new treatment regimen were explored *in vitro* and *in vivo*.

Building on the body of work involving the use of physical enhancers for transdermal drug delivery, I then began testing their use in the GI tract. In Chapter 4, I explored the use of microneedles in the GI tract to achieve the systemic delivery of biologics, which are currently limited to injection. Indeed, microinjections in the GI tract were found to afford superior kinetics compared to traditional injections. Furthermore, a model pill with radially protruding needles was found to be safe and well tolerated in a large animal model.

In Chapter 5, I investigated the use of US in the GI tract. US was found to enhance the delivery of model permeants in all tissue types compared to passive

delivery. Indeed, enhancement was up to an order-of-magnitude *ex vivo*. Further testing demonstrated the mechanism of enhancement to be a result of transient cavitation. Testing *in vivo* demonstrated that two modes of US administration are safe: axial in swine and radial in mice. Axially-emitted US was found to be safe and well tolerated for rectal delivery in swine. Further, the delivery of mesalamine, a therapeutic used clinically for the treatment of inflammatory bowel disease, was enhanced 22-fold. Finally, the clinical relevance of such enhancement was tested using radial US in mice. Specifically, mice with experimental colitis induced were found to recover significantly faster when US was administered rectally. This supports the continued investigation of US in the GI tract.

6.2. Areas of Potential Impact for Transdermal Technologies

Skin-permeabilizing methods have matured to the point where they may now make a positive impact on the treatment and prevention of diseases. Discussed here is the application of skin-permeabilizing methods to the areas of protein delivery, vaccination, and sensing.

6.2.1. Protein Delivery

The potential advantages of transdermal drug delivery are especially pertinent for protein delivery. Because of their degradation and low absorption in the GI tract, proteins cannot be administered orally. Additionally, certain proteins, such as interferons, must be delivered in a sustained manner, which the

transdermal route could allow for [1]. As a result, transdermal protein delivery has been a goal of researchers for years [1]. The delivery of human erythropoietin alfa (35 kDa) coated onto a microneedle patch, for example, was investigated in rats and found to achieve comparable pharmacokinetics to subcutaneous injection, the standard delivery method [2]. Additionally, the kinetics of insulin delivery to mice from dissolving microneedles has been shown to be comparable to that of subcutaneous injection [3]. Addressing the issue of what can be coated onto microneedles, other studies have examined coating formulations to deliver the model proteins bovine pancreatic ribonuclease A (13.7 kDa) and chicken ovalbumin (45 kDa) [4], [5]. Both studies found that the model proteins could be delivered into skin *in vitro*, with dosage and release kinetics dependent on the coating chemistry.

US and iontophoresis have also been investigated for protein delivery. US has previously been shown to enable the delivery of insulin (5.8 kDa), interferon gamma (17 kDa), and erythropoietin (35 kDa) [1]. More recently, it has been shown to effectively deliver a synthetic cytokine (12.7 kDa) and achieve serum levels comparable to those obtained by the combined use of microneedles and iontophoresis [6]. Studies utilizing iontophoresis alone have shown the delivery of ribonuclease A as well, in addition to cytochrome c (12 kDa), ribonuclease T1 (11.2 kDa), and oligonucleotides for the stimulation of anti-tumor activity [7]-[9]. Interestingly, delivery was shown to be due to electromigration for all proteins, despite electroosmosis being thought to be the dominant contribution to the flux of larger molecules [10]. The delivery of ribonuclease A was found to be greater

than that of ribonuclease T1, even though it is larger and has a lower net charge. This suggests that more than simply a molecule's charge to mass ratio influences its delivery by iontophoresis [9]. It should be noted that in all studies, treatments were carried out for up to 8 hours. It remains to be seen whether the cumulative dose, delivered over such a period of time, is clinically meaningful.

Combination methods have also been investigated for their ability to deliver proteins. One study tested the delivery of both bovine insulin (5.8 kDa) and bovine serum albumin (66 kDa) using the simultaneous application of microneedles and iontophoresis [11]. *In vitro* results showed a synergistic enhancement in the cumulative amount of each protein delivered using the combination, compared to either method alone [11].

6.2.2. Vaccination

There has been considerable interest on the use of skin-permeabilizing methods for vaccination. The dendritic cell-rich environment present in the epidermis makes the skin an attractive site for vaccination. Specifically, Langerhans cells (LCs), epidermal resident immune cells, cover 25% of the skin's area [12]. Second, immunizations administered transdermally typically require minimal amounts of antigenic material to be delivered in order to elicit an immune response. Further, delivery into the LC-rich environment can be dose-sparing compared to traditional intramuscular immunizations that deliver antigenic material to the muscle where much lower populations of immune cells reside [13].

Current needle-based vaccinations have two major limitations: First, for non-replicating vaccines, adjuvants or viral vectors are necessary to induce robust, long-lived immune responses. Both are important for activating the immune system but have serious disadvantages, including their inherent immunogenicity and systemic toxicity responsible for many of the side effects of vaccinations [14]. Furthermore, non-replicating vaccines cannot elicit cytotoxic T cells, which are thought to be essential for clearing viral infections and killing cancer cells [15]. Transdermal-based technologies have the potential to solve these serious side effects.

US, for example, has been investigated for its ability to elicit immune responses using the model antigen tetanus toxoid [16], [17]. The US-based treatments were found to effectively permeabilize the skin and allow diffusion of the tetanus toxoid. This resulted in comparable antigen-specific serum antibody titers to those elicited using intramuscular injection. More significant was the fact that US allowed for an order-of-magnitude dose sparing [17]. This is due to the activation of LCs after US application. It was found that even in the absence of antigen, LCs were activated in the epidermis as a result of the US treatment alone, suggesting that the US treatment itself is an immunization adjuvant [17]. This was further confirmed by a different research team, who found that antibody titers did not correlate with the extent of skin permeabilization, and therefore, with the amount of antigen that was delivered [16]. With relatively few research reports in this area, the use of US for immunization is a rich area for study, and it

remains to be seen whether this treatment protocol can be used to tune the specific response achieved *in vivo*.

Electroporation has seen broader use in the area of immunization, particularly with DNA-based vaccines. DNA-based vaccines are gaining in importance, particularly because of their favorable safety profile compared to vector-based methods. DNA vaccines, however, have traditionally been unable to elicit potent immune responses because they were not internalized by the cell nucleus [18]. By creating transient pores in the cellular membrane, electroporation enables the efficient uptake of the DNA material. One recent study found comparable titer levels induced through the use of electroporation and anthrax protective antigen compared to an FDA-approved anthrax vaccine [18]. More interestingly, it was found that the electroporation method induced the largest levels of anti-antigen antibodies one year after immunization [18].

Electroporation has also been used to vaccinate human subjects with an HIV-1 DNA vaccine [19]. Cell-mediated immunity was found to be increased over 70-times compared to vaccination without electroporation. In addition to more robust responses, electroporation also facilitated a dose-sparing effect. Local pain and tenderness were found to be greater in the groups receiving electroporation. Despite the positive immune response, the pain and bulky equipment required will most likely limit the impact electroporation has, especially in the developing world.

Microneedles have attracted the most attention due to their ease-of-use. Many groups have examined the use of microneedles for immunization against a

range of diseases. For example, superior titers and dose-sparing over traditional injection have been reported for measles [20], rotavirus [21], and various strains of influenza [22]-[24]. For influenza immunization, one study utilized dissolving microneedles to deliver inactivated influenza virus (strain A/PR/8/34, H1N1) [24]. The authors found that microneedles afforded superior responses compared to intramuscular injection in mice, including conferring protection against a lethal challenge. Additionally, challenges three months post immunization resulted in more efficient viral clearance in the microneedle group.

Microneedles have also been used for the delivery of DNA-based vaccines [25], [26]. While electroporation is considered to be the gold-standard for DNA vaccination, one group tested the method of DNA-containing polymer films loaded onto microneedles [26]. This allowed for the DNA to be reproducibly delivered into the epidermis and released by the microneedles. Adjustment of the polymer formulation allowed for control over the duration of the film persistence [26]. Using model HIV antigens, the group found that the use of their "multilayer tattooing" resulted in a strong T-cell response, with antigen specific $CD8^+$ T cells exceeding 5% of the total circulating population. This was comparable to the response seen for electroporation [26]. While adjuvants and immunostimulatory molecules were used to elicit responses, this is an exciting result, which, if proven safe in clinical trials, could greatly simplify DNA-based vaccines.

6.2.3. Sensing

In addition to delivery, skin-permeabilizing technologies can also be used to extract material for sensing. There is considerable interest in non-invasive sensing of metabolites, especially glucose, for diabetic populations [27]. The two main methods employed are US and microneedles, because both can provide a high degree of skin permeabilization, maximizing the amount of material that is extracted. Iontophoresis has also been used for the extraction of a number of analytes, including glucose and potassium [28], [29]. However, because of its limited impact on skin permeability, it is more limited in the types of analytes that can be detected.

US has seen significant use for skin permeabilization for the detection of interstitial glucose, with the first human trials occurring in the early 2000's [27]. These trials used an off-the-shelf transducer to permeabilize the skin for subsequent glucose detection. The authors showed good correlation between blood glucose levels and those found in interstitial fluid. Additionally, readings could be taken for over 15 hours while the skin remained highly permeable [27]. While this study utilized bulkier equipment, other studies have focused on the use of smaller equipment affording personalized calibration of skin permeabilization [30]. Chuang et al. showed the utility of non-invasive glucose monitoring in a variety of patient populations. More recently, cymbal transducer arrays have been integrated with glucometers to make wearable monitors [31].

Microneedles have similarly been investigated for their ability to extract and sense analytes. Recent studies have focused on the use of hollow

microneedles with various electrodes loaded within the microneedle [32], [33]. These detection methods use electrochemical reactions, in which the electrodes have been chemically modified to react with the metabolite of interest, generating a current. This method has been used for the detection of hydrogen peroxide, ascorbic acid, and lactate [32], [33]. The hollow microneedles were shown to remain intact within the skin and the electrodes exhibited specificity for the metabolites of interest.

Other studies have utilized solid microneedles with functionalized surfaces. One study looked at the use of conducting polymers for the sensing of glucose [34]. The polymers are loaded with glucose oxidase and then coated onto metal microneedles. The authors found that their stand-alone patch had acceptable sensitivity over the entire physiological glucose range, and was stable in wet or dry conditions for prolonged storage times [34]. Other studies have examined the detection of large antibodies [35]. By functionalizing the surface of the microneedles with influenza strains, the authors were able to show detection of antibodies *in vivo* after animals were vaccinated against those strains [35]. While the detection of large molecules is interesting, this technology is in its infancy. It requires significant post-processing to quantify the extent of capture by the microneedles, and is limited to a "yes" or "no" response, rather than to real-time concentration-dependent monitoring.

Two important issues surrounding non-invasive sensing are the amount of material that can be extracted over a given period of time and the correlation of interstitial analyte levels with those of blood. A lag-time has been determined to

exist between blood glucose levels and those found in interstitial fluid, for example [27]. As a result, there has been interest in the non-invasive extraction of blood for collection and later testing. Indeed, there are reports of the use of high-aspect ratio microneedles for blood extraction [36], [37]. There is also commercial interest in this area [38].

6.3. Outlook for Transdermal Drug Delivery

The SC limits the number of drugs that can diffuse across the skin. As a result, many methods have been studied for their ability to permeabilize the SC. The three most common permeabilization methods include US, microneedles, and electrical techniques. However, so far, none of these methods have made much of a clinical impact. This is primarily due to bulky equipment complicating use and patient compliance, expensive manufacturing methods, and safety concerns, in addition to the kinetics of delivery achievable with these methods.

US can permeabilize a large area of skin. However, treatment times can be long, and so far, the equipment required is bulky and expensive. This highlights the need for focused studies on the use of US for specific applications where the technology would solve an unmet need. Examples include delivery of small molecules with poor oral delivery or the delivery of larger molecules that require small doses. However, the kinetics of delivery must be considered in addition to the total dose achieved. It remains to be seen whether this method is appropriate for vaccination.

Regardless, US offers many advantages and deserves further investigation. First, US permeabilizes the largest area out of all of the permeabilization methods considered and specifically targets the top layer of the skin, making it painless. Second, further work into the miniaturization of this technology could enable wearable patches, reducing cost and increasing convenience for the patient. This will increase commercial interest in US, especially since reformulation would allow for further exclusivity periods of approved drugs. Finally, the area of US-assisted vaccination has seen relatively little investigation. US has the benefit of acting as an adjuvant, recruiting immune cells to the site of antigen administration. This could eliminate the need for toxic chemical adjuvants. The types of immune responses that can be induced also has not been investigated. The ability of US to induce cytotoxic T cells in cancer immunotherapy, for example, would be quite interesting.

Microneedles have received considerable interest because of advances in manufacturing and their overall ease of use. However, they are not useful for all applications. The relative area of permeabilization is small, being localized to the sites of needle insertion. Use of microneedles (or any other permeabilization method) as a pretreatment followed by the application of drug or a patch only complicates use, decreasing patient compliance. This effectively limits the application of microneedles to those where the therapeutic may be delivered simultaneously with the microneedles. This is why vaccination is an attractive application. Patches can be mass-produced and coated or loaded with minimal amounts of antigen. Further, patients could self-administer the patch, a feature

that, so far, is exclusive to microneedles. This is especially important for use in developing countries. The need for adjuvants, while associated with a myriad of side effects, will be acceptable, particularly if microneedles can induce responses against viruses and cancers that currently lack a vaccine.

Electrically-based delivery methods will likely see more limited use. Like US, they require electrical input, making them more expensive and difficult to implement than microneedles. Additionally, only electroporation induces permeability, albeit to a lesser extent than US. Finally, both electroporation and iontophoresis can elicit pain and discomfort from the start of treatment. Iontophoresis in particular is quite limited on its own. While uncharged species can experience some enhancement, it is significantly reduced compared to charged species. Additionally, delivery typically takes hours, which may not make the kinetics of delivery clinically relevant. Until these devices are further miniaturized, combination with another permeabilization method will only complicate treatment regimens, reducing compliance.

However, like microneedles, vaccination is an interesting application for electrically-based methods, specifically electroporation. Currently injected vaccines against viruses must use live vectors that themselves can elicit immune responses, limiting the ability to continually boost. The use of DNA-based vaccines is now feasible because of electroporation allowing efficient cellular uptake of the material. This could potentially enable immunization against cancers and viruses. Whether electrical methods or microneedles are more widely used for vaccination will most likely depend on which technology is

approved first. However, microneedles would seem to have the advantage due to their simplicity.

Transdermal drug delivery is an important route of administration due to its benefits over oral and needle-based methods. There is significant room for development and implementation of these methods but work must be tailored to the individual advantages afforded by each method. Studies addressing unmet clinical needs that would benefit specifically from the advantages offered by a particular method will drive innovation. By simultaneously considering effectiveness and convenience, these methods have the potential to positively impact patients and physicians alike.

6.4. Proposed Future Research Directions for GI-Based Delivery

The use of physical methods of administration in the GI tract, such as microneedles and US, provide an alternative means of delivery, requiring minimal reformulation of the drug, providing a potentially broad delivery platform. Similarly, these methods have the potential to deliver macromolecules. Microneedle-based technology, for example, has been extensively evaluated for transdermal drug and vaccine delivery [39] to many parts of the body, including the perianal skin area for the treatment of fecal incontinence [40]. Unlike the skin, the GI tract is insensate and therefore provides a unique opportunity for the use of needle-based delivery systems. The work presented in Chapter 4 of this thesis details a platform technology, and clearly demonstrates for the first time superior kinetics and safety of the deployment of microneedles in the GI tract.

Building on this preliminary study, it is crucial to develop and better understand the use of physical enhancers for oral drug delivery. With regards to microneedles, it is important to elucidate the effect of needle shape, length, and geometry on tissue interaction including puncture force. Additionally, it is hypothesized that needle geometry could be used to control the transit time of a model device through the GI tract. This would have important implications for delivery kinetics and release parameters. In addition to needle geometry, formulation could be investigated. Specifically, the use of bio-resorbable needles that could dislodge from the pill and slowly release drug into the tissue could provide a mechanism for controlled-release of drugs [41].

The work presented in Chapter 5 could also be built upon by developing US technology for deployment in an ingestible form to permeabilize the GI tissue to enhance drug delivery. Despite being investigated for transdermal drug delivery, ultrasound has never been investigated for use in the GI tract until now. This line of research, therefore, presents ample opportunity for significant study and impact. Indeed, future study could focus on the development of ingestible US devices to enable systemic delivery. Implementation of such a device has the potential to enable increased oral bioavailability based on safe and reversible permeabilization of the GI tract, thereby requiring lower drug doses for comparable efficacy.

Building on the work presented in this thesis on GI-based drug delivery could have tremendous impact and broaden our knowledge of delivery in the GI tract. The use of physical enhancers for oral delivery is an unexplored area rich

for academic and clinical investigation. It has the potential to enable oral delivery of substances such as nanoparticles, monoclonal antibodies, or vaccines to modulate mucosal immune responses [42]-[44]. Additionally, it has the potential to enable the delivery of new classes of therapeutics such as DNA and RNA-based treatments, whose delivery requires overcoming several biological barriers [45]-[47].

6.5. References

[1] S. Mitragotri, D. Blankschtein, and R. Langer, "Ultrasound-mediated transdermal protein delivery.," *Science*, vol. 269, no. 5225, pp. 850–853, Aug. 1995.

[2] E. E. Peters, M. Ameri, X. Wang, Y.-F. Maa, and P. E. Daddona, "Erythropoietin-Coated ZP-Microneedle Transdermal System: Preclinical Formulation, Stability, and Delivery," *Pharm Res*, vol. 29, no. 6, pp. 1618–1626, Jan. 2012.

[3] J. D. Kim, M. Kim, H. Yang, K. Lee, and H. Jung, "Droplet-born air blowing: Novel dissolving microneedle fabrication," *Journal of Controlled Release*, vol. 170, no. 3, pp. 430–436, Sep. 2013.

[4] E. M. Saurer, R. M. Flessner, S. P. Sullivan, M. R. Prausnitz, and D. M. Lynn, "Layer-by-Layer Assembly of DNA- and Protein-Containing Films on Microneedles for Drug Delivery to the Skin," *Biomacromolecules*, vol. 11, no. 11, pp. 3136–3143, Nov. 2010.

[5] K. van der Maaden, H. Yu, K. Sliedregt, R. Zwier, R. Leboux, M. Oguri, A.

Kros, W. Jiskoot, and J. A. Bouwstra, "Nanolayered chemical modification of silicon surfaces with ionizable surface groups for pH-triggered protein adsorption and release: application to microneedles," *Journal of Materials Chemistry B*, vol. 1, pp. 4466–4477, 2013.

[6] S. Katikaneni, G. Li, A. Badkar, and A. K. Banga, "Transdermal delivery of a ~13 kDa protein—an in vivocomparison of physical enhancement methods," *Journal of Drug Targeting*, vol. 18, no. 2, pp. 141–147, Feb. 2010.

[7] K. Kigasawa, K. Kajimoto, T. Nakamura, S. Hama, K. Kanamura, H. Harashima, and K. Kogure, "Noninvasive and efficient transdermal delivery of CpG-oligodeoxynucleotide for cancer immunotherapy," *Journal of Controlled Release*, vol. 150, no. 3, pp. 256–265, 2011.

[8] S. Dubey and Y. N. Kalia, "Non-invasive iontophoretic delivery of enzymatically active ribonuclease A (13.6kDa) across intact porcine and human skins," *Journal of Controlled Release*, vol. 145, no. 3, pp. 203–209, Aug. 2010.

[9] S. Dubey and Y. N. Kalia, "Electrically-assisted delivery of an anionic protein across intact skin: Cathodal iontophoresis of biologically active ribonuclease T1," *Journal of Controlled Release*, vol. 152, no. 3, pp. 356–362, Jun. 2011.

[10] R. H. Guy, Y. N. Kalia, M. B. Delgado-Charro, V. Merino, A. López, and D. Marro, "Iontophoresis: electrorepulsion and electroosmosis," *Journal of Controlled Release*, vol. 64, no. 1, pp. 129–132, Feb. 2000.

[11] M. J. Garland, E. C. Salvador, K. Migalska, D. A. Woolfson, and R. F. Donnelly, "Dissolving polymeric microneedle arrays for electrically assisted transdermal drug delivery," *Journal of Controlled Release*, vol. 159, no. 1, pp. 52–59, 2012.

[12] G. M. Glenn, D. N. Taylor, X. Li, S. Frankel, A. Montemarano, and C. R. Alving, "Transcutaneous immunization: A human vaccine delivery strategy using a patch - Nature Medicine," *Nature Medicine*, vol. 6, no. 12, pp. 1403–1406, Dec. 2000.

[13] S. T. Reddy, A. J. van der Vlies, E. Simeoni, V. Angeli, G. J. Randolph, C. P. O'Neil, L. K. Lee, M. A. Swartz, and J. A. Hubbell, "Exploiting lymphatic transport and complement activation in nanoparticle vaccines," *Nat Biotechnol*, vol. 25, no. 10, pp. 1159–1164, Sep. 2007.

[14] S. K. Ghosh and R. Roy Chowdhury, "Synthetic adjuvants for vaccine formulations: phytol derivatives," *Expert Opin. Drug Deliv.*, vol. 10, no. 4, pp. 437–450, Apr. 2013.

[15] D. Chen, K. F. Weis, Q. Chu, C. Erickson, R. Endres, C. R. Lively, J. Osorio, and L. G. Payne, "Epidermal Powder Immunization Induces both Cytotoxic T-Lymphocyte and Antibody Responses to Protein Antigens of Influenza and Hepatitis B Viruses," *Journal of virology*, vol. 75, no. 23, pp. 11630–11640, Dec. 2001.

[16] A. Dahlan, H. O. Alpar, P. Stickings, D. Sesardic, and S. Murdan, "Transcutaneous immunisation assisted by low-frequency ultrasound," *International Journal of Pharmaceutics*, vol. 368, no. 1, pp. 123–128, Feb.

2009.

[17] A. Tezel, S. Paliwal, Z. Shen, and S. Mitragotri, "Low-frequency ultrasound as a transcutaneous immunization adjuvant," *Vaccine*, vol. 23, no. 29, pp. 3800–3807, May 2005.

[18] B. D. Livingston, S. F. Little, A. Luxembourg, B. Ellefsen, and D. Hannaman, "Comparative performance of a licensed anthrax vaccine versus electroporation based delivery of a PA encoding DNA vaccine in rhesus macaques," *Vaccine*, vol. 28, no. 4, pp. 1056–1061, Jan. 2010.

[19] S. Vasan, A. Hurley, S. J. Schlesinger, D. Hannaman, D. F. Gardiner, D. P. Dugin, M. Boente-Carrera, R. Vittorino, M. Caskey, J. Andersen, Y. Huang, J. H. Cox, T. Tarragona-Fiol, D. K. Gill, H. Cheeseman, L. Clark, L. Dally, C. Smith, C. Schmidt, H. H. Park, J. T. Kopycinski, J. Gilmour, P. Fast, R. Bernard, and D. D. Ho, "In Vivo Electroporation Enhances the Immunogenicity of an HIV-1 DNA Vaccine Candidate in Healthy Volunteers," *PLoS ONE*, vol. 6, no. 5, p. e19252, May 2011.

[20] C. Edens, M. L. Collins, J. Ayers, P. A. Rota, and M. R. Prausnitz, "Measles vaccination using a microneedle patch," *Vaccine*, vol. 31, no. 34, pp. 3403–3409, Jul. 2013.

[21] S. Moon, Y. Wang, C. Edens, J. R. Gentsch, M. R. Prausnitz, and B. Jiang, "Dose sparing and enhanced immunogenicity of inactivated rotavirus vaccine administered by skin vaccination using a microneedle patch," *Vaccine*, vol. 31, no. 34, pp. 3396–3402, Jul. 2013.

[22] F. S. Quan, Y. C. Kim, J. M. Song, H. S. Hwang, R. W. Compans, M. R.

Prausnitz, and S. M. Kang, "Long-Term Protective Immunity from an Influenza Virus-Like Particle Vaccine Administered with a Microneedle Patch," *Clinical and Vaccine Immunology*, vol. 20, no. 9, pp. 1433–1439, Aug. 2013.

[23] Y.-C. Kim, F.-S. Quan, R. W. Compans, S.-M. Kang, and M. R. Prausnitz, "Formulation and coating of microneedles with inactivated influenza virus to improve vaccine stability and immunogenicity," *Journal of Controlled Release*, vol. 142, no. 2, pp. 187–195, Mar. 2010.

[24] S. P. Sullivan, D. G. Koutsonanos, M. del Pilar Martin, J. W. Lee, V. Zarnitsyn, S.-O. Choi, N. Murthy, R. W. Compans, I. Skountzou, and M. R. Prausnitz, "Dissolving polymer microneedle patches for influenza vaccination," *Nature Medicine*, vol. 16, no. 8, pp. 915–920, Jul. 2010.

[25] X. Chen, A. S. Kask, M. L. Crichton, C. McNeilly, S. Yukiko, L. Dong, J. O. Marshak, C. Jarrahian, G. J. P. Fernando, D. Chen, D. M. Koelle, and M. A. F. Kendall, "Improved DNA vaccination by skin-targeted delivery using dry-coated densely-packed microprojection arrays," *Journal of Controlled Release*, vol. 148, no. 3, pp. 327–333, Dec. 2010.

[26] P. C. DeMuth, Y. Min, B. Huang, J. A. Kramer, A. D. Miller, D. H. Barouch, P. T. Hammond, and D. J. Irvine, "Polymer multilayer tattooing for enhanced DNA vaccination," *Nature Materials*, vol. 12, no. 4, pp. 367–376, Jan. 2013.

[27] J. Kost, R. Langer, S. Mitragotri, R. A. Gabbay, and M. Pishko, "Transdermal monitoring of glucose and other analytes using ultrasound,"

Nature Medicine, vol. 6, no. 3, pp. 347–350, Mar. 2000.

[28] C. McCormick, D. Heath, and P. Connolly, "Towards blood free measurement of glucose and potassium in humans using reverse iontophoresis," *Sensors & Actuators: B. Chemical*, vol. 166, no. 0, pp. 593–600, May 2012.

[29] N. S. Oliver, C. Toumazou, A. E. G. Cass, and D. G. Johnston, "Glucose sensors: a review of current and emerging technology," *Diabetic Medicine*, vol. 26, no. 3, pp. 197–210, Mar. 2009.

[30] H. Chuang, M.-Q. Trieu, J. Hurley, E. J. Taylor, M. R. England, and S. A. Nasraway, "Pilot Studies of Transdermal Continuous Glucose Measurement in Outpatient Diabetic Patients and in Patients during and after Cardiac Surgery," *Journal of diabetes science and technology (Online)*, vol. 2, no. 4, p. 595, Jul. 2008.

[31] E.-J. Park, J. Werner, J. Beebe, S. Chan, and N. B. Smith, "Noninvasive Ultrasonic Glucose Sensing with Large Pigs (~200 Pounds) Using a Lightweight Cymbal Transducer Array and Biosensors," *Journal of Diabetes Science and Technology*, vol. 3, no. 3, pp. 517–523, Apr. 2009.

[32] P. R. Miller, S. D. Gittard, T. L. Edwards, D. M. Lopez, X. Xiao, D. R. Wheeler, N. A. Monteiro-Riviere, S. M. Brozik, R. Polsky, and R. J. Narayan, "Integrated carbon fiber electrodes within hollow polymer microneedles for transdermal electrochemical sensing," *Biomicrofluidics*, vol. 5, no. 1, p. 013415, 2011.

[33] J. R. Windmiller, N. Zhou, M.-C. Chuang, G. Valdés-Ramírez, P.

Santhosh, P. R. Miller, R. Narayan, and J. Wang, "Microneedle array-based carbon paste amperometric sensors and biosensors," *Analyst*, vol. 136, no. 9, p. 1846, 2011.

[34] M. A. Invernale, B. C. Tang, R. L. York, L. Le, D. Y. Hou, and D. G. Anderson, "Microneedle Electrodes Toward an Amperometric Glucose-Sensing Smart Patch," *Adv. Healthcare Mater.*, pp. n/a–n/a, Aug. 2013.

[35] J. W. Coffey, S. R. Corrie, and M. A. F. Kendall, "Early circulating biomarker detection using a wearable microprojection array skin patch," *Biomaterials*, vol. 34, no. 37, pp. 9572–9583, Dec. 2013.

[36] C. G. Li, K. Lee, C. Y. Lee, M. Dangol, and H. Jung, "A Minimally Invasive Blood-Extraction System: Elastic Self-Recovery Actuator Integrated with an Ultrahigh- Aspect-Ratio Microneedle," *Adv. Mater.*, vol. 24, no. 33, pp. 4583–4586, Jul. 2012.

[37] C. G. Li, C. Y. Lee, K. Lee, and H. Jung, "An optimized hollow microneedle for minimally invasive blood extraction," *Biomed Microdevices*, vol. 15, no. 1, pp. 17–25, Jul. 2012.

[38] C. M. Schoellhammer, D. Blankschtein, and R. Langer, "Skin permeabilization for transdermal drug delivery: recent advances and future prospects.," *Expert Opin. Drug Deliv.*, vol. 11, no. 3, pp. 393–407, Jan. 2014.

[39] M. R. Prausnitz, "Microneedles for transdermal drug delivery," *Advanced drug delivery reviews*, vol. 56, no. 5, pp. 581–587, 2004.

[40] C. Baek, M. Han, J. Min, M. R. Prausnitz, J.-H. Park, and J. H. Park,

"Local transdermal delivery of phenylephrine to the anal sphincter muscle using microneedles.," *J Control Release*, vol. 154, no. 2, pp. 138–147, Sep. 2011.

[41] G. Traverso, C. M. Schoellhammer, A. Schroeder, R. Maa, G. Y. Lauwers, B. E. Polat, D. G. Anderson, D. Blankschtein, and R. Langer, "Microneedles for Drug Delivery via the Gastrointestinal Tract," *Journal of Pharmaceutical Sciences*, pp. n/a–n/a, Sep. 2014.

[42] A. C. Watkinson, "Transdermal and Topical Drug Delivery Today," no. 18, H. A. E. Benson and A. C. Watkinson, Eds. John Wiley & Sonsedition, 2012.

[43] A. Cerutti, "Location, location, location: B-cell differentiation in the gut lamina propria," *Mucosal Immunol*, vol. 1, no. 1, pp. 8–10, Jan. 2008.

[44] Q. Zhu, J. Talton, G. Zhang, T. Cunningham, Z. Wang, R. C. Waters, J. Kirk, B. A. R. Eppler, D. M. Klinman, Y. Sui, S. Gagnon, I. M. Belyakov, R. J. Mumper, and J. A. Berzofsky, "Large intestine-targeted, nanoparticle-releasing oral vaccine to control genitorectal viral infection," *Nature Publishing Group*, pp. 1–7, Jul. 2012.

[45] "Microneedles for drug and vaccine delivery," vol. 64, no. 14, pp. 1547–1568, Nov. 2012.

[46] C. V. Pecot, G. A. Calin, R. L. Coleman, G. Lopez-Berestein, and A. K. Sood, "RNA interference in the clinic: challenges and future directions," *Nat Rev Cancer*, vol. 11, no. 1, pp. 59–67, Jan. 2011.

[47] M. P. Morrow and D. B. Weiner, "DNA Drugs Come of Age," *Scientific*

American, vol. 303, no. 1, pp. 48–53, Jul. 2010.